Impact of FLT3 internal tandem duplications (FLT3-ITD) on functional biology and sensitivity to therapy depending on their location

Dissertation

zur Erlangung des akademischen Grades

doctor rerum naturalium

(Dr. rer. nat.)

genehmigt durch die Fakultät für Naturwissenschaften

der Otto-von-Guericke-Universität Magdeburg

von M.Sc., Patricia Arreba Tutusaus

geb. am 21 Mai 1987 in Barcelona (Spanien)

Gutachter: Prof. Dr. med. Florian Heidel

Prof. Dr. rer. nat. Frank-D Böhmer

eingereicht am: 21 Juni 2016

verteidigt am: 16 November 2016

Learn from yesterday,
Live for today,
Hope for tomorrow.
The important thing is not to stop questioning

- Albert Einstein-

Table of Contents

Zusammenfassung

Die akute myeloische Leukämie ist häufig mit dem Auftreten von Mutationen im *FLT3* Gen assoziiert. Die häufigste Form der FLT3-Mutation ist eine interne Tandemduplikation (ITD). Die Behandlung der AML mit FLT3-Längenmutation (ITD) bleibt eine klinische Herausforderung, da diese Art von Leukämie selbst nach allogener Stammzelltransplantation eine hohe Rückfallquote aufweist. FLT3-Kinase-Inhibitoren besitzen nachgewiesene klinische Aktivität in klinischen Studien und können in Kombination mit Chemotherapie das Überleben der Patienten verbessern. So werden die FLT3-Kinase –Inhibitoren Midostaurin (PKC412) und Quizartinib (AC220) derzeit in fortgeschrittenen klinischen Studien eingesetzt und zeigen ein vielversprechendes klinisches Ansprechen.

Lange Zeit wurde geglaubt, dass ITD Mutationen ausschließlich in der Juxtamembran-Domäne (JMD) des FLT3-Rezeptors auftreten. Dadurch wird die autoinhibitorische Funktion der Domäne zerstört, was zu einem konstitutiv aktiven FLT3-Rezeptor und der nachgeschalteten Signalwege führt. Kürzlich konnten wir nachweisen, dass ein signifikanter Anteil (30 %) der FLT3-ITD Mutationen in der Tyrosin- Kinase-Domäne 1 (TKD1) lokalisiert ist. In einer multivariablen Analyse wurde die Lage der ITD-Mutation im „beta1-Sheet" der TKD1 als negativer prognostischer Faktor beschrieben. Dieser Einfluss war unabhängig von anderen unvorteilhaften prognostischen Faktoren wie z.B. der Allel-Last. In Vordaten aus unserer Abteilung hatten sich Hinweise ergeben, dass die Lokalisation von FLT3-ITDs in der TKD1 mit einer geringeren Tyrosin-Kinase Inhibitor Sensitivität der betroffen Zellen vergesellschaftet sein könnte.

In der vorliegenden Arbeit wurden verschiedene FLT3-ITD Mutationen (JMD vs. TKD1) *in vitro* untersucht und zum ersten Mal funktionell *in vivo* charakterisiert. Das Transformationspotential und die Aktivierung nachgelagerter Signalknoten, wie z.B. Stat5 und Erk1/2, waren vergleichbar zwischen den verschiedenen FLT3-ITD Varianten unabhängig von der Lage der FLT3-Längenmutation. Im Gegensatz zu JMD-ITDs zeigten TKD1-ITD Mutationen *in vivo* sowohl eine geringere Penetranz der Erkrankung als auch eine verzögerte Leukämieentwicklung. Andererseits konnte die im Zellkulturmodell gezeigte geringere Sensitivität der TKD1-ITDs gegenüber Kinase-Inhibitor Behandlung auch *in vivo* rekapituliert werden. Mit Hilfe von Gen-Expressionsanalysen konnten zwischen JMD-ITD und TKD1-ITD Mutationen differentiell regulierte ‚Gene-Sets' identifiziert werden. Hier zeigten sich vor allem DNA-Reparatur-assoziierte Gene dereguliert. Dieser Befund aus den Genexpressionsanalysen konnte in murinen Zelllinien nach Bestrahlung ebenfalls nachgewiesen werden. Nach Induktion

von DNA-Bruch zeigten TKD1-ITD Mutanten weniger Doppelstrangbrüche im Vergleich zu JMD-ITD Mutationen, was auf ein vermehrtes Level an DNA-Reparaturmechanismen hinweisen könnte.

Zusammenfassend können unsere Untersuchungen erstmals funktionell belegen, dass die Lage der ITD Mutationen innerhalb der FLT3-Kinase das biologische Verhalten der betroffenen Zellen und deren Sensitivität gegenüber Kinase-Inhibitor Therapie beeinflusst.

Abstract

Treatment of patients harboring internal tandem duplications within the *FLT3* gene (FLT3-ITD) remains a clinical challenge in acute myeloid leukemia (AML) as this subset of leukemia shows high incidence of relapse, even after allogeneic stem-cell transplantation. A long-term goal in AML treatment is the design of personalized therapies restricted to distinct recurrent mutations in order to eliminate residual pre-leukemic and leukemic clones. Inhibitors of the FLT3-mutated receptor, known as tyrosine kinase inhibitors (TKIs), have proven activity in advanced clinical trials and an improvement in progression free survival when combined with chemotherapy. For a long time, ITD mutations have been believed to exclusively occur within the juxtamembrane domain (JMD) of the FLT3 receptor. However, a molecular subset of FLT3-ITD mutations located in the tyrosine kinase domain 1 (TKD1) has recently been defined in FLT3-ITD positive AML patients. In multivariable analyses, location of ITD mutations within the beta1-sheet of FLT3 (TKD1-ITD) was identified as an unfavorable prognostic factor for achievement of complete remission and overall survival, independently of other prognostic factors such as allelic ratio. Furthermore, previous work in our group showed that TKD1-ITD mutations conferred less sensitivity to kinase inhibitor therapy *in vitro*. The purpose of this dissertation was to characterize the biology and the sensitivity to FLT3-targeted therapy of additional FLT3-ITD mutations depending on their location site (JMD vs. TKD1) *in vitro* and, for the first time, *in vivo*. Transforming potential and activation of downstream signaling nodes were comparable between previously characterized mutations and novel variants isolated from leukemia samples *in vitro*. However, TKD1-ITD mutations revealed reduced penetrance as well as prolonged onset of leukemia development when compared to JMD-ITDs *in vivo*. Furthermore, previous findings could be recapitulated since TKD1-ITDs showed less sensitivity to TKI treatment *in vivo*. Lastly, gene-expression data from human and murine cells harboring FLT3-ITD mutations provided differentially regulated gene-sets (JMD vs. TKD1), among which DNA damage and repair mechanisms were selected as potential mediators of drug sensitivity. Here, DNA damage was quantified in murine cells suggesting increased DNA repair in TKD1-ITD mutants. Taken together, the present study provides evidence that location of ITD mutations within the FLT3 receptor tyrosine kinase may determine differential oncogenic potential and sensitivity to targeted treatment in patients.

Figures

Tables

Abbreviations

5-FU	5'-fluorouracil
AA	Amino acids
AL	Activation loop
ALL	Acute lymphocytic leukemia
AML	Acute myeloid leukemia
APS	Ammonium persulfate
ATP	Adenosine triphosphate
Bad	Bcl-2-associated death
Bax	Bcl-2-associated X
Bcl-2	B-cell lymphoma 2
Bcl-x$_L$	B-cell lymphoma-extra large
BMT	Bone marrow transplant
bp	Base pairs
BSA	Bovine serum albumin
C/EBPA	CCAAT/Enhancer binding protein alpha
CD135	Cluster of differentiation antigen 135
CFU	Colony-forming unit
CLP	Common lymphoid progenitors
CMP	Common myeloid progenitors
CN-AML	Cytogenetically normal-AML
CN-LOH	Copy-neutral loss of heterozygosity
CO$_2$	Carbon dioxide
CR	Complete remission
CSF-1-R	Macrophage colony-stimulating factor receptor
ddNTP	Dideoxynucleotide triphosphates
DMEM	Dulbecco's modified eagle's medium
DMSO	Dimethyl sulfoxide
DNA	Deoxyribonucleic acid
dNTP	Deoxynucleotide triphosphates
DPBS	Dulbecco's phosphate-buffered saline
DSB	Double strand break
EDTA	Ethylenediaminetetraacetic acid
EGTA	Ethylene glycol tetraacetic acid
EtBr	Ethidium bromide
FACS	Fluorescence-activated cell sorting
FBS	Fetal bovine serum
FL	FLT3 ligand
Flk2	Fetal liver kinase 2

FLT3	FMS-related tyrosine kinase-3
FLT3-AL	FLT3 point mutation
FOXO	Forkhead box O
GAB2	GRB2-associated-binding protein 2
G-CSF	Granulocyte-colony stimulating factor
GEP	Gene-expression profiling
GMP	Granulocyte-Macrophage progenitors
GFP	Green fluorescent protein
H_2O	Hydrogen oxide
HR	Homologous recombination
HRP	Horseradish peroxidase
HSC	Hematopoietic stem cells
HSPC	Hematopoietic stem and progenitor cells
IRES	Internal ribosome entry site
ITD	Internal tandem duplication
JM-B	JM binding motif
JMD	Juxtamembrane domain
JMD-ITD	FLT3-ITD within the JMD
JM-S	JM switch motif
JM-Z	JM zipper or linker peptide segment
KCl	Potassium chloride
LB	Lysogeny broth
LC	Leukemic cells
M-CSF	Macrophage-colony-stimulating factor
MAPK	Mitogen-activated protein kinase
Mcl-1	Myeloid cell leukemia 1
MDS	Myelodysplastic syndromes
MEP	Megakaryocyte-Erythroid progenitors
$MgCl_2$	Magnesium chloride
$MgSO_4$	Magnesium sulfate
MIY	MSCV IRES YFP
MoMSV	Moloney murine sarcoma virus
MSCV	Murine stem cell virus
NaCl	Sodium chloride
NaF	Sodium fluoride
NHEJ	Nonhomologus end-joining
OD	Optical density
OS	Overall survival
PBS	Phosphate-buffered saline
PCR	Polymerase chain reaction
PDGF-R	Platelet-derived growth factor receptor

PEG	Polyethylene glycol
PI3K	Phosphoinositide 3-kinase
PIG	Puromycin IRES GFP
PTP	Protein tyrosine phosphatase
Rb	Retinoblastoma
RGS2	Regulator of G-protein signaling 2
RNA	Ribonucleic acid
ROS	Reactive oxygen species
RPMI	Roswell Park memorial institute
RTK	Receptor tyrosine kinase
RUNX1	Runt-related transcription factor 1
SCF	Stem cell factor
SDS	Sodium dodecyl sulfate
SDS-PAGE	SDS polyacrylamide gel electrophoresis
SFEM	Serum-free expansion medium
SH2	Src homology 2
SHC	SH2-containing sequence protein
SHIP	SH2-containing inositol 5'-phosphatase
SOC	Super optimal broth with catabolite repression
TBE	Tris-borate-EDTA
TEMED	Tetramethylethylenediamine
TKD1	Tyrosine kinase domain 1
TKD1-ITD	FLT3-ITD within the TKD1
TKD2	Tyrosine kinase domain 2
TKD2-ITD	FLT3-ITD within the TKD2
TKI	Tyrosine kinase inhibitor
Tm	Melting temperature
TPO	Thrombopoietin
UV	Ultraviolet
V	Volt
VitE	Vitamin E
WBC	White blood cell
YFP	Yellow fluorescent protein
γH2AX	Phosphorylated H2AX

1. Introduction

1.1. The hematopoietic system and leukemia development

Hematopoiesis is a hierarchical and dynamic process that sustains a steady-state production of cellular blood components (Parcells et al., 2006). At the top of the hierarchy, a limited pool of hematopoietic stem cells (HSC) balances self-renewal and differentiation potential to maintain hematopoiesis throughout the adult lifetime. In this way, hematopoietic stem cells give rise to more committed cells that progressively lose their self-renewal capacity and undergo specific differentiation to develop functional mature hematopoietic cells, which belong either to erythroid, myeloid or lymphoid lineages (Parcells et al., 2006; Herdrich and Weinberger, 2013) (Figure 1).
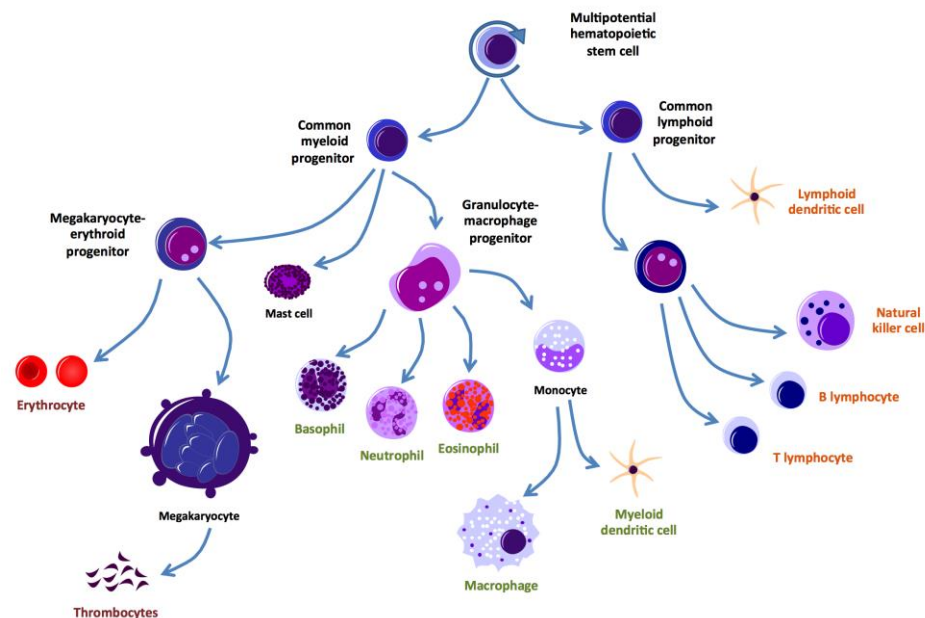
Figure 1. Scheme of the hierarchical hematopoietic system. Multipotent hematopoietic stem cells balance self-renewal and differentiation potential to maintain blood production throughout the adult lifetime. HSCs differentiate into two different types of oligolineage-restricted progenitors that ultimately give rise to mature blood cells. Common lymphoid progenitors (CLP) give rise to lymphoid cells (orange), including dendritic cells, natural killer cells, B-lymphocytes and T-lymphocytes. Common myeloid progenitors (CMP) give rise to granulocyte-macrophage progenitors (GMP), which eventually differentiate into myeloid cells (green) including dendritic cells, macrophages and granulocytes (basophils, neutrophils and eosinophils); and megakaryocyte-erythroid progenitors (MEP), which eventually produce thrombocytes (platelets) and erythrocytes (red).

During aging of the hematopoietic system, genetic alterations arise in hematopoietic stem and progenitor cells (HSPC) of otherwise healthy individuals. Accumulation of genetic events leads to development of clonal hematopoiesis. These genetic aberrations may pre-dispose development of hematopoietic disorders like myelodysplasia or acute leukemia. Leukemias

involve a group of heterogeneous blood malignancies characterized by an uncontrolled growth of white blood cells (Passegué et al., 2003). In the course of the disease, transformed cells proliferate at higher rates and fail in their differentiation causing an accumulation of non-functional leukemic cells (LC) in the organism. Leukemias include several disorders that are classified by the cellular origin - myeloid or lymphoid - and the progression of the disease - chronic or acute. While chronic leukemia has a more indolent course with transformed cells in more differentiated stages, acute leukemia is more aggressive due to its faster progression and accumulation of immature cells (*blasts*) (Sell, 2005).

1.2. Acute myeloid leukemia

Acute myeloid leukemia (AML) is characterized by an abnormal clonal growth of myeloid precursors with impaired differentiation (Herdrich and Weinberger, 2013). As a result, a high frequency of immature myeloblasts circulates in the bloodstream, and blast cells accumulate in the bone marrow interfering with the production of normal blood cells (Ferrara and Schiffer, 2013). This lack of normal hematopoiesis leads to a bone-marrow failure and a clinical picture marked by thrombocytopenia (bleedings), neutropenia (infections) and reduction of red blood cells (anemia) (Herdrich and Weinberger, 2013). In addition, accumulation of myeloblasts in extramedullary organs like spleen, lung or brain may occur (Kumar, 2011). According to epidemiological and survival data, AML is the most common type of acute leukemia diagnosed in adults accounting for more than 60% of acute leukemia. Disease incidence strongly correlates with population aging, and the majority of AML patients are above the age of 65 increasing the average age to 67 (Kumar, 2011). In addition, survival is also influenced by co-morbidities and higher incidence of adverse prognostic factors (Estey and Döhner, 2006). Overall, survival rate is low and declines with increasing age. Long-term survival in younger patients (<60 years) is 40-45%, while elderly patients' survival is below 20% (Grove and Vassiliou, 2014).

Conventional treatment for AML has two phases: remission induction and consolidation therapy. Induction therapy aims to eradicate leukemic cells and achieve complete remission (CR) in patients, a status that is defined as bone marrow with less than 5% blasts, absence of extramedullary leukemia, neutrophil count >1000/µl and platelet count >100000/µl (Estey and Döhner, 2006; Grove and Vassiliou, 2014). Since more than three decades, standard induction therapy combines two chemotherapeutic agents: anthracycline, which targets DNA and RNA synthesis and inhibits the topoisomerase II enzyme preventing DNA transcription and

replication, and cytarabine that interferes with DNA synthesis (Kumar, 2011). After induction, consolidation therapy aims to eliminate residual leukemic cells and to achieve a durable complete remission. Depending on several factors, e.g., age of the patient, co-morbidities or cytogenetic abnormalities, options for consolidation therapy include chemotherapy, autologous stem-cell transplantation and allogeneic stem-cell transplantation (Kumar, 2011; Herdrich and Weinberger, 2013). Unfortunately, despite achieving complete remission with standard therapy, disease relapse is a recurrent clinical problem emerging in more than half of the patients (50% to 70%) (Kumar, 2011). Recent studies have reported re-emergence of drug-resistant leukemic clones or evolution of pre-leukemic cells into leukemic clones as main origins of relapse (Ding et al., 2012; Kronke et al., 2013; Parkin et al., 2013; Corces-Zimmerman et al., 2014; Shlush et al., 2014).

1.2.1. Clonal hematopoiesis and genetic pathogenesis in AML

AML development is a stepwise process in which hematopoietic stem and progenitor cells acquire mutations that may cooperate to transform a functionally normal cell into a leukemic clone. This model of oncogenesis, known as clonal hematopoiesis, is a long-term process related to aging that requires driver mutations in order to induce a clonal expansion of healthy hematopoietic cells (Jaiswal et al., 2014; McKerrell et al., 2015). The acquisition of an initiating driver mutation confers fitness advantage to immature hematopoietic cells resulting in a pre-leukemic clone, which retains itself random passenger mutations accumulated over time. During clonal expansion, new passenger mutations are acquired until a cooperating driver mutation hits the pre-leukemic clone and gives rise to a *founding clone* that ultimately originates a full-blown acute leukemia (Figure 2) (Welch et al., 2012; Genovese et al., 2014). Hence, despite the genetic heterogeneity of AML - more than 200 different mutations have been described in AML (Döhner et al., 2010) - the majority of these aberrations may be considered as random background mutations (passenger mutations) and the combination of a reduced number of drivers would be sufficient for disease development (Welch et al., 2012; Cancer Genome Atlas Research Network, 2013; Wakita et al., 2016).
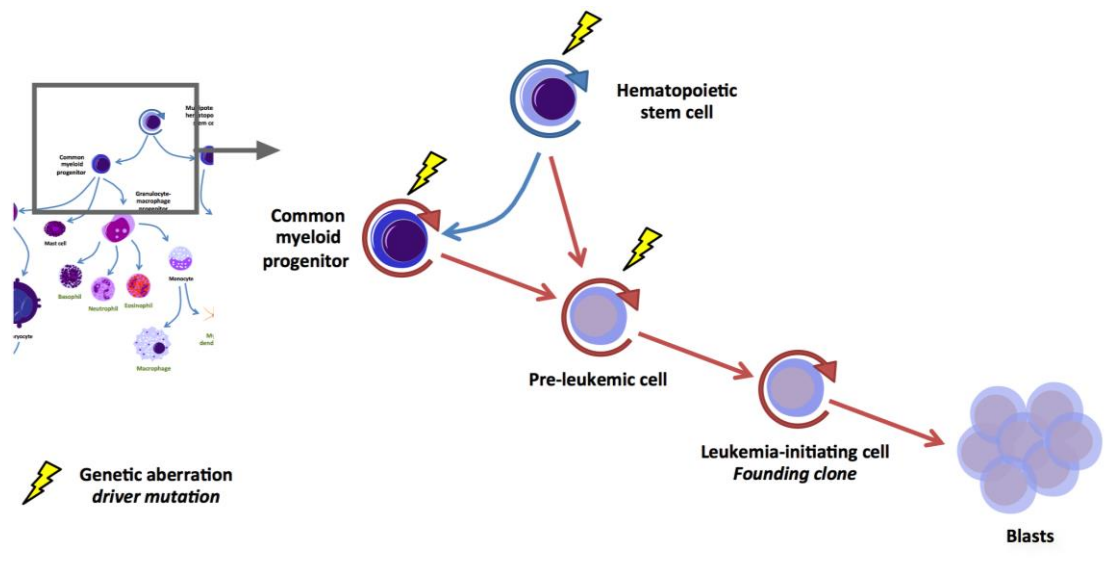
Figure 2. Scheme of clonal hematopoiesis in AML development. The sequential acquisition of genetic aberrations (driver mutations) in hematopoietic stem and progenitor cells gives rise to pre-leukemic clones and, subsequently, leukemia-initiating cells (*founding clone*), which are characterized by enhanced proliferation and loss of differentiation capacity. Uncontrolled overgrowth of the *founding clone* leads to further accumulation of undifferentiated cells (*blasts*) in the bone marrow interfering with the development of normal blood cells.

In 2002, Gilliland and Griffin already defined a *two-hit model* to explain the onset of AML. According to the model, leukemogenesis requires two classes of mutations (Gilliland, 2001; Gilliland and Griffin, 2002b). Class I mutations, which are defined as gain-of-function mutations, represent genes encoding signaling molecules (e.g., FLT3-ITD, N-RAS and c-KIT mutations) that enhance cellular proliferation and resistance to apoptosis. These mutations are considered as later events in the transformation. Class II mutations are thought to be initiating lesions that affect transcription factors and impair hematopoietic differentiation. Here, chromosomal abnormalities (e.g., PML-RARA or RUNX1-RUNX1T1) and mutations in transcription factors (e.g., C/EBPA or RUNX1) are included (Estey and Döhner, 2006; Ferrara and Schiffer, 2013). Although this model fits with the sequential acquisition of driver mutations and the molecular phenotype of arrest of cellular differentiation and enhancement of proliferation, it is currently known that leukemogenesis encompass a more complex network with many other driver mutations involved in the transformation process (Figure 3) (Passegué et al., 2003; Cancer Genome Atlas Research Network, 2013; Ferrara and Schiffer, 2013; Mazzarella et al., 2014). Overall, there is large mutational heterogeneity between AML patients, which increases due to subclones originated side-by-side within individuals. Nowadays, a main challenge in leukemia research is to discriminate these recurrent driver mutations from non-functional passenger mutations in order to better understand the molecular mechanism of disease and, importantly, to design therapies that are more effective

4

against the *founding clone* and also pre-leukemic clones. Moreover, there is a continuous search for well-defined prognostic groups in order to improve diagnosis and patients' outcome (Kumar, 2011; Herdrich and Weinberger, 2013). To date, the cytogenetic analysis is commonly used to define molecular pathogenesis and stratify AML patients into different risk groups. Recurrent chromosomal abnormalities are well-established as diagnostic and prognostic factors. For instance, patients with PML-RARA or RUNX1-RUNX1T1 variations are associated with favorable risk, whereas monosomal karyotype or more complex alterations are related to poor prognosis (Patel et al., 2012; Herdrich and Weinberger, 2013). Nevertheless, nearly 50% of *de novo* AML patients are cytogenetically normal (CN-AML) forming a heterogeneous intermediate risk group with high mutational and clinical variability. There is a need to establish recurrent somatic mutations as new prognostic factors for a better risk stratification of CN-AML (Kohlmann et al., 2010; Grossmann et al., 2012; Mrozek et al., 2012; Patel et al., 2012; Li et al., 2013; Kurosawa et al., 2016). For instance, mutations in the transcription factor C/EBPA1 have been designated as a favorable factor (Döhner et al., 2010; Taskesen et al., 2011). Moreover, mutations in the gene *NPM1* encoding for nucleophosmin - one of the most common aberrations in AML - are associated with a favorable outcome in patients without FLT3-ITD, while patients harboring wild-type *NMP1* and FLT3-ITD belong to the intermediate risk group. Mutations in the receptor tyrosine kinase FLT3 (FLT3-ITD) are the second most frequent aberrations in AML and are associated with unfavorable outcome (Döhner et al., 2010; Grossmann et al., 2012; Linch et al., 2014; Rapin et al., 2014).
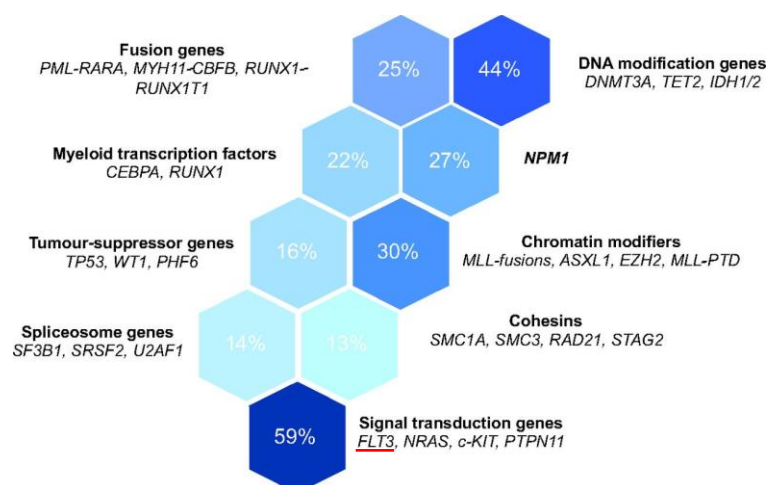
Figure 3. Overview of genetic aberrations in *de novo* AML sorted by their biological function. Recurrent somatic mutations identified in AML patients are classified into different biological functions. Genes associated to each functional group are listed, and the frequency of each group in AML is displayed (Figure from Grove and Vassiliou, 2014).

1.3. FMS-related tyrosine kinase-3 (FLT3)

1.3.1. FLT3 expression and function in hematopoiesis

FMS-related tyrosine kinase-3 (FLT3), also known as fetal liver kinase 2 (Flk2) or cluster of differentiation antigen 135 (CD135), is a member of the receptor tyrosine kinase (RTK) class III family that includes the macrophage colony-stimulating factor receptor (CSF-1-R), the stem cell factor receptor (c-Kit) and the platelet-derived growth factor receptor (PDGF-R) (Rosnet et al., 1993; Stirewalt and Radich, 2003; Parcells et al., 2006). Human *FLT3* is located on chromosome 13q12.2 and consists of 24 exons encoding a 993 amino acid mature protein (Shibuya et al., 1989; Rosnet et al., 1991b; Agnes et al., 1994). Two isoforms have been identified: a protein of about 130-140 kDa and a membrane-bound protein of 160 kDa produced after post-translational N-linked glycosylation (Lyman et al., 1993; Maroc et al., 1993; Naoe and Kiyoi, 2004). When compared to the murine homologue, there is an 85% identity at the amino acid level between human and mouse FLT3 receptor (Rosnet et al., 1991a; Shurin et al., 1998; Parcells et al., 2006). The FLT3 receptor is primarily expressed in committed myeloid and lymphoid progenitors, but also in a subset of dendritic precursor cells and, with a variable expression, in more mature monocytic lineages (Matthews et al., 1991; Brasel et al., 1995; Rosnet et al., 1996; Turner et al., 1996; Kikushige et al., 2008; Boyer et al., 2011). Besides these hematopoietic lineages, murine *Flt3* mRNA has also been detected in lympho-hematopoietic organs, such as liver, thymus, spleen and placenta, and non-hematopoietic organs such as gonads and brain (Rosnet et al., 1991a; Maroc et al., 1993; deLapeyriere et al., 1995; Meshinchi and Appelbaum, 2009).

In normal hematopoiesis, FLT3 is known to promote proliferation, survival and differentiation of early myeloid and lymphoid precursors, while no growth effect has been observed on progenitors of erythrocyte, megakaryocyte, eosinophil or mast cell lineages (Hudak et al., 1995). Furthermore, the characterization of mice deficient in *Flt3* indicated a role of the receptor tyrosine kinase in multipotent stem cells and lymphoid differentiation (Mackarehtschian et al., 1995). However, its function is also highly dependent on the cell type and the combination with other growth factors. Several *in vitro* studies in human and murine hematopoietic cells have reported a colony-stimulating activity of the FLT3 ligand (FL) on multilineage and myeloid progenitors in combination with other cytokines, such as SCF, G-CSF, IL-11 and IL-3 (Broxmeyer et al., 1995; Gabbianelli et al., 1995; Hirayama et al., 1995; Hudak et al., 1995; Shah et al., 1996; Haylock et al., 1997). FL also potentiates, either alone or in combination with IL-10 and IL-7, the regeneration of B-cell and T-cell lineages *in vivo*, and supports the proliferation of lymphoid and early B-lymphoid progenitors in combination with

cytokines such as IL-6, IL-7, IL-11, SCF and G-CSF (Hirayama et al., 1995; Namikawa et al., 1996; Ray et al., 1996; Wils et al., 2007; Tsuboi et al., 2008).

1.3.2. FLT3 structure and activation

The FLT3 receptor tyrosine kinase contains five extracellular immunoglobulin-like domains, a single-helix transmembrane domain and a cytoplasmic region that comprises a juxtamembrane domain (JMD) and two tyrosine kinase domains (TKD1/TKD2), split by a kinase-insert domain (Griffith et al., 2004; Naoe and Kiyoi, 2004). The JMD can be divided into three distinctive topological regions: the JM binding motif (JM-B), the JM switch motif (JM-S) and the zipper or linker peptide segment (JM-Z). The JM-B (Tyr572-Met578) is a short finger-like segment, which interacts with practically each structural component required in the activation of the kinase. The JM-S (Val579-Val592) forms a two-stranded antiparallel ß twist motif, which includes two key tyrosine residues (Tyr^{589} and Tyr^{591}). Last, the JM-Z (Asp593-Trp603) followed by the JM hinge region (Asp604-Asn609) is located at the C-terminus of the JMD. The JM-Z domain folds up beside the TKD1 and includes another key tyrosine residue (Tyr^{599}), which is conserved across the PDGF-R family (Griffith et al., 2004). Furthermore, the protein kinase region contains the catalytic site as well as the ATP binding site. The TKD1 (N globe) presents five-stranded anti-parallel ß-sheets (ß1-ß5) with a nucleotide-binding loop between the strands ß1 and ß2 by the side of an α-helix, termed αC. The second structure, the TKD2 (C globe), is primarily α-helical including seven α-helices (αD-E, αEF, αF-I) but also three ß-strands (ß6-ß8) and a catalytic loop. Lastly, the activation loop (AL) is a long flexible peptide that constitutes two additional ß-strands (ß10-11) (Griffith et al., 2004) (Figure 4A).

Wild-type FLT3 resides as an inactive monomeric protein in the plasma membrane. In this auto-inhibited conformation, the JM-S motif ensures a rigid orientation of the framework and interposes both tyrosine residues (Tyr^{589} and Tyr^{591}) toward the TKD2, while the JM-B motif interacts with key structural domains, including the glycine-rich loop, the αC domain and the activation loop, to prevent the rotation of TKD1 toward TKD2. Moreover, the activation loop strategically folds between TKD1 and TKD2 blocking the access to the active site and the ATP-binding site. In addition, the residue Tyr^{599} has been suggested to ensure the proper orientation to the JM hinge region (Griffith et al., 2004; Toffalini and Demoulin, 2010; Chan, 2011) (Figure 4B).
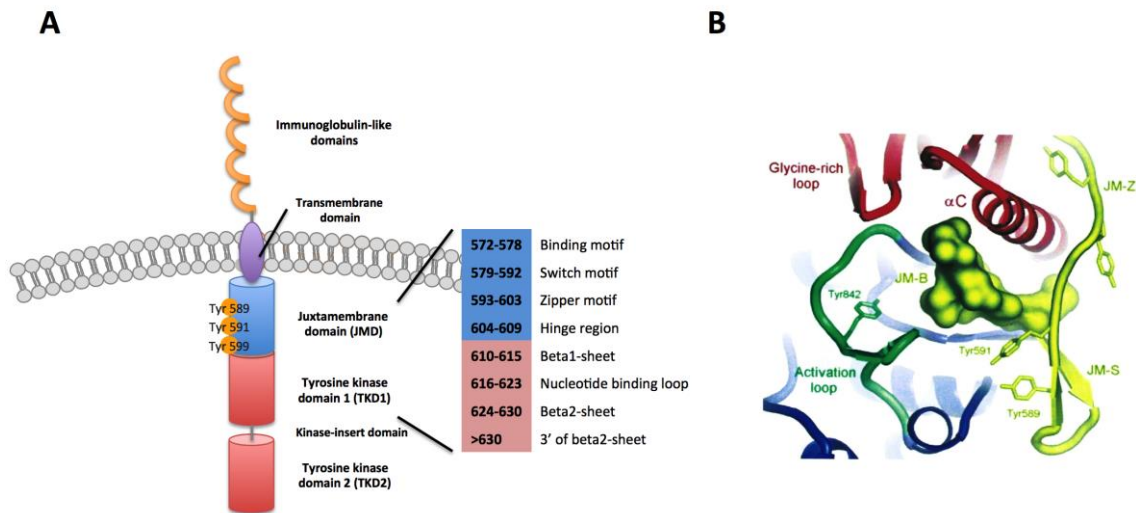
Figure 4. Schematic representation of the FLT3 receptor and crystal structure of the auto-inhibited conformation.
A) FLT3 receptors localize at the plasma membrane (grey) and consist of five extracellular immunoglobulin-like domains that form the extracellular domain (orange), a single-helix transmembrane domain (violet), and a cytoplasmatic domain containing a juxtamembrane domain (blue) and two tyrosine kinase domains (red) split by a kinase-insert domain. The JMD is divided into three distinctive topological regions: the binding motif, the switch motif and the zipper motif followed by the hinge region. Key tyrosine residues Tyr^{589}, Tyr^{591} and Tyr^{599} are highlighted in the JMD. The TKD1 contains five ß-sheets, in which the nucleotide loop links the strands ß1 and ß2. The TKD2 contains the binding and active sites as well as the C-terminal activation loop. Amino acid length of each JMD region and the beginning of the TKD1 are shown (Adapted from Kayser et al., 2009). **B)** Three-dimensional model of the cytoplasmatic domain in an inactive conformation including the JMD (yellow), TKD1 (red), TKD2 (blue) and the AL (green). The crystal structure highlights the interaction of the JM-B with the glycine-rich loop, the αC and the AL; while, both Tyr residues within the JM-S are orientated toward the TKD2 (Image from Griffith et al., 2004).

Binding to the FL promotes dimerization of FLT3 receptors and concomitant changes in their conformation that enable the trans-phosphorylation of conserved tyrosine residues in the JMD: Tyr^{589}, Tyr^{591} and Tyr^{599} (Heiss et al., 2006; Verstraete et al., 2011; Heldin and Lennartsson, 2013). As a result, the auto-inhibited conformation is disrupted, revealing the catalytic subunit and the ATP-binding pocket. Phosphorylation and activation of FLT3 leads to the recruitment and subsequent phosphorylation of cytoplasmic adaptor proteins, which in turn promote intracellular signal transduction through effector proteins (Stirewalt and Radich, 2003). Several studies have reported a more detailed picture of the downstream signaling cascade through the expression of chimeric FLT3 receptors and the native FLT3 protein *in vitro*. Specific tyrosine residues act as docking sites for adaptor proteins, such as GBR2 (Growth factor receptor-bound protein 2), SHC (SH2-containing sequence proteins), SHIP (SH2-containing inositol 5'-phosphatase), SHP2 (protein tyrosine phosphatase), c-Cbl (proto-oncogene) and GAB2 (GRB2-associated-binding protein 2) (Zhao et al., 2000, Naoe et al., 2001; Tse et al., 2001; Levis et al., 2002; Levis et al., 2006). Phosphorylation of these adaptor proteins results in the activation of both, the phosphatidylinositol 3-kinase (PI3K)/AKT signaling cascade, which is involved in cell metabolism and cell cycle progression, and the mitogen-

activated protein kinase (MAPK) signaling cascade that regulates cell survival and proliferation (Dosil et al., 1993; Casteran et al., 1994; Rottapel et al., 1994; Lavagna-Sevenier et al., 1998; Zhang and Broxmeyer, 2000). Both signaling pathways also regulate and prevent apoptosis through members of the B-cell lymphoma 2 (Bcl-2) family, including pro-apoptotic (Bad and Bax) and anti-apoptotic (Bcl-2 and Bcl-x$_L$) proteins (Lisovsky et al., 1996; Chang et al., 2003a; Chang et al., 2003b). Moreover, the PI3K/AKT signaling pathway inhibits the expression of pro-apoptotic proteins through the phosphorylation and inactivation of FOXO (Forkhead box O) transcription factors (Chang et al., 2003a). To ensure a proper physiological response, inactivation of the FLT3 receptor is modulated by protein tyrosine phosphatases (PTP), such as DEP-1 and STS1/STS2, as well as the c-Cbl protein, which induces FLT3 ubiquitination and subsequent degradation (Sargin et al., 2007; Arora et al., 2011; Oshikawa et al., 2011; Böhmer et al., 2013; Zhang et al., 2015). Overall, FLT3 signaling regulates cellular proliferation, survival and apoptosis (Turner et al., 1996; Shurin et al., 1998; Parcells et al., 2006; Chan, 2011) (Figure 5).

Apoptosis   Survival and/or proliferation
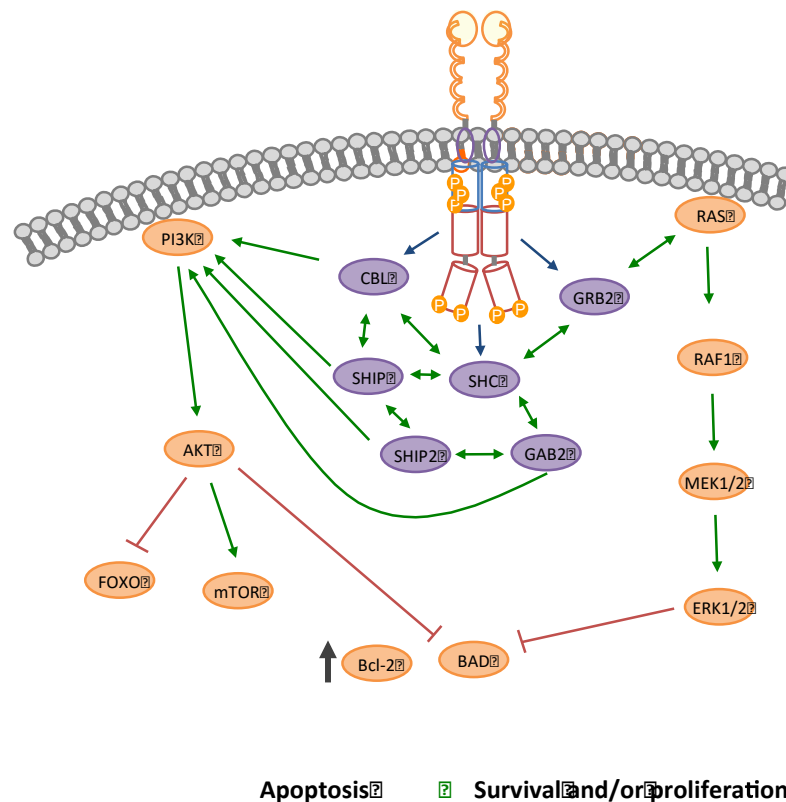
Figure 5. Schematic model of signaling pathways downstream the FLT3 receptor tyrosine kinase. Upon binding to the ligand, FLT3 receptor homodimerization triggers the activation of PI3K/AKT and MAPK signaling pathways (orange) through different adaptor proteins (purple), supporting survival, proliferation and inhibition of apoptosis. Blue arrows point to adaptor proteins that directly bind to FLT3, green arrows represent signaling cascades, and red arrows represent inhibitory pathways (Adapted from Stirewalt and Radich, 2003; Swords et al., 2012).

1.4. FLT3 receptor in acute myeloid leukemia

As mentioned above, FLT3 signaling plays a crucial role in hematopoietic development, controlling important cellular functions like proliferation and apoptosis, and thus a deregulated function of the kinase disrupts the cellular homeostasis and is involved in leukemogenesis (Levis et al., 2005). As one of the most commonly mutated genes in AML, somatic mutations within the receptor tyrosine kinase occur in 30-40% of newly diagnosed patients with a higher incidence in CN-AML (Yokota et al., 1997; Patel et al., 2012). Although several mutations have been identified in AML patients, two main gain-of-function aberrations are known to induce a constitutive activation of FLT3 promoting growth-factor independent proliferation and apoptosis resistance: internal tandem duplications (ITD) and point mutations (Gilliland and Griffin, 2002a; Fröhling et al., 2007).

Internal tandem duplications have been an object of research since 1996, when they were first identified in AML patients (Nakao et al., 1996; Kiyoi et al., 1998). As the most frequent FLT3 aberration, the prevalence rate in AML is about 25-30%. However, these duplications are also found at much lower frequencies in related diseases, such as myelodysplastic syndrome (MDS) and acute lymphocytic leukemia (ALL) (Yokota et al., 1997). An ITD results from the duplication of a fragment of the coding sequence and its insertion in a direct head-to-tail orientation (Stirewalt and Radich, 2003). The length of the duplication varies from 3 base pairs (bp) to more than 400 bp, and the insertion is always in-frame with the possible addition of nucleotides at the ITD junction in order to preserve the original reading frame (Schnittger et al., 2002; Kayser et al., 2009). The underlying mechanism involved in the formation of ITDs remains unknown, however Kiyoi and colleagues suggested that the DNA sequence corresponding to codon 593 and 602 potentially forms a palindromic intermediate that might lead to DNA-replication error and duplication (Kiyoi et al., 1998). The second most common mutation is a missense point mutation that occurs in 5-10% of AML cases but also, at lower frequencies, in MDS and ALL patients. Point mutations are mainly found within the activation loop (FLT3-AL) at the second tyrosine domain (e.g., D835Y, N676K) (Abu-Duhier et al., 2001; Yamamoto et al., 2001; Gilliland and Griffin, 2002b; Meshinchi and Appelbaum, 2009; Huang et al., 2016).

As mentioned earlier, a key issue in the field is the identification of molecular drivers that lead to leukemic transformation. In this context, several findings have provided substantial evidence that FLT3-ITD may be considered as a driver mutation. FLT3-ITD mutations provide human and murine HSPCs with enhanced proliferation and survival potential that gives advantage to cell fitness (Lee et al., 2007; Li et al., 2007). Moreover, FLT3-ITD knock-in mice

develop a myeloproliferative disorder and only require an additional genetic aberration, such as NUP98-HOXD13 or TET2, to induce a complete AML phenotype (Schessl et al., 2005; Lee et al., 2007; Li et al., 2008; Greenblatt et al., 2012; Zorko et al., 2012; Shih et al., 2015). Xenotransplantation experiments have also shown that FLT3-ITD mutations are present in the engrafting cells, implying that FLT3-ITD occurs at the level of the leukemic clone (Levis et al., 2005; Cheung et al., 2010). Moreover, a large majority of FLT3-ITD positive AML patients (>80%) present the mutation both at diagnosis and relapse, suggesting that ITDs are somatic mutations implicated in disease development (Kottaridis et al., 2002; Wakita et al., 2013; Garg et al., 2015; Madan et al., 2016). In addition, recently published data on the clonal evolution of AML patients harboring FLT3-ITD mutations has suggested aberrations in the *FLT3* gene as secondary genetic events. While several leukemia-associated mutations, such as TET2 or NPM1, were already found in residual hematopoietic stem cells (pre-leukemic clones), FLT3-ITD mutations were exclusively present in AML cells (Jan et al., 2012). Furthermore, FLT3-ITD mutations are considered to be an important genetic event in the progression of myelodysplasias towards secondary acute myeloid leukemia (Shih et al., 2004; Takahashi et al., 2013; Badar et al., 2015; Meggendorfer et al., 2015). Nevertheless, the real contribution of FLT3-ITD as driver mutation has also been questioned due to the lack of significant activity of several FLT3-targeting drugs in clinical studies. The failure to eradicate leukemic cells harboring FLT3 mutations suggested that these genetic aberrations are merely passenger mutations (Testa and Pelosi, 2013). However, recent studies have demonstrated the effectiveness of other inhibitors and the development of resistance at the level of the kinase domain during relapse, reinforcing the role of activating FLT3 aberrations as recurrent driver mutations in leukemogenesis (Man et al., 2012; Pauwels et al., 2012; Smith et al., 2012a).

1.4.1. FLT3-ITD-mediated transformation

The insertion of genetic material into the *FLT3* sequence leads to a disruption of the auto-inhibitory conformation while promoting a constitutive activation of the kinase in the absence of endogenous ligand (Schlessinger, 2003; Griffith et al., 2004). Structural changes seem to destabilize the orientation of the cytoplasmic region substantially enough to place important tyrosine sites toward the catalytic site, resulting in the *cis*-phosphorylation of the receptor (Rocnik et al., 2006; Toffalini and Demoulin, 2010; Chan, 2011). Consequently, constitutive auto-phosphorylation of FLT3 leads to increased proliferation and cell survival through the activation of downstream signaling pathways such as PI3K/AKT and MAPK as well as the JAK/STAT pathway. Although activation of STAT5 is not involved in wild-type FLT3 signaling, it

plays a crucial role in FLT3-ITD-mediated transformation (Mizuki et al., 2000; Zhang et al., 2000; Birkenkamp et al., 2001; Kiyoi et al., 2002; Spiekermann et al., 2003; Brandts et al., 2005; Rocnik et al., 2006; Nabinger et al., 2013; Arreba-Tutusaus et al., 2016). Several studies have demonstrated growth-factor independent proliferation and block of differentiation in murine cell lines transduced with FLT3-ITD mutations as well as in human leukemia cell lines harboring ITDs (Hayakawa et al., 2000; Mizuki et al., 2000; Kiyoi et al., 2002; Zheng and Small, 2005). Besides hyperproliferation, constitutive activation of the receptor tyrosine kinase FLT3 also mediates an anti-apoptotic response via phosphorylation of the pro-apoptotic protein Bad and concomitant release of the anti-apoptotic proteins Bcl-2 and Bcl-x$_L$, up-regulation of the anti-apoptotic protein Mcl-1 and phosphorylation of the Foxo3 protein, which prevents up-regulation of the pro-apoptotic protein Bim (Scheijen et al., 2004; Yang et al., 2005; Kim et al., 2006; Irish et al., 2007; Nordigarden et al., 2009; Yoshimoto et al., 2009; Zhou et al., 2011). Further *in vitro* studies using FLT3-ITD mutated cells have reported the repression of genes involved in myeloid differentiation, such as RGS2 (regulator of G-protein signaling 2), C/EBPA (CCAAT/enhancer-binding protein alpha) and the transcription factor PU.1 (Mizuki et al., 2003; Schwable et al., 2005; Radomska et al., 2006). In fact, gene-expression analyses in cultured cells and clinical samples have revealed more than 700 genes associated with FLT3-ITD activation, proving a broad range of cellular functions that may be relevant in FLT3-ITD-mediated transformation (Mizuki et al., 2003; Neben et al., 2005; Bullinger et al., 2008; Caldarelli et al., 2013). For instance, FLT3-ITD mutations are known to enhance the expression of proteins involved in the Wnt signaling pathway, including the receptor Frizzled 4, the beta-actin protein and the target gene c-myc (Tickenbrock et al., 2005). Furthermore, FLT3-ITD mutations are known to increase the production of reactive oxygen species (ROS) and enhance oxidative stress associated to DNA damage. Thus, FLT3-ITD mutations lead to high levels of double strand breaks (DSB) and aberrant DNA repair though homologous recombination (HR) and non-homologus end-joining (NHEJ) pathways (Gaymes et al., 2002; Sallmyr et al., 2008a; Fan et al., 2010; Woolley et al., 2012; Hole et al., 2013; Stanicka et al., 2015). High levels of ROS production also lead to oxidation and inactivation of the tyrosine phosphatase DEP-1 protein involved in FLT3 inactivation (Godfrey et al., 2012; Jayavelu et al., 2016).

1.4.2. Murine models to investigate the oncogenic potential of FLT3 mutations

In vivo animal models are essential to address specific experimental questions that remain unanswered using exclusively *in vitro* approaches. In particular, murine models represent an excellent organism to study human AML owing to molecular, cellular and developmental

similarities between species (McCormack et al., 2005; Fortier and Graubert, 2010). Two main models are commonly used to investigate recurrent genetic aberrations in AML development. First, the murine bone marrow transplantation (BMT) model is based on the retroviral transduction of an oncogene of interest in primary murine hematopoietic cells followed by their transplantation in lethally irradiated recipient mice. Generally, the retroviral vector incorporates a reporter gene (e.g., GFP) to determine transduction efficiency, to select transduced cells and/or to track transformed cells after transplant (Persons et al., 1997; Fortier and Graubert, 2010). The stable expression of FLT3-ITD mutations in murine bone marrow cells results in a fatal myeloproliferative-like disorder characterized by an increased white blood cell (WBC) count (leukocytosis) and spleen enlargement produced by extramedullary infiltration (splenomegaly) (Kelly et al., 2002; Grundler et al., 2005). In contrast, a FLT3 point mutation (i.e., D835Y) develops a lymphoid-like disorder with a lower disease penetrance (Grundler et al., 2005). Here, the strain background seems to be decisive in the transformation process since FLT3-ITD mutations exclusively develop a lethal hematopoietic disorder in BALB/c and not in C57BL/6 mice (Kim et al., 2008). Inbred BALB/c mice are known to harbor hypomorphic alleles of the tumor suppressor gene Cdkn2a resulting in a reduce activity of the cyclin-dependent kinase inhibitor protein p16INK4a and a defective ability to inhibit retinoblastoma (Rb) phosphorylation, which may increase the susceptibility to develop a proliferative-like disorder (Zhang et al., 1998; Mori, 2010). Second, the generation of genetically engineered mouse models has also been an important tool to investigate human AML. These models allow a regulated expression of a gene of interest with a stable transmission to the offspring (Fortier and Graubert, 2010). FLT3-ITD murine transgenic and knock-in models recapitulate a myeloproliferative-like phenotype but with a six to eleven times longer period of latency when compared to BMT models. The first human FLT3-ITD transgenic mice, generated by Lee and colleagues in 2005, were driven by the exogenous *vav* promoter that controls transgene expression broadly throughout the entire hematopoietic compartment (Lee et al., 2005). These mice mainly developed a myeloproliferative phenotype characterized by increased production of platelets (thrombocytosis), myeloid hyperplasia in the bone marrow and extramedullary hematopoiesis in the spleen but, unlike the BMT and the knock-in models, without leukocytosis. Additionally, two of seven founder mice developed clonal immature B- and T-lymphoid diseases. Besides the transgenic mice, two FLT3 knock-in models are currently available, both engineered by the insertion of a human ITD into exon 14 of the murine *Flt3* locus (Lee et al., 2007; Li et al., 2008). Lee and colleagues generated a mouse harboring a 21 bp ITD (previously described by Kelly et al., 2002). Heterozygous and homozygous animals developed myeloproliferative disease characterized by dose-dependent myeloid hyperplasia,

leukocytosis and splenomegaly. Moreover, FLT3-ITD conferred hematopoietic stem and progenitor cells with increased proliferation capacity and survival (Lee et al., 2007). Li and co-workers generated a knock-in model comprising an 18 bp ITD mutation. As a result, heterozygous animals developed a myeloproliferative phenotype comparable to the other knock-in model (Li et al., 2008). Further investigations on hemizygous animals revealed that loss of wild-type FLT3 contributes to myeloid expansion and development of a more severe phenotype (Li et al., 2008; Li et al., 2011). Moreover, both knock-in models could demonstrate that FLT3-ITD expression primed immature hematopoietic cells to enhanced myeloid expansion and decreased development into B-cells. In fact, FLT3-ITD-mediated overproliferation and disease development has been related to a deregulation in the quiescence and homeostasis of HSCs, which became rapidly depleted. (Chu et al., 2012). In contrast, knock-in of FLT3-AL (i.e., D835Y) induced a less aggressive myeloproliferative disease, in which HSC homeostasis remained unaffected (Chu et al., 2012; Bailey et al., 2013).

1.4.3. The clinical implications of FLT3-ITD mutations

From a clinical outlook, FLT3-ITD mutations are considered as a relevant prognostic factor and promising therapeutic target. Besides being one of the most frequent mutations in AML, FLT3-ITD mutations are more common in CN-AML patients and are associated with a higher incidence of relapse and poor overall survival (OS), which categorizes them as a powerful predictor of disease outcome (Kottaridis et al., 2001; Fröhling et al., 2002; Patel et al., 2012). However, there is a high heterogeneity among ITDs, which seems to influence its prognostic significance and the clinical outcome of FLT3-ITD positive AML patients. Features like loss of wild-type FLT3 by copy-neutral loss of heterozygosity (CN-LOH) and FLT3-ITD high allelic burden, which implicates a threshold of >0.50, have been associated with an unfavorable outcome (Whitman et al., 2001; Thiede et al., 2002; Kayser et al., 2009; Kharazi et al., 2011; Schnittger et al., 2012; Linch et al., 2014). In addition, recently published data has suggested the allelic ratio as useful predictive marker in the selection of consolidation therapy. Allogeneic stem-cell transplantation after remission therapy seems to be beneficial to reduce relapse risk in patients with high allelic ratio (Brunet et al., 2012; Laboure et al., 2012; Schlenk et al., 2014). In a more controversial way, the length of the duplicated fragment may also be prognostically relevant. Stirewalt et al. and, more recently, Kim et al. have stated that longer ITD mutations correlate with a decreased OS in FLT3-ITD AML patients, while other studies have reported that ITD length has no impact on clinical outcome (Ponziani et al., 2006; Stirewalt et al., 2006; Schnittger et al., 2012; Kim et al., 2015).

Given the impact of FLT3-ITD mutations on disease development and prognosis, there is a tremendous interest in developing FLT3-targeted therapies (Kayser and Levis, 2014). Over the past decade, several small molecules have been reported as tyrosine kinase inhibitors (TKI). The majority of these molecules are heterocyclic inhibitors that block the binding of ATP to the active site in a competitive fashion and, therefore, prevent auto-phosphorylation and concomitant activation of downstream pathways (Gilliland and Griffin, 2002b; Shawver et al., 2002). However, none of these inhibitors has received so far a complete approval for clinical use (Konig and Levis, 2015). First generation inhibitors - e.g., Midostaurin (PKC412) or Sorafenib (BAY 43-9006) - target a wide spectrum of kinases including FLT3-ITD and FLT3-AL mutations. Although these compounds have shown a promising effect in preclinical studies, early clinical trials have reported in many cases poor pharmacokinetic and long-term efficacy under monotherapy, leading to the emergence of resistance (Weisberg et al., 2002; Stone et al., 2004; Stone et al., 2005; Heidel et al., 2006; Levis et al., 2006; Fischer et al., 2010; Stölzel et al., 2010; Konig and Levis, 2015). Ongoing trials are investigating the combination of these inhibitors with conventional chemotherapy or other targeted treatments in order to improve the therapeutic outcome (Knapper et al., 2006; Kiyoi, 2015a). Recently, the SORAML trial and the global phase III CALGB 10603/RATIFY trial (Abstract #6, ASH annual meeting 2015) have reported beneficial results in the addition of Sorafenib (SORAML) and Midostaurin (RATIFY) to standard chemotherapy (Röllig et al., 2015; Stone et al, 2015). Second generation inhibitors - e.g., Quizartinib (AC220) or KW-2449 - exhibit a higher selectivity and sensitivity against activating FLT3 mutations (Chao et al., 2009; Zarrinkar et al., 2009). For instance, AC220 has demonstrated a strong potency, safety and long effective half-life in early clinical trials, reaching phase III trials (Wander et al., 2014; Konig and Levis, 2015).

In most cases, the failure observed in clinical trials involves resistance mechanisms, which are commonly classified into primary and secondary resistance (Kindler et al., 2010; Smith and Shah, 2012). Primary or inherent resistance prevails in approximately 30% of FLT3-mutated AML patients and includes the activation of compensatory pathways, a lower potency against leukemic cells or a differential sensitivity to TKIs among the FLT3 mutations (Clark et al., 2004; Knapper et al., 2006; Mead et al., 2008; Breitenbuecher et al., 2009a; Damdinsuren et al., 2015; Kiyoi, 2015b). Secondary resistance develops either due to acquisition of additional mutations within the targeted kinase, auto- or paracrine effects, overexpression of FLT3 or the acquisition of additional mutations in FLT3-independent signaling pathways (Weisberg et al., 2002; Bagrintseva et al., 2004; Cools et al., 2004; Heidel et al., 2006; Furuichi et al., 2007; Bubnoff et al., 2009; Zhou et al., 2009; Stölzel et al., 2010; Sato et al., 2011; Smith et al.,

2012b). Nowadays, the identification of cellular mechanisms deregulated by FLT3 mutations is crucial to better understand the disease biology and to overcome resistance (Mehta et al., 2013; Onishi et al., 2015; Hirade et al., 2016).

1.5. Novel location sites of ITD mutations within the tyrosine kinase domain 1

For many years, it has been assumed that location of ITD mutations occurs exclusively within the JMD of the receptor tyrosine kinase. However, sequencing analysis of FLT3-ITD mutated AMLs revealed that almost one third of FLT3-ITD mutations are located within the TKD1 region (Breitenbuecher et al., 2009b; Kayser et al., 2009; Schnittger et al., 2012). A summary of the distinct regions harboring ITD mutations is illustrated in Figure 6.
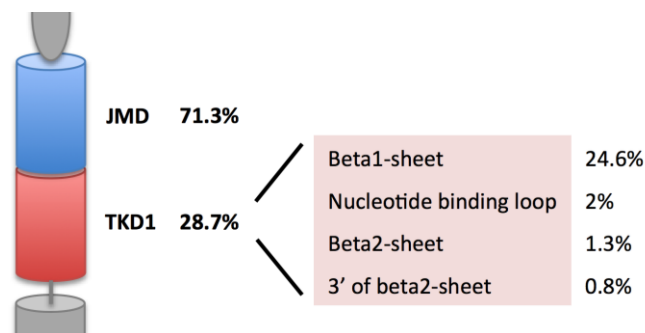
Figure 6. Summary of ITD integration sites. The localization of FLT3-ITD mutations was analyzed in 753 FLT3-ITD positive AML patients. Although a higher percentage of FLT3-ITDs was localized within the JMD (71.3%), a significant number of ITDs was located in the TKD1 (28.7%) including the ß1-sheet with the highest frequency (24.6%), the nucleotide binding loop (2%), the ß2-sheet (1.3%) and 3' ß2-sheet regions (0,8%) (Adapted from Breitenbuecher et al., 2009b).

On the basis of this important observation, retrospective studies have evaluated the clinical impact of this novel location in FLT3-ITD positive AML patients after remission and post-remission therapy. As a result, ITD mutations located within the TKD1 (TKD1-ITD) could be identified as an unfavorable prognostic factor: patients harboring TKD1-ITD mutations showed a worse clinical outcome with a reduction in CR, relapse-free survival and OS when compared to JMD-located ITDs (Kayser et al., 2009; Schlenk et al., 2014) (Figure 7A). Of note, location of the ITD mutation had stronger influence on clinical outcome than other features like size of the duplication or allelic burden. Moreover, a correlation between the ITD length and the functional regions was found with longer ITDs inserted into the more C-terminal region. A closer look at the duplicated sequences showed that 96.1% of the ITDs contained at least one of the specific tyrosine residues included at the ends of the sequence (Tyr591-Tyr599): **Y**VDFREYE**Y** (Kayser et al., 2009) (Figure 7B). In order to characterize the functional biology of

this novel group of ITD mutations, Breitenbuecher and colleagues characterized for the first time a prototype FLT3-ITD mutation located within the TKD2 region (ITDA627E). Murine 32D cells transfected with the ITDA627E showed a constitutive auto-phosphorylation of the FLT3 receptor and activation of the downstream signaling effector STAT5. Transplantation of these cells into syngeneic mice induced a lethal myeloproliferative disease, suggesting a transforming potential of non-JMD FLT3-ITD mutations (Breitenbuecher et al., 2009b). Interestingly, this particular mutation also revealed a primary resistance mechanism against TKIs through the up-regulation of the anti-apoptotic protein Mcl-1 (Breitenbuecher et al., 2009a). This data suggests that TKD-ITD mutations confer a constitutive activation of the FLT3 receptor comparable to *standard* JMD-ITD mutations but with a distinct sensitivity to TKIs. More recently, our group has investigated the functional biology of single FLT3-ITD mutations derived from JMD- and TKD1-ITD positive patients using *in vitro* experimental approaches. We have analyzed the sensitivity of different FLT3-ITD mutations to TKIs in regard to the ITD location (JMD vs. TKD1) (Ballaschk, Dissertation, 2014; Mack, Dissertation, 2014). When compared to JMD-ITDs, TKD1-ITDs revealed a similar signaling phenotype and transforming potential in two different murine hematopoietic cell lines (Ba/F3 and 32D). However, a distinct response to standard TKIs (AC220 and PKC412) was observed between JMD-ITDs and TKD1-ITDs. Upon TKI treatment, TKD1-ITD transduced cells showed primary resistance characterized by decreased cell death when compared to JMD-ITDs. Thus, despite the comparable transforming capacity between both ITD groups *in vitro*, these data suggests that the ITD location might influence the sensitivity of FLT3-ITD mutations to TKIs.
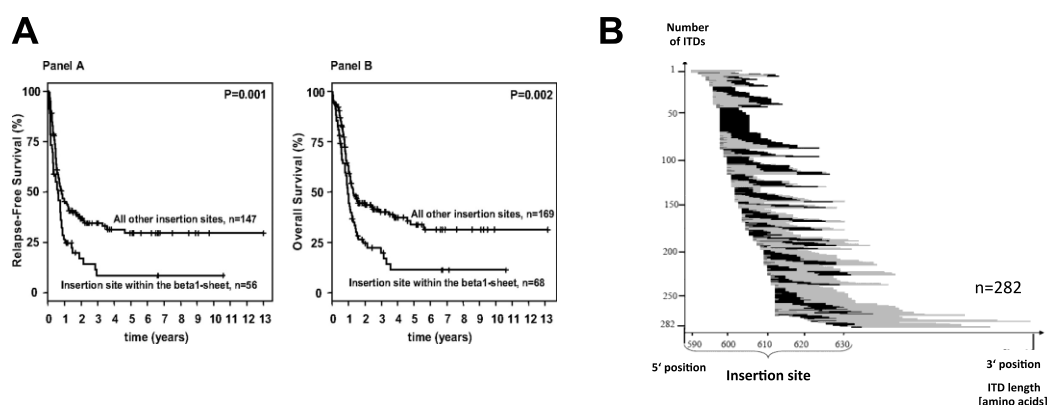
Figure 7. Influence of ITD insertion site on the clinical outcome of FLT3-ITD positive AML patients. The localization of FLT3-ITD mutations was analyzed in 241 patients. **A)** Relapse-free survival (Panel A) and overall survival (Panel B) analysis of chemotherapy treated FLT3-ITD positive AML patients according to the ITD location. Patients harboring TKD1-ITD mutations (ß1-sheet) showed worse outcome when compared to all other insertion sites. **B)** Representation of each ITD insertion site shows a correlation between ITD length and region of insertion that longer ITD mutations localized more c-terminal. Duplication of the motif Tyr591-Tyr599 is highlighted in black (Figures from Kayser et al., 2009)

2. Aims of the project

Recent studies have defined a molecular subset of FLT3-ITD mutations (TKD1-ITD) as an unfavorable prognostic factor for achievement of complete remission and overall survival independently of other features such as allelic ratio. Furthermore, previous work in our group showed that one specific non-JMD mutation conferred decreased sensitivity to kinase inhibitor therapy *in vitro* (Breitenbuecher et al., 2009a). The purpose of this dissertation was to characterize the biological properties, the sensitivity to FLT3-targeted therapy and the functional consequences of multiple FLT3-ITD mutations depending on their location site (JMD vs. TKD1) *in vitro* and *in vivo.*

This work has been organized in three main aspects:

a. Functional characterization of novel FLT3-ITD mutations *in vitro:* The first section in this thesis expands the characterization of FLT3-ITD mutations *in vitro*. Two novel FLT3-ITD mutations were isolated from FLT3-ITD positive AML patients and characterized accordingly*.* Their transforming potential and sensitivity to specific FLT3 inhibitors was investigated and compared to previously studied mutations. The goal of this section was to provide solid evidence for the divergence in FLT3-ITD mutations in regard to the ITD location (JMD vs. TKD1).

b. Functional characterization of FLT3-ITD mutations *in vivo:* In the second part of this project, I investigated the oncogenic potential of several FLT3-ITD mutations (JMD-ITD and TKD1-ITD) *in vivo.* A bone marrow transplantation model was chosen to examine the biological properties of FLT3-ITD mutations depending on their location (JMD vs. TKD1). Moreover, sensitivity to the FLT3-TKI PKC412 was tested *in vivo* comparing JMD-ITD and TKD1-ITD transforming mutations.

c. Assess for mechanistic consequences of distinct ITD-location: The third section provides first evidence of mechanisms involved in the biological divergence between activating FLT3 mutations. Gene expression data was used to identify potential pathways deregulated in TKD1-ITDs compared to JMD-ITD mutations. Here, DNA damage and repair pathways were identified to be deregulated and thus were investigated in murine cell lines harboring either JMD-ITD or TKD1-ITD mutations.

3. Materials

3.1. Organisms

3.1.1. Bacteria

Table 1. List of bacteria strains used in this work, genotype and company.

Strain	Genotype	Company
TOP10	F- mcrA Δ(mrr-hsdRMS-mcrBC) φ80lacZΔM15 ΔlacX74 recA1 araD139 Δ(ara-leu)7697 galU galK rpsL (StrR) endA1 nupG	Invitrogen™, Carlsbad, CA, USA
Stellar	F–, endA1, supE44, thi-1, recA1, relA1, gyrA96, phoA, Φ80d lacZΔ M15, Δ (lacZYA - argF) U169, Δ (mrr - hsdRMS - mcrBC), ΔmcrA, λ–	Clonetech Laboratories, Mountain View, CA, USA

3.1.2. Cell lines

Table 2. List of cell lines used in this work, origin, and company.

Cell line	Origin	Company
Ba/F3 parental	Murine pre-B cell	(ACC 300) DSMZ Braunschweig, Germany
32D parental	Murine bone marrow cell	(ACC 441) DSMZ Braunschweig, Germany
WEHI 3B	Murine myelomonocytic leukemia cell	(ACC 26) DSMZ Braunschweig, Germany
Phoenix	Human embryonic kidney fibroblasts (293T)	(CRL-3215) ATCC Manassas, VA, USA

Table 3. List of cell lines generated in this work.

Cell line	Description
Ba/F3 FLT3_ITD598/599(12) PIG	Murine pre-B cell with stable expression of ITD598/599(12) PIG
Ba/F3 FLT3_ITD598/599(22) PIG	Murine pre-B cell with stable expression of ITD598/599(22) PIG
Ba/F3 FLT3_ITDK602R(7) PIG	Murine pre-B cell with stable expression of ITDK602R(7) PIG
Ba/F3 FLT3_ITDL601H(10) PIG	Murine pre-B cell with stable expression of ITDL601H(10) PIG

19

Cell line	Description
Ba/F3 FLT3_ITDFV605YF(14) PIG	Murine pre-B cell with stable expression of ITDFV605YF(14) PIG
Ba/F3 FLT3_ ITDE611V(32) PIG	Murine pre-B cell with stable expression of ITDE611V(32) PIG
Ba/F3 FLT3_ITDG613E(33) PIG	Murine pre-B cell with stable expression of ITDG613E(33) PIG
32D FLT3_ITD598/599(12) PIG	Murine bone marrow cells with stable expression of ITD598/599(12) PIG
32D FLT3_ITD598/599(22) PIG	Murine bone marrow cells with stable expression of ITD598/599(22) PIG
32D FLT3_ITDK602R(7) PIG	Murine bone marrow cells with stable expression of ITDK602R(7) PIG
32D FLT3_ITDL601H(10) PIG	Murine bone marrow cells with stable expression of ITDL601H(10) PIG
32D FLT3_ITDFV605YF(14) PIG	Murine bone marrow cells with stable expression of ITDFV605YF(14) PIG
32D FLT3_ ITDE611V(32) PIG	Murine bone marrow cells with stable expression of ITDE611V(32) PIG
32D FLT3_ITDG613E(33) PIG	Murine bone marrow cells with stable expression of ITDG613E(33) PIG
Ba/F3 FLT3_ITD598/599(12) YFP	Murine pre-B cell with stable expression of ITD598/599(12) YFP
Ba/F3 FLT3_ITDK602R(7) YFP	Murine pre-B cell with stable expression of ITDK602R(7) YFP
Ba/F3 FLT3_ ITDE611V(32) YFP	Murine pre-B cell with stable expression of ITDE611V(32) YFP

3.1.3. Mouse models

Table 4. List of mouse strains used in this work, type and origin.

Strain	Type	Company
BALB/cByJRj	Inbred mouse	Janvier Labs, Saint Berthevin Cedex, France

3.2. Plasmids

Table 5. List of plasmids used in this work, description and origin.

Plasmid (size in kb)	Description	Origin
FLT3_WT pAL (~9.5)	Moloney Murine Sarcoma Virus (MoMSV) retroviral expression system; expresses wild-type FLT3	Mizuki et al., 2000
FLT3_ITD598/599(12) pAL (~9.5)	Moloney Murine Sarcoma Virus (MoMSV) retroviral expression system; expresses FLT3_ITD598/599(12)	Mizuki et al., 2000
FLT3_ITD598/599(22) pMSCV (~9)	Murine Stem Cell Virus (MSCV) retroviral expression system; puromycin as selection marker; expresses FLT3_ITD598/599(22)	Armstrong Lab, MSKCC, New York, NY; USA
FLT3_ITDK602R(7) pMSCV (~9)	Murine Stem Cell Virus (MSCV) retroviral expression system; puromycin as selection marker; expresses FLT3_ITDK602R(7)	Armstrong Lab, MSKCC, New York, NY, USA
FLT3_ITDE611V(32) pAL (~9.5)	Moloney Murine Leukemia Virus (MoMuLV) retroviral expression system; expresses FLT3_ITDE611V(32)	Mack, Dissertation, 2014
FLT3_ITDG613E(33) pAL (~9.5)	Moloney Murine Leukemia Virus (MoMuLV) retroviral expression system; expresses FLT3_ITDG613E(33)	Mack, Dissertation, 2014
pMSCV PIG (~7.6)	Murine Stem Cell Virus (MSCV) retroviral expression system; puromycin as selection marker; green fluorescent protein (GFP) as reporter gene	#21654 Addgene, Cambridge, MA, USA
pMSCV MIY (~6.5)	Murine Stem Cell Virus (MSCV) retroviral expression system; yellow fluorescent protein (YFP) as reporter gene	Armstrong Lab, MSKCC, New York, NY, USA
FLT3_ITDE611V(32) pMSCV MIY (~9.5)	Murine Stem Cell Virus (MSCV) retroviral expression system; YFP as reporter gene; expresses FLT3_ITDE611V(32)	Armstrong Lab, MSKCC, New York, USA
K73 Eco envelope (~9.7)	Murine Leukemia Virus (MLV) expression system; expresses ecotropic envelope protein	Armstrong Lab, MSKCC, New York, NY, USA
M57DAW gag-pol (~8.1)	Murine Leukemia Virus (MLV) expression system; expresses gag-pol protein	Armstrong Lab, MSKCC, New York, NY, USA

Table 6. List of plasmids generated in this work, description and origin.

Plasmid (size in kb)	Description	Origin
FLT3_ITD598/599(12) pMSCV PIG (~10.6)	Murine Stem Cell Virus (MSCV) retroviral expression system; puromycin as selection marker; GFP as reporter gene; expresses FLT3_ITD598/599(12)	Generated in this work in collaboration with Mack, Dissertation, 2014
FLT3_ITD598/599(22) pMSCV PIG (~10.6)	Murine Stem Cell Virus (MSCV) retroviral expression system; puromycin as selection marker; GFP as reporter gene; expresses FLT3_ITD598/599(22)	
FLT3_ITDK602R(7) pMSCV PIG (~10.6)	Murine Stem Cell virus (MSCV) retroviral expression system; puromycin as selection marker; GFP as reporter gene; expresses FLT3_ ITDK602R(7)	
FLT3_ITDE611V(32) pMSCV PIG (~10.6)	Murine Stem Cell virus (MSCV) retroviral expression system; puromycin as selection marker; GFP as reporter gene; expresses FLT3_ITDE611V(32)	
FLT3_ITDG613E(33) pMSCV PIG (~10.6)	Murine Stem Cell virus (MSCV) retroviral expression system; puromycin as selection marker; GFP as reporter gene; expresses FLT3_ITDG613E(33)	
FLT3_ITDL601H(10) pMSCV PIG (~10.6)	Murine Stem Cell virus (MSCV) retroviral expression system; puromycin as selection marker; GFP as reporter gene; expresses FLT3_ ITDL601H(10)	Generated in this work
FLT3_ITDFV605YF(14) pMSCV PIG (~10.6)	Murine Stem Cell virus (MSCV) retroviral expression system; puromycin as selection marker; GFP as reporter gene; expresses FLT3_ITDFV605YF(14)	
FLT3_ITD598/599(12) pMSCV YFP (~9.5)	Murine Stem Cell virus (MSCV) retroviral expression system; YFP as reporter gene; expresses FLT3_ ITD598/599(12)	
FLT3_ITDK602R(7) pMSCV YFP (~9.5)	Murine Stem Cell virus (MSCV) retroviral expression system; YFP as reporter gene; expresses FLT3_ ITDK602R(7)	
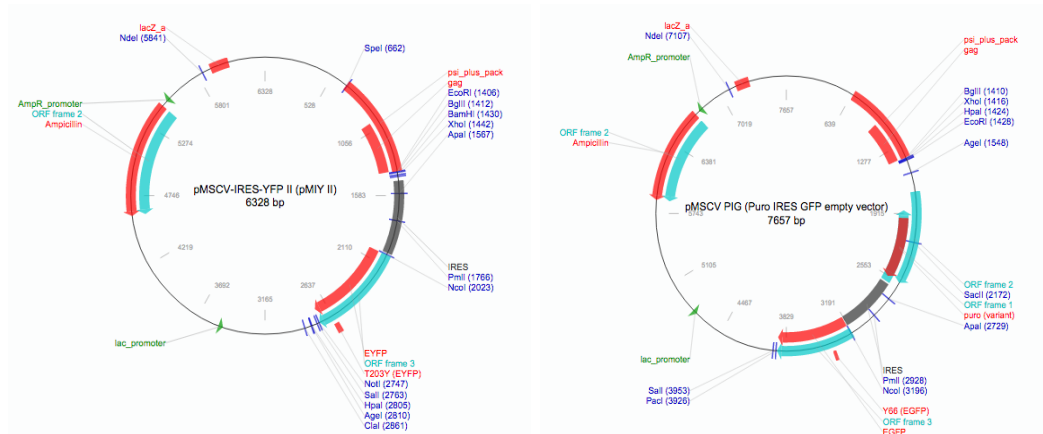
Figure 8. Vector backbone of plasmids used in this work. pMSCV_MIY (MSCV IRES YFP) (left); pMSCV_PIG (Puro IRES GFP) (right).

3.3. Oligonucleotides

Table 7. List of oligonucleotides used in this work, sequence and size.

Oligoname	Sequence (5'→3')	Size (bp)
Seq_FLT3_For1	aaattagggaaggatggccg	20
Seq_FLT3_For2	ctgagatttgatccgagtcc	20
Seq_FLT3_For3	tctctttcagagctgtctgc	20
Seq_FLT3_For4	gtgccaagggaattgtatgc	20
Seq_FLT3_For5	tgaacacttcttccaggtcc	20
Seq_FLT3_Rev1	atctgcttccatcacactgc	20
Seq_FLT3_Rev2	aactcctcagaccacattgc	20
Seq_FLT3_Rev3	gtgctgtgcatacaattccc	20
Seq_FLT3_Rev4	actcaagatgatgacccagc	20
Seq_FLT3_Rev5	ataatgcaatcctgctgggc	20
MSCV_PIG_for	cccttgaacctcctcgttcgacc	23
MSCV_PIG_rev	cagcggggctgctaaagcgcatgc	24
Itdfw_pig_bgl2	cgccggaattcgctctcatgccggcgttggcgcgcgac	38
Itdre_pig_xho	attcgttaacctcgagctacgaatcttcgacctgagc	37
Itdfw_mig_eco	ctaggcgccggaattccatgccggcgttggcgcgcgac	38
Itdre_mig_xho	tcgagttttтctcgagctacgaatcttcgacctgagc	37
FLT3_fow (diagnosis)	gcaatttaggtatgaaagccagc	23
FLT3_rev (diagnosis)	cttтcagcattтtgacggcaacc	23

3.4. Antibodies

3.4.1. Flow cytometry antibodies

Table 8. List of flow antibodies used in this work, available fluorochrome(s), clone and company.

Antibody	Fluorochrome(s)	Clone	Company
Mac-1 (CD11b)	PB; APC/Cy7	M1/70	BioLegend®, San Diego, CA, USA
Gr-1 (Ly-4G/Ly-6C)	PerCP/Cy5.5; PB; APC	RB6-8C5	BioLegend®, San Diego, CA USA
CD3	APC/Cy7	17A2	BioLegend®, San Diego, CA, USA
CD8	PerCP/Cy5.5; PE/Cy7	53-6.7	BioLegend®, San Diego, CA, USA
B220 (CD45R)	APC	RA3-6B2	BioLegend®, San Diego, CA, USA
PI	Channel PE	-	Sigma-Aldrich®, St Louis, MO, USA
Sytox® Blue Dead Cell Stain	Channel PB	-	Invitrogen™, Carlsbad, CA, USA

3.4.2. Western Blot antibodies

Table 9. List of antibodies used in this work, epitope, size, dilution factor and company.

Antibody	Epitope	Size [kDa]	Dilution	Company
Anti-phospho FLT3	Tyr591	130, 160	1:1000	Cell Signaling®, Danvers, MA, USA
Anti-FLT3	C-Terminus (C20)	130, 160	1:200	Santa-Cruz Biotechnology®, Dallas, TX, USA
Anti-phospho STAT5A/B	Tyr694/699	92, 94	1:1000	Merk Millipore
Anti-STAT5A	C-Terminus (L20)	92	1:100	Cell Signaling®, Danvers, MA, USA
Anti-phospho p44/p42 MAPK (Erk1/2)	Tyr202/Tyr204	42, 44	1:2000	Cell Signaling®, Danvers, MA, USA
Anti-p44/p42 MAPK (Erk1/2)	C-Terminus	42, 44	1:2000	Cell Signaling®, Danvers, MA, USA

Antibody	Epitope	Size [kDa]	Dilution	Company
Anti-GAPDH	Internal region	36	1:5000	Meridian Life Science®, Memphis, TN, USA
Anti-α-Mouse IgG-HRP	IgG	-	1:2000	Santa-Cruz Biotechnology®, Dallas, TX, USA
Anti-α-Rabbit IgG-HRP	IgG	-	1:2000	Cell Signaling®, Danvers, MA, USA

3.4.3. Immunocytochemistry antibodies

Table 10. List of antibodies used in this work, epitope, fluorochrome, dilution factor and company.

Antibody	Epitope	Fluorochrome	Dilution	Company
Anti-phospho H2A.X	Ser139	-	1:50	Cell Signaling®, Danvers, MA, USA
Anti-α-rabbit IgG-Cy3	F(ab') fragment	Cy3	1:100	Sigma-Aldrich®, St Louis, MO, USA
DAPI	-	PB (461nm)	20 µg/ml	Sigma-Aldrich®, St Louis, MO, USA

3.5. Chemicals and reaction kits

3.5.1. Chemicals

Table 11. List of chemicals used in this work, grouped by company.

Company	Product(s)
Bayer, Leverkusen, Germany	Ciprobay 400 mg, Xylazine (Rompun 2%)
Becton Dickinson (BD), Franklin Lakes, NJ, USA	Pharm Lysis Buffer
Baxter, Deerfield, IL, USA	Isoflurane
Carl Roth®, Karlsruhe, Germany	All other chemicals
Dako, Hamburg, Germany	Mounting Medium
Fischar®, Saarbrücken, Germany	Formalin 4.0%
GIBCO	Neomycin

Company	Product(s)
Gibco® by Life Technologies	DMEM + GlutaMAX™, DPBS (1x), Fetal Bovine Serum (FBS), IMDM + GlutaMAX™, L-glutamine, MEM Non-essential Amino Acids, Opti-MEM®, RPMI 1640, Sodium pyruvate, Penicillin-Streptomycin, 0,05% Trypsin-ETDA
Hoffmann-La Roche, Basel, Switzerland	cOmplete™ phosphatase Inhibitor cocktail, FuGENE® Transfection Reagent, PhosSTOP™ phosphatase inhibitor cocktail
InvivoGen, San Diego, CA, USA	Plasmocin
JTBaker®, Center Valley, PA, USA	Methanol
LC Laboratories, Woburn, MA, USA	Midostaurin (PKC412)
Merk Millipore, Billerica, MA, USA	Distilled water for molecular biology
New England Biolabs® (NEB), Ipswich, MA, USA	Restriction enzymes: BglII, EcoR HF, XhoI
Novartis, Basel, Switzerland	Midostaurin (PKC412), Quizartinib (AC220)
PanReac AppliChem, Darmstadt, Germany	Puromycin
PeproTech®, Rocky Hill, NJ, USA	Recombinant murine IL-3, IL-6, Stem Cell Factor (SCF), Thrombopoietin (TPO)
Pfizer, New York, NY, USA	Ketamine (Ketavet® 100 mg/ml)
Pharmacy, Magdeburg University	5-Fluorouracil
Selleckchem, Munich, Germany	Crenolanib (CP-868596)
Serva, Heidelberg, Germany	Tween® 20
Sigma-Aldrich®, St Louis, MO, USA	2-Mercaptoethanol, D-a-tocopheryl (VitE), EDTA, Trypan Blue Solution, May-Grünwald Stain, Giemsa stain modified
STEMCELL Technologies™, Vancouver, Canada	Methylcellulose MethoCult #3231
TAKARA Bio, Shiga, Japan	RetroNectin®

3.5.2. Reaction kits

Table 12. List of reaction kits used in this work.

Product	Company
Bio-Rad Protein Assay (Bradford)	BioRad, Hercules, CA, USA
CellTiter 96® Aqueous One Solution Proliferation Assay (MTS)	Promega, Fitchburg, WI, USA

Product	Company
FastStart™ High Fidelity Kit	Hoffmann-La Roche, Basel, Switzerland
Immobilon Western HRP Substrat	Merk Millipore, Billerica, MA, USA
In Fusion® HD Cloning Kit	Clonetech Laboratories, Mountain View, CA, USA
QIAprep® Spin Miniprep Kit	Qiagen, Hilden, Germany
QIAquick® Gel Extraction Kit	Qiagen, Hilden, Germany
QIAquick® PCR purification Kit	Qiagen, Hilden, Germany
PureLink® HIPure Plasmid Maxiprep Kit	Invitrogen™, Carlsbad, CA, USA

3.6. Software

Table 13. List of software used in this work, application and company.

Software	Application	Company
DNASTAR Lasergene 8	Sequencing	DNASTAR Inc., Madison, WI, USA
FlowJo Software	Analyze Flow data	Tree Star Inc., Ashland, OR, USA
Fusion FX-7	Detect chemiluminescence	Peqlab Biotechnologie, Erlangen, Germany
GraphPad Prism 6	Analyze data	GraphPad Software Inc., La Jolla, CA, USA
ImageJ	Analyze images	Wayne Rasband, NIH, USA
InFusion® Primers	Create primers	Clonetech Laboratories, Mountain View, CA, USA
TECAN Magellan Software	Absorbance reader	TECAN, Männedorf, Switzerland

4. Methods

4.1. Molecular biology

4.1.1. Bacterial transformation

All plasmids used in this work were purified following bacterial transformation.

Bacterial transformation is defined as the transfer of an exogenous genetic material (foreign DNA) into a bacterial cell, known as a competent cell. To transform competent cells, a heat-pulse destabilizes the bacterial wall allowing the uptake of the foreign DNA. The presence of an origin of replication within the foreign DNA enables an independent replication, providing high amounts of genetic material that can eventually be extracted and purified.

To perform a bacterial transformation, competent cells (Top10 or Stellar cells) were first thawed slowly on ice. Fifty microliters (μl) of competent cells were carefully mixed with 1.5-2 μl of plasmid into a 1.5 ml Eppendorf tube. The mixture was placed for 30 minutes on ice followed by a heat-pulse of 42°C for 30 seconds. Cells were immediately cooled down for 2 minutes on ice with the intention of stabilizing the transformation. Next, transformed cells were resuspended in 250 μl of pre-warmed SOC medium and incubated for 1 hour at 37°C and 225 rpm. In parallel, a LB-Agar plate containing Ampicillin (50 μg/ml) was pre-warmed at room temperature. By adding Ampicillin to LB-Agar plates, growth of unspecific bacteria was avoided since only the foreign DNA expresses an Ampicillin resistance gene. One third of the transformed cells (100 μl) were spread on the LB-Agar plate using a L-shaped cell spreader (previously sterilized with ethanol). After 24 hours incubation at 37°C (Heraeus Holding incubator, Thermo Scientific, Waltham, MA, USA), a bacterial culture was prepared by selecting and dissolving a single colony in 7 ml of LB-medium containing Ampicillin (50 μg/ml). Bacterial cultures were always incubated for 12-18 hours at 37°C in a shacking incubator (Carl Roth, Karlsruhe, Germany).

To ensure aseptic conditions during the manipulation of bacteria, the work was performed under sterile conditions.

LB-medium

Pepton	10 g
Yeast extract	5 g
NaCl	5 g
Agar	15 g
ddH$_2$O	up to 1000 ml

LB-Agar plates[1]

LB-medium	500 ml
Agar	7.5 g

SOC medium

Yeast extract	0.5%
Tryptone	2%
NaCl	10 mM
Glucose	20 mM
MgCl$_2$	10 mM
MgSO$_4$	10 mM
KCl	2.5 mM

4.1.2. Bacterial glycerol stock

In order to preserve transformed bacteria, 800 µl of bacterial culture was mixed with 200 µl of 86% sterile glycerol into 1.2 ml cryovials. Cryovials were stored at -80°C for future use. To recover a culture, the bacteria were scraped off and grown overnight in LB-medium containing Ampicillin, as explained above.

4.1.3. DNA purification

DNA was purified from bacterial cultures using a QIAprep® Spin Miniprep Kit (Qiagen, Hilden, Germany) (<20 µg) according to the manufacturer's manual. Briefly, the overnight culture was

---

[1] Solution was autoclaved and cooled down before adding Ampicillin (50 mg/ml)

spun down by centrifugation and lysed to break and precipitate all bacterial structures. Lysate was applied to the QIAprep® module, and, after a washing step, pure DNA was eluted with 30 µl ddH$_2$O into a 1.5 ml Eppendorf. Bigger bacterial cultures were useful when higher amounts of DNA were required. In this case, a pre-culture (7 ml LB + Ampicillin (50 µg/ml)) was set up for 6 hours and poured into 200 ml LB-medium containing Ampicillin (50 µg/ml). After overnight incubation, the purification of plasmid DNA was done using a PureLink® HIPure Plasmid Maxiprep Kit (Qiagen, Hilden, Germany) (500-800 µg) according to the manufacturer's manual. Maxiprep procedure was similar to a Miniprep, but DNA was eluted with 750 µl ddH$_2$O in a 1.5 ml Eppendorf tube. DNA was stored at -20°C for future use.

4.1.4. DNA concentration

DNA concentration and purity was determined using a NanoDrop™ spectrophotometer (Thermo Scientific, Waltham, MA, USA). A spectrophotometer detects the amount of UV light that is absorbed by 1 µl of sample at wavelengths 260 nm and 280 nm, measuring the optical density (OD). This OD is then converted to a concentration value by the software since an OD at 260 nm of 1 equals 50 µg/ml of dsDNA. In addition, since nucleic acids have the higher absorbance at 260 nm and proteins at 280nm, the OD$_{260}$/OD$_{280}$ ratio provides information about the purity of the sample. Pure DNA has an OD$_{260}$/OD$_{280}$ ratio of ~1.8, and pure RNA has an OD$_{260}$/OD$_{280}$ ratio of ~2.0.

4.1.5. Polymerase chain reaction (PCR)

The polymerase chain reaction (PCR) method is commonly used to amplify a specific DNA sequence. The reaction comprises three main steps and requires a DNA polymerase, specific primers and deoxynucleotide triphosphates (dNTPs):

1) Denaturation step: template DNA melts and separates in single stranded DNA (ssDNA) by applying high temperatures.

2) Annealing step: specific primers stick to the template DNA allowing the synthesis of new strands by a DNA polymerase. In this step, it is critical to ensure the hybridization of the primers with the ssDNA by selecting an optimal annealing temperature related to the primers melting temperature (Tm).

3) Elongation step: the DNA polymerase synthesizes a complementary strand by adding dNTPs to the primer extreme (3'-OH). The temperature in this step depends on the polymerase, and the time depends on the length of the amplified sequence (approximately 1 min per kb).

In this work, all PCRs were performed using a FastStart High Fidelity PCR system (Hoffmann- La Roche, Basel, Switzerland) and a PeqSTART x2 thermocycler (Peqlab Biotechnologie, Erlangen, Germany).

Table 14. PCR mix commonly used.

Component	Volume
DMSO	1 µl
PCR Buffer 10x	5 µl
dNTP	1 µl
Primer_for [10 pmol]	2 µl
Primer_rev [10 pmol]	2 µl
DNA-template	100 ng
Taq Polymerase	0.5 µl
ddH$_2$O	up to 50 µl

Table 15. Representative PCR program used for FLT3-ITD amplification.

Step	Cycles	Time	Temperature
Initial denaturation	1	2 min	95°C
Denaturation		30 sec	94°C
Annealing	30	30 sec	65°C
Elongation		3 min	72°C
Final elongation	1	5 min	72°C
Cooling	-	∞	4°C

4.1.6. Restriction enzyme digestion of plasmid DNA

Restriction endonuclease digestion is commonly used to cleave DNA. Restriction enzymes are bacterial enzymes that recognize small palindromic regions (6-8 bases) and cut the DNA in a particular site (Smith, 1993). In this work, DNA digestion was performed during cloning to generate compatible and specific ends.

The restriction reaction was set up on ice adding the enzyme(s) last. Reaction buffer and BSA (100 µg/ml) were chosen according to the enzyme(s) features. The digestion was incubated for 2 hours at 37°C followed by 20 minutes at 65°C to inactivate the enzyme(s). Digested DNA was stored at -20°C.

Table 16. Restriction mix.

Component	Volume
Plasmid DNA	2 µg
Buffer 10x	5 µl
BSA 10x	5 µl
Enzyme 1	1 µl
Enzyme 2	1 µl
ddH$_2$O	up to 50 µl

4.1.7. Agarose gel electrophoresis

To confirm PCR amplification or to purify a digested plasmid, samples were separated using an agarose gel electrophoresis. Gel electrophoresis separates negatively charged DNA that moves toward a positive electrode by applying an electrical field through a gel matrix. Short DNA fragments always migrate more quickly than large ones, and the size(s) of the DNA fragment(s) can be determined by comparison with a DNA ladder (Figure 9). The gel matrix consists of agarose, a polysaccharide polymer, and its resolution depends on the concentration (0.75% to 2%). Low percentage gels separate better big DNA fragments and vice versa (Takahashi et al., 1969). To prepare a 1% gel, 1 g of agarose was dissolved in 100 ml TBE (1x) buffer by applying heat but preventing the solution from boiling over. DNA samples were mixed with 1/5 loading dye and run at 80-120 V until the dye line reached ¾ of the gel. A GeneRuler™ 1kb DNA ladder (Thermo Scientific, Waltham, MA, USA) was included during the electrophoresis. To visualize DNA, the gel was placed inside a bath containing Ethidium bromide (400 µl EtBr in 1000 ml ddH$_2$O) and analyzed with a UV-Gel documentation system (Peqlab Biotechnologie, Erlangen, Germany). Therefore, to confirm a PCR amplification, a small portion of PCR product was run in an agarose gel, and the rest was purified using a QIAquick® PCR purification Kit (Qiagen, Hilden, Germany). Furthermore, to purify a digested plasmid, the entire product was run along with an undigested probe as a negative control. Then, the fragment of interests was cut from the gel and purified using a QIAquick® Gel Extraction Kit (Qiagen, Hilden, Germany).

TBE 10x Buffer

Tris   900 mM

EDTA   900 mM

Boronic acid   10 mM

Loading dye 6x

Glycerin   50%

SDS   1%

EDTA   125 mM

Bromophenol blue   0.05%

Xylene cyanol   0.05%
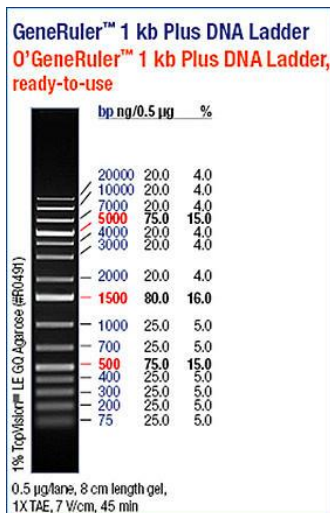
Figure 9. Gene Ruler™ 1kb DNA ladder used in this work.

4.1.8. In-Fusion® Cloning

In-Fusion® cloning kit (Clontech Laboratories, Mountain View, CA, USA) was used for directional cloning of DNA fragments into vector systems. This approach is based on the fusion of DNA fragments (e.g., PCR product) with linearized vectors by recognizing a 15 bp overlap at their ends. The first step was the design of specific primers that always included 1) the same cutting site(s) used to linearize the vector and 2) 15 bp extensions (5') complementary to the ends of the vector. Once the PCR product and the linearized vector were purified, In-Fusion cloning reaction was prepared, incubated for 15 minutes at 50°C and immediately placed on

ice. The amount of vector and insert depended on their size. In addition, a reaction with the linearized vector alone was used as negative control, and the kit included a positive control. Once the reaction was completed, competent cells were transformed with 2.5 µl of the cloning product. Next day, colonies were selected and grown in LB cultures as described before. To select positive clones, purified plasmid DNA was digested with specific enzymes and run in an agarose gel. Finally, selected clones were sent for sequencing.

Table 17. In-Fusion® reaction.

Component	Volume
5x In-Fusion® HD enzyme	2 µl
Linearized vector	50-200 ng
Insert	10-200 ng
ddH$_2$O	up to 10 µl

4.1.9. Sequencing

Sequencing of selected clones was done using the method of Sanger (Sanger et al., 1977). Similar to a PCR reaction, this method requires a template DNA, primers, a DNA polymerase, dNTPs and chain-terminating dideoxynucleotide triphosphates (ddNTP). Briefly, the DNA polymerase keeps generating a new complementary DNA strand until a ddNTP is incorporated. DdNTPs lack the 3-OH group required to bind two nucleotides and, therefore, block the chain-reaction. Since each ddNTP (A, G, T, C) is conjugated to a different fluorochrome, their insertion site can be detected and related with the length of the amplified fragment providing a final DNA sequence.

In this work, all sequencing was performed by GATC Biotech (Cologne, Germany), and the results were analyzed with the DNASTAR Lasergene 8 software (DNASTAR Inc., Madison, WI, USA).

4.2. Cell biology

4.2.1. General cell culture

All cell lines used in this work are listed in Table 2 and Table 3.

4.2.1.1. Culture of cell lines

Murine Ba/F3 and 32D cells were cultured in RPMI 1640 medium supplemented with 10% FBS, 29 ml Additiva, 50 µg/ml Penicillin-Streptomycin and 2.5 mg/ml Plasmocin. Medium for parental cells and cells transduced with wild-type FLT3 was supplemented with 10% IL-3. IL-3 was collected from WEHI-3B conditioned media. Cell passaging was done every 2-3 days with a seeding density of 3×10^5 cells/ml.

Human Phoenix cells were used as retroviral packaging cells. Cells were cultures in DMEM (1x) + GlutaMAX™ medium supplemented with 10% FBS, 50 µg/ml Penicillin-Streptomycin, 1% L-Glutamine and 2.5 mg/ml Plasmocin. Cell passaging was done every 2-3 days with a 70-80% confluence. Since Phoenix cells are adherent cells, 0.05% Trypsin-EDTA was used to detach cells after a pre-wash with DPBS (1x). All cells were incubated at 37°C, 5% CO_2 levels and a relative humidity of <80% in a CO_2 Incubator CB210 (Binder, Tuttlingen, Germany)

Additiva[2]

DPBS 1x	100 ml
PBS 1x + ß-mercaptoethanol [0.35 µl/ml]	100 ml
HEPES 1M ph7.2	100 ml
Sodium pyruvate [100 nM]	100 ml
L-glutamine [200 mM]	100 ml
Non-Essential amino acids 10x	60 ml
Asparagine [10 mg/ml]	20 ml

4.2.1.2. Cryopreservation

All cell lines were preserved in order to guarantee a continuous stock. Fresh cultured cells were washed and re-suspended with freezing medium at a density of 1.5×10^6 cells/ml (Phoenix cells) or 5×10^6 cells/ml (Ba/F3 and 32D). Cryovials were placed in a Nalgene® freezing container (Thermo Scientific, Waltham, MA, USA) at -80°C for 48 hours and then stored in liquid nitrogen. To recover a cell culture, cells were immediately unfrozen at 37°C and washed once with 15 mL DPBS (1x).

---

[2] Additiva was filtered before use under sterile conditions.

Freezing medium

Culture medium   70%

FBS   20%

DMSO   10%

4.2.1.3. Cell counting

Cell counting was done mixing 10 µl of cell suspension with 90 µl of Trypan Blue obtaining a 1:10 dilution. Then, 10 µl from this dilution were placed in a hemocytometer (Neubauer counting chamber), and viable cells were counted using a "Primo Vent" microscope (Zeiss, Oberkochen, Germany). Cell density was calculated using the following formula:

$$\frac{\text{number of cells}}{4} \text{ x diluted factor x } 10^4 = \frac{\text{cells}}{\text{ml}} \text{ in original suspension}$$

4.2.2. Virus production and infection

In this work, retroviral infections were performed with the intention of generating new cell lines that stably express a gene of interest.

4.2.2.1. Retroviral virus production

Replication-incompetent retroviral particles were generated using FuGene® Transfection Reagent (Hoffmann-La Roche, Basel, Switzerland) and Phoenix cells as packaging cells.

Phoenix cells (2×10^5 cells/ml) were plated in a 10 cm dish one day before transfection to reach approximately 80% confluence after 24 hours. To set up a transfection, 10 µg of the gene of interest, 10 µg of the gag-pol-expressing vector and 3 µg of the eco-envelope-expressing vector were added to 500 µl of Opti-MEM medium pre-warmed to room temperature. Next, 69 µl of FuGene® (1:3 ratio) were carefully added. The mixture was vortexed and incubated for 15 minutes at room temperature. Last, the mixture was added drop-by-drop onto the Phoenix cells containing freshly changed medium. The medium of transfected cells was changed 24 hours after transfection. Sixteen hours later, the first virus-containing supernatant was collected and filtered through a 0.45 µm filter. To collect additional virus-containing supernatant, 5ml of fresh medium was added, and virus-containing

supernatant was harvested 6-8 hours later. The virus-containing supernatant was placed on ice for immediate use or stored at -80°C.

4.2.2.2. Cell infection and selection

In this work, an ecotropic envelope MLV-based vector was used enabling the infection of murine cells in culture.

To transduce parental cell lines, 2×10^6 cells were plated in a six-well plate along with 3 ml of virus-containing supernatant. The infection plate was spun down at 33°C at 2000 rpm for 90 minutes and incubated overnight. Twenty-four hours later, virus-containing medium was replaced by the respective culture medium. Selection of transduced cells started 48 h after infection for one to two weeks before setting up experiments and preparing cryovials. However, the selection method depends on the characteristics of the retroviral vector system. In this work, two vectors systems were used: pMSCV-PIG (Puromycin IRES GFP) and pMSCV-MIY (MSCV IRES YFP). Cells transduced with PIG plasmids were selected with puromycin (1 µg/ml) and analyzed for GFP expression by flow cytometry; while, cells transduced with MIY plasmids were only analyzed by flow.

4.2.3. Fluorescence-based methods

4.2.3.1. Flow cytometry

Flow cytometry is a laser-based technology that identifies chemical and physical properties of single cells. Therefore, cells within a suspension can be classified by their size and granularity, as well as by the detection of fluorescence particles (e.g., antibodies). In this work, flow cytometry analysis was widely used, for example, to confirm the expression of a plasmid following a retroviral infection or to classify different cell populations within a cell suspension using antibodies (e.g., blood, bone marrow). In order to distinguish these populations, cells were incubated with antibodies linked to specific fluorochromes. All antibodies used for flow cytometry are listed in Table 8. All samples were analyzed using a FACSCanto™ II cytometer (Becton Dickinson, Franklin Lakes, NJ, USA), and post-acquisition analysis was done using FlowJo software (Tree Star Inc., Ashland, OR, USA).

4.2.3.2. Fluorescence-activated cell sorting

Following the same principle as in flow cytometry, fluorescence-activated cell sorting (FACS) separates cells depending on their fluorescence. Therefore, different cell populations, previously detected by flow cytometry, can also be separated and collected for further applications. All samples were sorted using a FACSAria™ III Sorter (Becton Dickinson, Franklin Lakes, NJ, USA).

4.2.3.3. Immunocytochemistry

Immunocytochemistry is a technique used to visualize the localization of a molecule of interest (e.g., protein) in single cells using a specific tag (e.g., antibody) and a fluorescence microscope.

In this work, 1×10^5 cells were spun down onto a microscope slide for 5 minutes at 1000 rpm. Immediately after, cells were fixed in methanol for 5 minutes at -20°C with the intention of minimizing changes in cell structure followed by incubation with acetone for 1 minute at room temperature to permeabilized the cell membrane. In order to obtain an immunological detection, slides were stained using an indirect method. First, slides were blocked with 5% BSA dissolved in DPBS (1x) for 1 hour. Next, slides were incubated with a specific primary antibody for 1 hour followed by an additional incubation with a secondary antibody covalently linked to a fluorophore. Both antibodies were freshly dissolved in 1% BSA. Cells were also stained with DAPI (1 µg/ml) for 10 minutes in order to localize the cell nucleus. The entire staining process was done inside a dark humidity chamber, and the slides were always washed three times with DPBS (1x) between incubation steps. Finally, slides were mounted with fluorescent mounting medium and stored at 4°C in the dark. Immunofluorescence images were acquired with an automated epi-fluorescence microscope (objective 40x/0.75 Plan-Neofluar) (Zeiss, Oberkochen, Germany). Images were further analyzed using ImageJ (Wayne Rasband, NIH, USA).

4.2.4. Cell biology

4.2.4.1. Methylcellulose colony formation assay

Methylcellulose-based medium is a semi-solid media that supports cell proliferation and differentiation of single cells. It can be used for multiple applications depending on the media composition. In this work, methylcellulose without cytokines (#3231; STEMCELL Technologies, Vancouver, Canada) was used to test clonogenicity of transformed FLT3-ITD cell lines. Cells

were plated in 3 ml of methylcellulose (1000 cells/ml), and colony numbers were counted after 10 days. Only oncogenic transformed cells were able to proliferate and generate colonies (clones) in the absence of cytokines.

4.2.4.2. Cell proliferation Assay (MTS)

Proliferation and cell viability was quantified employing a colorimetric methyl-thiazol-tetrazolium-based assay (MTS). The MTS assay is based on the reduction of tetrazolium dye into formazan by the NAD(P)H-dependent cellular oxidoreductase enzyme present in living cells. The amount of produced formazan is measured by quantifying its absorbance at a certain wavelength (490 nm). In this work, 5000 cells were plated into a well of a 96-well plate and incubated for 24 hours. Next day, 20 µl of MTS dilution was added and incubated for 2-3 additional hours. Plate absorbance was quantified using a Sunrise™ plate reader (TECAN, Männedorf, Switzerland).

4.2.4.3. Apoptosis assay

Apoptotic cells can be detected by adding propidium iodide into a cell suspension followed by flow cytometry analysis. Propidium iodide is an intercalating agent and a fluorescent molecule with a maximum emission at 617 nm that binds to the DNA. Thereby, the staining with propidium iodide distinguishes apoptotic cells from viable cells according to the DNA content; cells with a DNA content less than 2n ("subG1 cells") are defined as apoptotic (Nicoletti et al., 1991). To analyze apoptosis, 3×10^4 cells were plated in a well of a 6-well plate and incubated under different culture conditions. After 24 hours, cells were harvested, washed once with DPBS (1x) and directly stained with propidium iodide (100 ng/ml). Apoptosis was measured by flow cytometry and analyzed using FlowJo software (Tree Star Inc., Ashland, OR, USA).

4.3. Protein biochemistry

4.3.1. Cell lysis

To analyze the protein composition within a pool of cells, these were lysed and analyzed using Western blot assays. Depending on the composition of the buffer, different cellular fractions can be extracted (e.g., nucleus or cytoplasm). In this work, a whole cell lysis buffer supplemented with protease and phosphatase inhibitors, which stabilize proteins and

phosphorylated amino acids, was used. Cells were harvested, washed two times with ice-cold DPBS (1x) and resuspended in freshly prepared lysis buffer. The amount of buffer depends on the cell number. After 30 minutes on ice, the lysate was centrifuged for 15 minutes at 4°C and 13000 rpm. Supernatant was collected into a new tube and stored at -80°C.

Japan buffer (stored at 4° C)

HEPES pH 7.4	50 mM
Glycerol	10%
NaCl	150 mM
Triton-X	1%
$MgCl_2$	1.5 mM
EGTA	5 mM

Lysis buffer 1 mL (100 µl/10^6 cells)

Japan buffer	800 µl
cOmplete 20x	50 µl
PhosStop 10x	100 µl
NaF [1M] (optional)	50 µl

4.3.2. Protein concentration

Protein concentration was measured using the colorimetric Bradford dye-binding method based on the changes in the absorbance of the dye Coomassie brilliant blue G-250. Once the dye binds to basic and aromatic amino acid residues, the blue anionic form stabilizes; while, the red cationic form stays unbound. The amount of bounded form is measured by its absorbance at 595 nm, which is proportional to the amount of protein in the sample (concentration). However, to obtain the concentration of unknown samples, the absorbance values need to be compared to a standard curve. To measure protein concentration, 200 µl of Bio-Rad Bradford reagent, previously diluted 1:5 with ddH_2O, were pipetted in a well of a 96-well plate along with either 2 µl of protein standard (Bovine serum albumin (BSA) [mg/ml]: 0, 0.25, 0.5, 0.75, 1, 1.25, 1.5) or 1 µl of the unknown sample (in duplicates). After 5 minutes incubation, plate absorbance and protein concentration were measured using a Sunrise™ plate reader and the TECAN Magellan Software (TECAN, Männedorf, Switzerland)

4.3.3. SDS-PAGE / Western blotting

Western blot is commonly used to detect specific proteins within cell lysate following three main steps:

1) SDS polyacrylamide gel electrophoresis (SDS-PAGE): gel electrophoresis separates denatured and reduced proteins that move toward a positive electrode by applying an electrical field through a gel matrix. Proteins are separated by their molecular weight - small proteins migrate faster than big ones -, and the size(s) can be determined by comparison with a prestained protein ladder. The gel matrix consists of polyacrylamide, and its resolution depends on the concentration. Low percentage gels separate better big proteins and vice versa. Previous to the gel electrophoresis, it is usually necessary to denature and reduce proteins using a loading buffer that contains the anionic detergent SDS and ß-mercaptoethanol. While SDS denatures and negatively charges proteins after boiling the sample at 95-100°C for 5 minutes, ß-mercaptoethanol reduces disulphide bridges.

2) Membrane transfer: separated proteins are transferred from the gel onto a nitrocellulose membrane. Following the same principle as in the electrophoresis, proteins move onto the membrane by applying an electric field along the blotting sandwich. Proteins are also fixed in the membrane by adding methanol in the transfer buffer.

3) Protein detection: detection of proteins is done using antibodies that recognize a specific epitope. After transfer, the nitrocellulose membrane is blocked with either 5% non-fat dry milk or 5% BSA (depending on the antibody) for 45 minutes to avoid unspecific binding. After several washes with TBST buffer, a primary antibody is added overnight at 4°C. It is important that the adequate amount of antibody is diluted in the recommended buffer. Unbound antibody is removed with several washing steps, followed by the incubation with a secondary antibody for 1 hour at room temperature. Depending on the detection systems, secondary antibodies can be linked to different molecules (e.g., fluorophores, horseradish peroxidase). In this work, secondary antibodies were linked to a reporter enzyme: horseradish peroxidase (HRP). A Fusion FX7 machine was used to detect chemiluminiscence after adding Immobilon Western HRP Substrate (Merk Millipore, Billerica, MA, USA). Additionally, a PageRuler™ prestained protein ladder (Thermo Scientific, Waltham, MA, USA) was included during electrophoresis to determine the molecular weight of the proteins (Figure 10).

Loading buffer (4x)

SDS	4%
Tris pH 6.8	250 mM
Glycerol	40%
ß-mercaptoethanol	20%
Bromophenol blue	0.01%

Separating gel	**8%**	**12%**
ddH$_2$O	9.3 ml	6.6 ml
30% Acrylamide	5.3 ml	8 ml
Tris [1M] pH8.8	5 ml	5 ml
SDS 10%	200 µl	200 µl
APS 10%	200 µl	200 µl
TEMED	20 µl	20 µl

Stacking gel (5%)

ddH$_2$O	3.4 ml
30% Acrylamide	830 µl
Tris [1M] pH6.8	630 µl
SDS 10%	50 µl
APS 10%	50 µl
TEMED	5 µl

Running buffer (10x)

Tris	30 g
Glycine	144 g
SDS	10 g
ddH$_2$O	up to 1000 ml

Transfer buffer (1x)

Running buffer 1x	100 ml
Methanol	200 ml
ddH$_2$O	700 ml

TBST buffer (10x)

Tris	0.2 M
NaCl	1.4 M
Tween	0.1%

Blocking buffer

TBST	40 ml
Non-fat dry milk	2 g
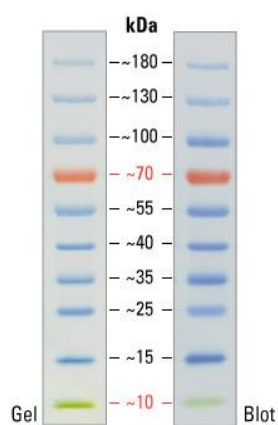
Figure 10. PageRuler™ Prestained Protein Ladder (10 to 180 kDa) used in this work.

4.4. Animal experiments

All mice were housed under pathogen-free conditions in the accredited Animal Research Facility at the Otto-von-Guericke University Medical Faculty, Magdeburg. All mice were euthanatized under carbon dioxide (CO$_2$) inhalation. All experiments were approved by the Landesverwaltungsamt Saxony-Anhalt (Protocol: 42502-2-1052).

4.4.1. Retroviral infection and bone marrow transplantation

Retroviral bone marrow transplantation (BMT) is based on the retroviral transfer of a gene of interest into hematopoietic stem and progenitors cells *ex vivo*, followed by transplantation of the respective cells into lethally irradiated recipient mice. This technique provides an *in vivo* model, for example, to analyze the pathophysiology of a genetic mutation or to test a therapeutic compound (Gavrilescu and Van Etten, Richard A, 2008). In this work, the retroviral bone marrow (BM) transplantation protocol was established according to previous publications (Kelly et al., 2002; Grundler et al., 2005). BM cells were always kept on ice and manipulated under sterile conditions. The protocol was divided into three main steps:

1) Isolation of primary bone marrow cells: Tibias, femurs and iliac crests were collected from humanely sacrificed 6-9 weeks old BALB/c donor mice 5 days after intraperitoneal injection of 5-fluorouracil (5-FU; 150 mg/kg). Commonly used for cancer treatment, 5-FU inhibits the nucleotide synthetic enzyme thymidylate synthase blocking the synthesis of the pyrimidine thymidine required for DNA duplication (Longley et al., 2003). In mice, the injection of 5-FU depletes mature bone marrow cells and induces cycling of immature and progenitor cells. Muscle and connective tissue were cleaned off, and single bones were crushed into fragments in a sterile mortar containing 5 ml of DPBS(1x)+1%FBS. Released bone marrow cells were collected and filtered into a 50 mL Falcon tube through a 70 µm cell strainer. Remaining bone marrow cells were rinsed with 5 ml of DPBS(1x)+1%FBS and filtered into the same tube. Cell suspension was centrifuged at 1400 rpm for 5 minutes at 4°C and resuspended in 2ml of Erylysis buffer (1x). After 3 minutes incubation on ice, cell were centrifuged, resuspended in 5 ml DPBS(1x)+1%FBS and filtered once again through a 70 µm cell strainer to obtain a single cell suspension.

2) Transduction of bone marrow cells: non-tissue treated 6-well plates were coated overnight with 2 ml retronectin (12.5 µg/ml) at 4°C. Plates were washed with sterile DPBS (1x), and 3 ml of virus-containing supernatant was centrifuged at 2000 rpm for 90 minutes at 33°C. After centrifugation, virus-containing supernatant was replaced by bone marrow cells previously resuspended in 5 ml of fresh virus-containing supernatant supplemented with murine growth factors (6 ng/ml IL-3, 10 ng/ml IL-6, 10 ng/ml TPO and 100 ng/ml SCF). Bone marrow cells were transduced twice within 24 hours using the same centrifugation program. Forty-eight hours after the first infection, the virus-containing supernatant was replaced by pre-warmed serum-free expansion medium (SFEM) supplemented with growth factors and puromycin (1 µg/ml).

3) Transplantation: after 24 hours of puromycin selection, cells were washed with DPBS(1x)+1%FBS, counted in a hemocytometer and analyzed for GFP expression by flow cytometry. Same GFP$^+$ cell numbers were injected along with supporter cells into the lateral tail vein of lethally irradiated (13Gy; Biobeam 800, Gamma-Service-Medical, Leipzig, Germany) 6-9 week old female recipient mice. Mice were housed with neomycin (2 mg/ml) in the drinking water for one week. Supporter bone marrow cells from a 6-9 week old female mouse were prepared as previously described. For irradiation, recipient mice were anesthetized with an intraperitoneal injection of Ketamine (100 mg/kg) and Xylacine (5 mg/kg).

4.4.2. Competitive retroviral BMT

The competitive transplant model was adapted from the retroviral BMT model. Here, the aim was to transplant two differentially transduced bone marrow populations in a single recipient mouse. Competitive bone marrow cells were harvested and infected as described above. Forty-eight hours after the first infection, GFP$^+$ and YFP$^+$ transduced cells were sorted and incubated in SFEM supplemented with growth factors. After 24 hours, same GFP$^+$ and YFP$^+$ cell numbers along with supporter cells were transplanted into the lateral tail vein of lethally irradiated (13Gy) 6-9 week old female recipient mice.

4.4.3. Homing assay

Equal numbers of sorted bone marrow cells previously transduced with retroviral constructs were transplanted into the lateral tail vein of lethally irradiated (13Gy) 6-9 week old female recipient mice. After 16 hours, single femurs were harvested, and single cell suspension was prepared as described above. Total cell numbers were counted, and the entire cell suspension was analyzed by flow cytometry to detect the percentage of transformed cells that reach the bone marrow.

4.4.4. Blood analysis

Transplanted mice were anesthetized with isoflurane, and retro-orbital blood was collected into EDTA-coated containers. To determine complete blood cell counts, 20 µl of blood cells were diluted 1:10 in NaCl solution and then measured using an ADVIA 2120 analyzer (Siemens, Munich, Germany). To determine the percentage of GFP$^+$ (or YFP$^+$) expressing cells, 20 µl of blood cells was erylysed, resuspended in DPBS(1x)+1%FBS and analyzed by flow cytometry.

Furthermore, blood smears were prepared on a microscope slide for further cytological characterization and confirmation of leukocytosis.

4.4.5. Primary cells cryopreservation

In order to preserve primary cells, approximately 20 x 10^6 cells were frozen down in cryovials as previously described (please see 4.2.1.2).

Freezing medium

SFEM   10%

FBS   80%

DMSO   10%

4.4.6. May-Grünwald-Giemsa staining

May-Grünwald-Giemsa staining was used to stain blood smears. This method is based on the electrostatic interaction between dyes and cell components. The May-Grünwald solution contains anionic eosin (acid dye) and cationic methylene blue (basic dye), and the Giemsa solution contains both dyes and additional azures (basic dye) derived from methylene blue. Basic dyes stain in bluish acidic cellular components such as DNA/RNA (nucleus) or granules of basophil granulocytes, and eosin stains in reddish positive charged components like red blood cells and granules of eosinophil granulocytes. In this work, microscope slides were immersed in the May-Grünwald solution for 5 minutes and briefly washed with distilled water. Next, the Giemsa solution, previously diluted with 9 volume of distilled water, was placed on the slides for 30 minutes and entirely removed with distilled water. Slides were air-dried and stored at room temperature.

4.4.7. PKC412 treatment *in vivo*

PKC412 stock solution was prepared and stored at 4°C for a maximum of 6 weeks. Prior to administration, PKC412 50 mg/g stock was melt for 5 minutes in a water bath at 37°C. In order to prepare a fresh PKC412 12 mg/g micro-emulsion, 24% of PKC412 50 mg/g stock was mixed with 76% of purified water and inverted to obtain a clear emulsion. The drug was administered (50 mg/kg) every 24 hours by gavage using a 22-gauge gavage needle (Lee et al., 2005).

PKC412 50 mg/g pre-concentrate (1 g)

PKC412	50 mg
VitE	340 mg
PEG 400	425 mg
Cornoel-glyceride	85 mg
Ethanol	100 mg

5. Results

5.1. Functional characterization of novel FLT3-ITD mutations *in vitro*

5.1.1. Isolation of novel FLT3-ITD mutations from AML patients and cloning into a retroviral expression vector system

In order to establish a constitutive expression of our gene of interest in murine primary hematopoietic bone marrow (BM) cells and cell lines, all FLT3 constructs were cloned into a retroviral pMSCV-PIG vector system (Figure 8). This expression vector contains a puromycin resistance gene and a green fluorescence protein (GFP) as reporter gene, both separated by an internal ribosome entry site (IRES). Cloning of wild-type FLT3 and previously reported FLT3-ITD mutations was done using an InFusion®HD Cloning Kit. Two novel FLT3-ITD mutations were isolated and cloned into the pMSCV-PIG vector. After screening several clinical samples, the first mutation was isolated from genomic material of a FLT3-ITD positive AML patient. Genomic DNA was previously prepared from bone marrow cells and stored in the tumor bank of our department. Clinical samples were drawn after obtaining written informed consent, and all experiments were performed according to the guidelines of the Helsinki declaration and approved by the local ethics committee. The second mutation was isolated from genomic material of MV4;11 cells, a well-characterized FLT3-ITD positive human cell line. This cell line was established from the blast cells of a 10-year-old boy with acute myelomonocytic leukemia (AML FAB M5) at diagnosis. The cells were described to carry a t(4;11)(q21;q23) chromosome translocation and a FLT3 internal tandem duplication (Lange et al., 1987; Quentmeier et al., 2003). The cloning strategy included the detection of positive clones by restriction digestion using an *Xho*I enzyme and agarose gel electrophoresis. The pMSCV-PIG vector (~7.6 kb) contains a single *Xho*I cutting site within the multiple cloning site, while the *FLT3* gene (~3kb) includes two *Xho*I cutting sites within its sequence. Hence, only positive pMSCV-PIG_FLT3 clones (~10.6 kb) showed three specific DNA fragments of ~490 bp, ~1.6 kb and ~8.5 kb (Figure 11A). Previously investigated FLT3-ITD mutations were amplified from verified plasmids, hence positive clones detected by digestion definitely included an ITD mutation within the *FLT3* sequence. The same was true for the ITD cloned from the genomic material of MV4;11 cells since this cell line expresses exclusively the mutated *FLT3* allele (homozygous) (Quentmeier et al., 2003). In contrast, FLT3-ITD positive AML patients are often heterozygous expressing both wild-type and mutated alleles. In this case, the selection of positive clones harboring the mutant allele was done using an additional PCR-based assay with primers flanking exons 14

and 15 of the *FLT3* gene. This screening method is commonly used in the diagnostic laboratory of our department to detect ITD mutations in AML patients. As illustrated in Figure 11B, DNA fragments amplified from FLT3-ITD positive clones were bigger than wild-type clones. FLT3-WT_PIG and *standard* FLT3-ITD_PIG (ITD598/599(12)) constructs were included as negative and positive controls, respectively. Last, all constructs were sent for sequencing in order to verify the *FLT3* sequence and define each ITD mutation (GATC, Cologne). DNA-sequencing data was analyzed with DNASTAR Lasergene 8 software (DNASTAR Inc., Madison, WI, USA).
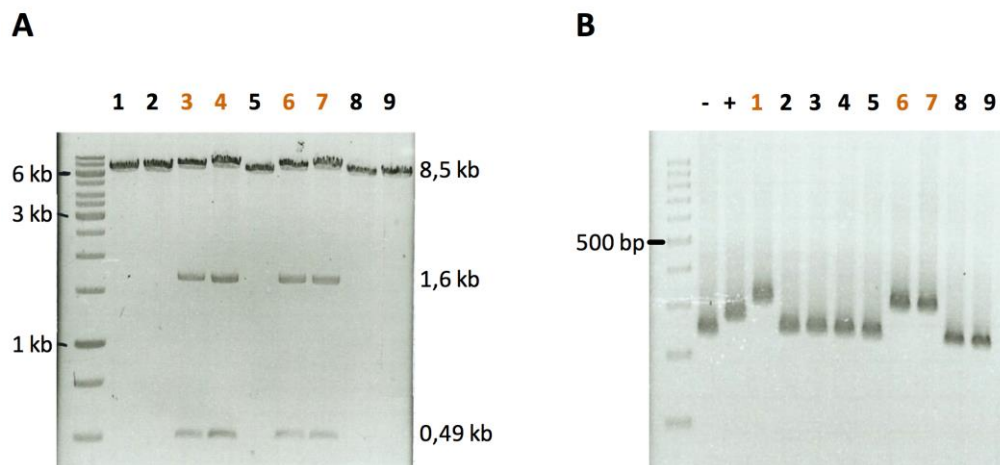
Figure 11. Selection of positive clones following restriction with *Xho*I. A) Agarose gel electrophoresis of several clones (plasmid DNA) previously digested with *Xho*I for 1 hour. Positive clones (lanes 3, 4, 6 and 7 (orange)) presented three fragments at ~8.5 kb, ~1.6 kb and ~490 bp. Representative gel from ITDG613E(33)_PIG cloning. **B)** Agarose gel electrophoresis of clones amplified by PCR using primers flanking exons 14 and 15 of the *FLT3* gene in order to detect the insertion of the FLT3 mutated allele. Positive clones (lanes 1, 6 and 7 (orange)) showed a higher size compared to wild-type FLT3 (negative control). A "standard" FLT3-ITD was used as positive control. Representative gel from ITDL601H(10).

Even though the ITD location site was the main feature of interest in this project, FLT3-ITD mutations are still fairly heterogeneous from patient to patient, for example, different duplication lengths or exchange of amino acids (AA) (Schnittger et al., 2002; Schnittger et al., 2012). In this work as well as in previous experimental studies in our department, each FLT3-ITD mutant was named under a specific nomenclature according to: 1) the ITD location defined by the codon position and 2) the length of the duplicated fragment defined by the number of AA indicated in brackets. Thus, three possible variants were observed: 1) an insertion between two codons, e.g., ITD598/599(12), 2) an insertion within a codon resulting in a point mutation with an AA exchange, the original AA stands before the codon position followed by the converted AA, e.g., ITDE611V(32) and 3) an insertion within the codon resulting in the exchange of more than one AA, e.g., ITDEV611VMT(32). According to this nomenclature, all FLT3-ITD mutations cloned into the pMSCV_PIG vector are represented in Figure 12.
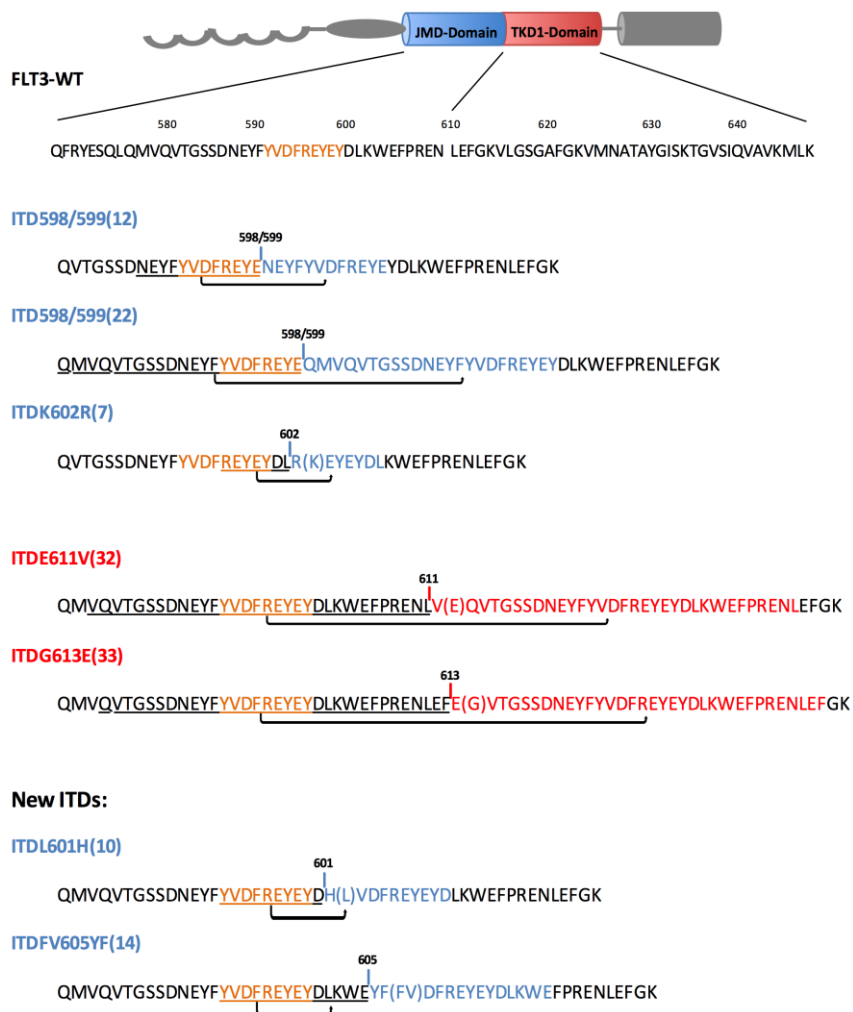
Figure 12. Schematic model of the wild-type FLT3 receptor tyrosine kinase and detailed presentation of the FLT3-ITD mutations. Extracellular domain, transmembrane domain and second tyrosine kinase domain are shaded gray, juxtamembrane domain and first tyrosine kinase domain are labeled and shaded blue and red, respectively. Wild-type FLT3 (WT) amino acid sequence includes parts of exon 13 and 14, which encode the juxtamembrane sequence and beginning of the first tyrosine kinase domain. Each FLT3-ITD mutation is represented: 1) duplicated residues are underlined in the wild-type sequence, 2) insertion site is indicated with a line and the AA position, 3) duplicated residues are inserted within the wild-type sequence (color matches with domain) and 4) if required, AA exchanged by an in-frame insertion of the duplicated sequence is shown in brackets. Specific tyrosine enriched amino acid motif is highlighted in orange in the wild-type sequence. First five FLT3-ITD mutants correspond to the previously investigated ITDs in our department, while the last two ITDs were isolated in this work.

Mutations within the JMD-ITD group include ITD598/599(12) (*standard* ITD mutant) (Mizuki et al., 2000), ITD598/599(22) and ITDK602R(7) (Kelly et al., 2002). Both ITD598/599(12) and ITD598/599(22) are located between the same codon positions; while, ITDK602R(7) is found within the codon 602 with an exchange of lysine (K) to arginine (R). All three ITD mutations are variable in regard to their length with 36 nucleotides, 66 nucleotides and 21 nucleotides, respectively. Mutations included in the TKD1-ITD group are: ITDE611V(32) and ITDG613E(33) (Mack, Dissertation, 2014). ITDE611V(32) localizes within the codon 611 with an exchange of glutamic acid (E) to valine (V) and a length of 96 nucleotides; while, ITDG613E(33) localizes

within codon 613 with an exchange of glycine (G) to glutamic acid (E) and a length of 99 nucleotides. Furthermore, both ITD mutations isolated in this work are located within the JMD-ITD group (Figure 12). ITDL601H(10), isolated from the MV4;11 cell line, localizes within the codon 601, exchanges leucine (L) to histidine (H) and includes 30 nucleotides. The mutation isolated from a FLT3-ITD positive AML patient, ITDFV605YF(14), localizes within the codon 605 with a double exchange of phenylalanine-valine (FV) to tyrosine-phenylalanine (YF) and a length of 42 nucleotides. As highlighted in Figure 12, all FLT3-ITD mutations include - entirely or only partially - the specific tyrosine enriched amino acid motif: **Y**VDFREYE**Y** (Vempati et al., 2007; Kayser et al., 2009).

5.1.2. Stable expression of FLT3-ITD mutations in murine hematopoietic cell lines

Transduction of Ba/F3 and 32D cell lines, IL-3 dependent murine pro-B lymphoid or myeloid cells, respectively, is a commonly used model to investigate the functional biology of oncogenes involved in signal transduction and cellular growth, including FLT3 mutations (Mizuki et al., 2000; Kelly et al., 2002; Spiekermann et al., 2003; Breitenbuecher et al., 2009b; Huang et al., 2013; Janke et al., 2014; Nonami et al., 2015). The fundamental rationale behind this is that constitutive expression of an oncogenic event confers IL-3 independent proliferation capacity, generating a cellular system useful to evaluate signaling and physiological properties of the gene of interest. In order to characterize both novel mutations - ITDL601H(10) and ITDFV605YF(14) - *in vitro*, new cell lines were generated in this work. In addition, wild-type FLT3 as well as previously reported FLT3-ITD mutations were included as controls: FLT3-WT_PIG, ITD598/599(12)_PIG, ITD598/599(22)_PIG, ITDK602R(7)_PIG, ITDE611V(32)_PIG and ITDG613E(33)_PIG (Ballaschk, Dissertation, 2014; Mack, Dissertation, 2014). FLT3_PIG constructs were packed in retroviral virus-particles followed by the transduction of Ba/F3 and 32D parental cells. Transduction efficiency was determined 48 hours after infection by analyzing the percentage of GFP-positive cells using flow cytometry (GFP$^+$). Parental cells (Ba/F3 and 32D) were used as GFP-negative control (GFP$^-$). The pMSCV-PIG vector also co-expresses a puromycin resistance gene allowing an effective selection of transduced cells via antibiotic treatment. Cells were selected with puromycin (1 ng/µl) in the presence of IL-3 starting 48 hours post-transduction. As observed in Figure 13, the percentage of GFP$^+$ cells was relatively low 48 h after infection but similar among the different FLT3 constructs (2%-6%). The percentage of viable GFP$^+$ cells increased up to 95% in wild-type FLT3 and FLT3-ITD transduced cells one week after selection with puromycin (Figure 13).

Previous studies in our and other groups have demonstrated cell autonomous growth of FLT3-ITD transduced Ba/F3 and 32D cells regardless of the ITD location (Breitenbuecher et al., 2009a; Ballaschk, Dissertation, 2014; Mack, Dissertation, 2014). To assess whether the novel ITD mutants also conferred IL3-independent growth, a pool of ITDL601H(10) and ITDFV605YF(14) transduced cells, previously selected with puromycin, was deprived of IL-3 for one week. ITD598/599(12), ITD598/599(22), ITDK602R(7), ITDE611V(32) and ITDG613E(33) mutants were used as positive control. Upon withdrawal of IL-3, only FLT3-ITD positive cells with proliferative advantage remained viable. After one week, cell viability was stabilized in both FLT3-ITDs and previously reported mutants with an increased expression of GFP up to 99% (Figure 13). As expected, viability of wild-type FLT3 transduced cells was unsustainable upon IL-3 withdrawal (Figure 13).

In summary, ITDL601H(10) and ITDFV605YF(14) constructs were stably expressed and conferred long-term IL3-independent growth to Ba/F3 and 32D cells, consistent with previous characterized FLT3-ITD mutations.
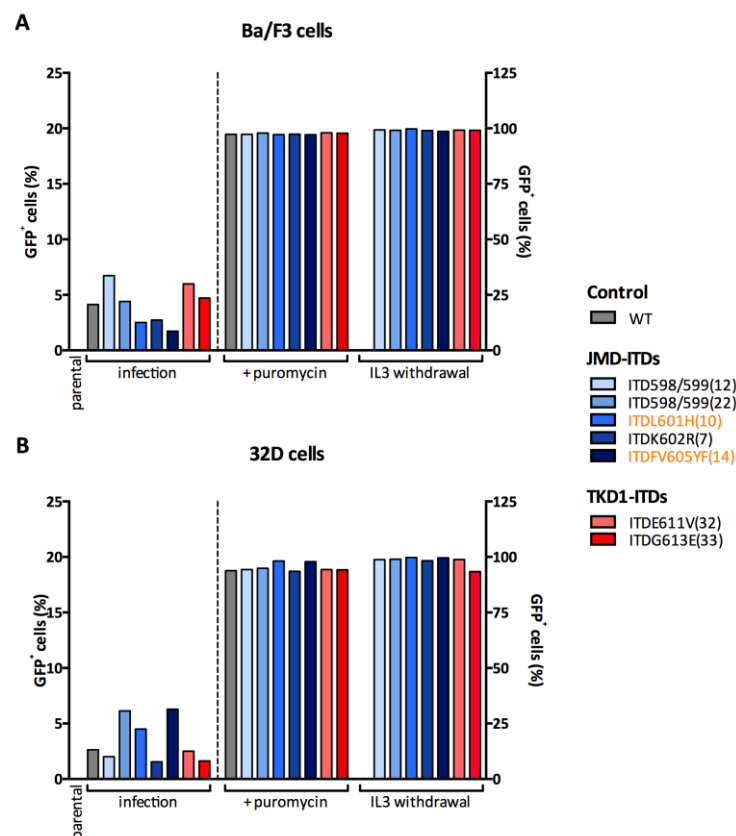
Figure 13. Stable transduction of murine cell lines (Ba/F3 and 32D) with the respective retroviral ITD constructs. A) Expression of the GFP reporter gene was analyzed by flow cytometry 48h after infection in Ba/F3 cells. Parental cells were used as GFP⁻ control. Transduced cells were selected with puromycin (1 ng/µl) in presence of IL-3. After one week, only stably transduced cells survived in culture indicated by high GFP levels. Stably transduced cells with transforming potential were selected following deprivation of IL-3. FLT3-ITD transduced cells were cultured in IL-3 free medium without puromycin. **B)** Similar results were observed in 32D cells. Data represents a single transduction.

5.1.3. Proliferation capacity and clonal growth of FLT3-ITD mutants

As demonstrated above, novel FLT3-ITD mutations as well as previously investigated mutations provided autonomous growth to Ba/F3 and 32D transduced cells. To further analyze the growth-factor independent transforming potential of each FLT3-ITD mutation, colony forming capacity was evaluated in methylcellulose-based medium as a readout of single cell clonogenicity (Mizuki et al., 2000; Kelly et al., 2002). Previous studies in our department investigated clonal growth of 1) Ba/F3 cells transfected with FLT3-ITD mutations cloned in a pAL-based vector system - ITD598/599(12)_pAL, ITDE611V(32)_pAL and ITDG613E(33)_pAL - and 2) 32D cells transduced with FLT3-ITD_PIG constructs - ITD598/599(12)_PIG, ITDK602R(7)_PIG, ITDE611V(32)_PIG and ITDG613E(33)_PIG. In both cases, all ITD mutants showed similar clonal growth regardless of the ITD location. In this work, clonal growth of both FLT3-ITD mutants - ITDL601H(10)_PIG and ITDFV605YF(14)_PIG - as well as additional FLT3-ITD mutants - ITD598/599(12)_PIG, ITD598/599(22)_PIG, ITDK602R(7)_PIG, ITDE611V(32)_PIG, and ITDG613E(33)_PIG – was analyzed in transduced Ba/F3 cells. Equal cell numbers were plated in methylcellulose-based medium without cytokines and incubated for 10 days. As a positive control, wild-type FLT3 expressing cells were cultured in methylcellulose supplemented with IL-3. Due to the absence of cytokines, only cells with autonomous growth were able to proliferate and generate colony-forming units (CFU) derived from a single cell. All transformed Ba/F3 mutants showed similar colony numbers comparable to wild-type FLT3 cells on IL-3 medium (Figure 14A) and regardless of ITD location site (Figure 14B). To confirm these results, the metabolic activity of each FLT3-ITD mutant was investigated using MTS-assays. Equal cell numbers of Ba/F3 transduced cells were plated, and proliferation was analyzed after 24 hours. Wild-type FLT3 transduced cells with or without IL-3 were used as positive and negative control, respectively. As observed in Figure 14C, all FLT3-ITD mutants showed similar factor-independent proliferation comparable to wild-type FLT3 cells supplemented with IL-3 and regardless of their location site (JMD vs. TKD1) (Figure 14D). As expected, wild-type FLT3 cells deprived of IL-3 failed to grow (Figure 14C).

Taken together, these results confirmed that both isolated FLT3-ITD mutations - ITDL601H(10)_PIG and ITDFV605YF(14)_PIG - mediate growth-factor independent proliferation that was comparable to previously characterized mutations regardless of the ITD location (JMD vs. TKD1).
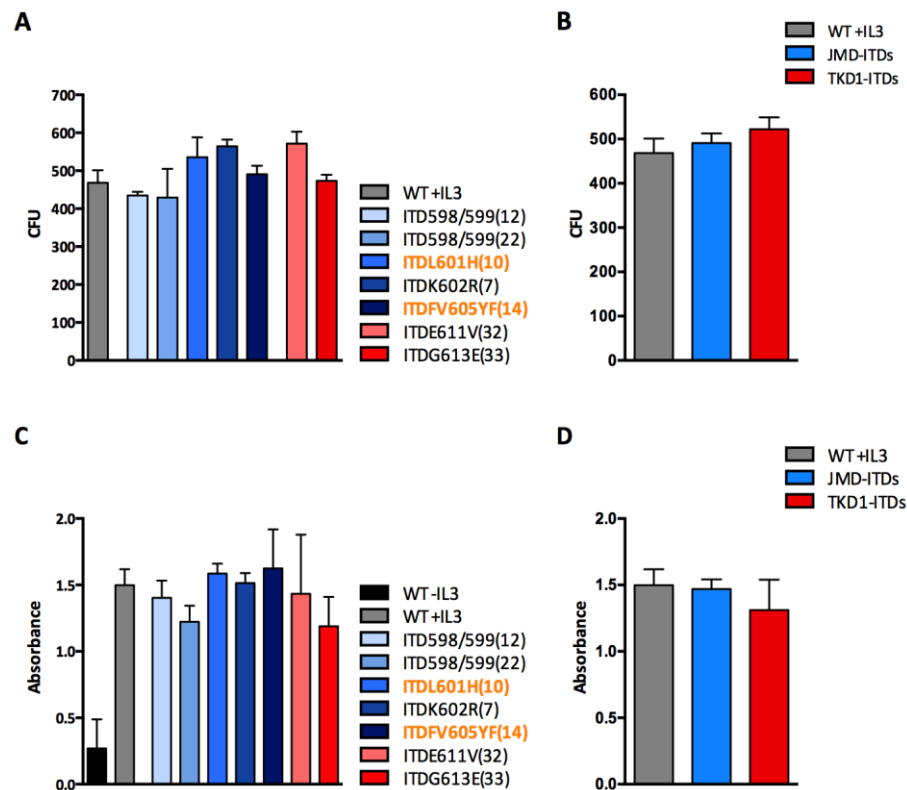
Figure 14. Transforming capacity and proliferation of FLT3-ITD mutations in stably transduced Ba/F3 cells. A) One thousand cells were plated in duplicate in methylcellulose (#3231, Stemcell Technologies) without cytokines. Colony-forming units were scored after 10 days of culture. Methylcellulose containing wild-type FLT3 cells was supplemented with IL-3 to support cellular growth. FLT3-ITD mutations showed high numbers of colonies in absence of cytokines comparable to wild-type FLT3 control (n=3 in duplicate; mean ±SEM). **B)** Clonal growth of FLT3-ITD mutants grouped by their insertion site (JMD vs. TKD1) and compared to wild-type FLT3 (mean ±SEM). **C)** Five thousand cells were plated in triplicate in IL-3 free medium. Cell metabolism was measured after 24 hours using MTS-assay. Wild-type FLT3 cells were cultured in medium supplemented with IL-3 to support cellular growth. FLT3-ITD mutations showed similar absorbance values indicating a comparable proliferative activity of FLT3-ITD mutated and wild-type FLT3 cells. Wild-type FLT3 cells were unable to proliferate in absence of IL-3 (n=3 in triplicate; mean ±SEM). **D)** Proliferation capacity of FLT3-ITD mutants grouped by their location site (JMD vs. TKD1) and compared to wild-type FLT3 (mean ±SEM).

5.1.4. Constitutive activation of the FLT3 receptor tyrosine kinase and its downstream targets STAT5 and ERK1/2 in FLT3-ITD mutants

Under basal conditions, the FLT3 receptor tyrosine kinase resides as an inactive monomer in the plasma membrane. Upon binding to its ligand, receptor dimerization leads to conformational changes enabling *trans*-phosphorylation of conserved tyrosine residues within the JMD. Internal tandem duplications have been described to bring these important tyrosine sites, such as Tyr^{589} and Tyr^{591}, next to the catalytic site leading to ligand-independent *cis*-phosphorylation of the receptor tyrosine kinase (Rocnik et al., 2006; Toffalini and Demoulin, 2010; Chan, 2011). Hence, the transforming capacity of FLT3-ITD mutants observed upon growth-factor withdrawal is sustained by a constitutive auto-phosphorylation of the receptor

and activation of downstream signaling pathways such as PI3K/AKT and MAPK, as well as STAT5 (Mizuki et al., 2000; Kiyoi et al., 2002; Spiekermann et al., 2003; Brandts et al., 2005; Rocnik et al., 2006). Constitutive activation of FLT3-ITD mutants - ITD598/599(12)_PIG, ITD598/599(22)_PIG, ITDK602R(7)_PIG, ITDE611V(32)_PIG, and ITDG613E(33)_PIG - has been previously reported in Ba/F3 and 32D cells (Ballaschk, Dissertation, 2014; Mack, Dissertation, 2014). To confirm a ligand-independent activation in the novel FLT3-ITD mutants, whole cell lysates were analyzed by Western Blot. As positive control, previously characterized FLT3-ITD mutations were included. After 4 hours starvation in medium containing 0.5% FBS, constitutive phosphorylation of FLT3 was detected with a specific phospho-antibody against FLT3 Tyr[591] (Figure 15A; lane 1). Immunoblot of total FLT3 protein confirmed comparable protein expression between the different mutants (Figure 15A; lane 2). Of note, two bands of about 130 kD and 160 kD were detected for FLT3 (Lyman et al., 1993; Maroc et al., 1993). Previous studies have shown that FLT3-ITD mutations significantly activate the downstream signaling molecule STAT5, which is not involved in wild-type FLT3 signaling (Choudhary et al., 2005; Grundler et al., 2005; Takahashi, 2011; Janke et al., 2014). In this work, constitutive phosphorylation of STAT5 was detected in all FLT3-ITD mutants using a specific phospho-antibody against STAT5 Tyr[694/699] (Figure 15A; lane 3). Total STAT5 was equally expressed in all samples (Figure 15A; lane 4). The enzyme GAPDH was used as loading control (Figure 15A; lane 5). Furthermore, all FLT3-ITD mutants showed a constitutive phosphorylation of ERK1/2, detected with a specific phospho-antibody against ERK1/2 Tyr[202/204] (Figure 15B; lane 5). Total ERK1/2 protein was equally expressed in all samples (Figure 15B; lane 6). FLT3-WT lysates were also analyzed after 4 hours starvation, without or with IL-3 (FLT3-WT -IL3 and FLT3-WT +IL3). As observed in Figure 15B, FLT3, STAT5 and ERK1/2 remained dephosphorylated under IL-3 deprivation, while STAT5 and ERK1/2, but not FLT3, were activated when IL-3 was added to the medium (Figure 15B). GAPDH was used as loading control (Figure 15B; lane 7).

Overall, these results confirmed that the transforming capacity of the novel FLT3-ITD mutations was supported by a constitutive auto-phosphorylation of the FLT3 receptor and activation of its downstream targets STAT5 and ERK1/2. These data showed a comparative transforming potential between all FLT3-ITD mutants, irrespectively of the ITD location site (JMD vs. TKD1).
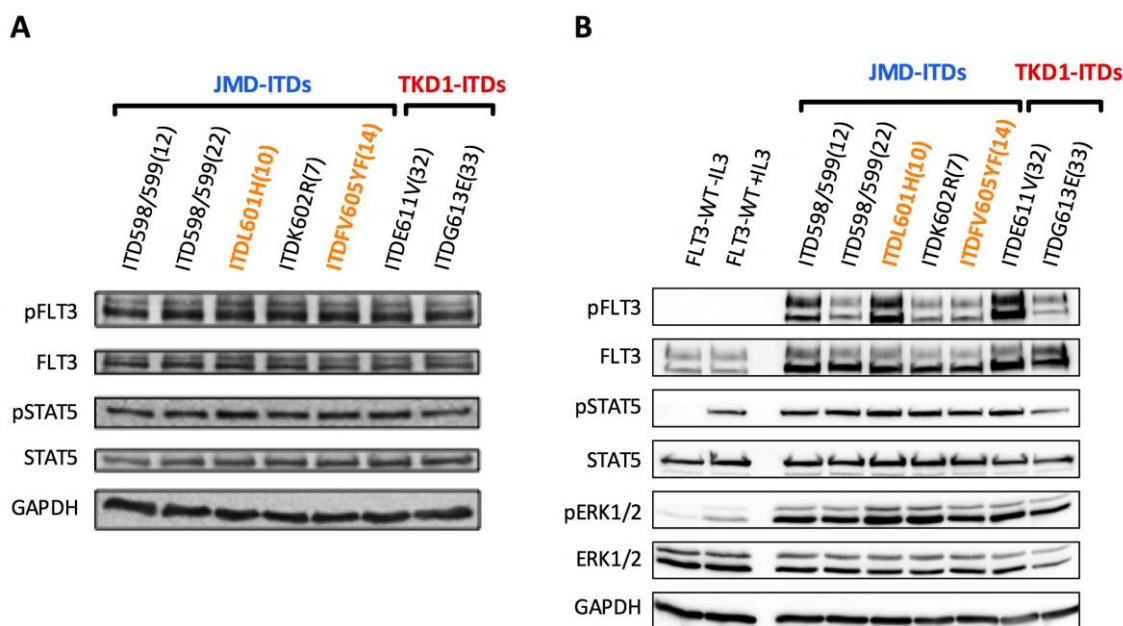
Figure 15. Western blot analysis of FLT3-ITD transduced Ba/F3 cells. A) Transduced cells were starved for 4 hours before preparation of total cell lysates. Novel FLT3-ITD mutants (orange) as well as previously characterized FLT3-ITD mutants showed equal FLT3 protein expression with a constitutive FLT3 phosphorylation (lane 1 and lane 2). Activation of the downstream signaling molecule STAT5 was detected in all FLT3-ITD mutants with equal levels of total STAT5 protein expression (lane 3 and lane 4). GAPDH was used as a loading control (lane 5). **B)** FLT3-ITD cell lysates were prepared as described above. FLT3-WT samples were cultured in medium either without or supplemented with IL-3. FLT3 receptor remained dephosphorylated in FLT3-WT, as well as the downstream molecules STAT5 and ERK1/2 (lane 1, lane 3 and lane 5). In the presence of IL-3, activation of STAT5 and ERK1/2 could be observed, but no FLT3 phosphorylation. Novel FLT3-ITD mutants as well as previously characterized FLT3-ITD mutants showed comparable ERK1/2 phosphorylation and total protein expression (lane 5 and lane 6). GAPDH was used as a loading control (lane 7). These blots are representative results of three independent experiments.

5.1.5. Sensitivity of ITDL601H(10) and ITDFV605YF(14) to tyrosine kinase inhibitors

Despite the advances in chemotherapy and hematopoietic stem cell transplantation, more than half of the AML patients remain uncured including patients that cannot undergo conventional chemotherapy due to comorbid conditions. As one of the most frequent and aggressive mutations in AML, the FLT3 receptor tyrosine kinase is considered as a promising therapeutic target (Konig and Levis, 2015). To date, a significant amount of tyrosine kinase inhibitors (TKIs) against mutated FLT3 are investigated in preclinical and clinical trials (Fischer et al., 2010; Kayser and Levis, 2014; Kiyoi, 2015a). Even though these studies have revealed promising results, the response of FLT3-ITD mutations to TKIs and chemotherapy seems to be heterogeneous. Mutations located within the TKD1 region have been associated with an unfavorable outcome after remission and post-remission therapy (Kayser et al., 2009; Schlenk et al., 2014). In addition, previous studies performed in our group revealed a differential sensitivity of FLT3-ITD mutants to TKIs depending on the ITD location site (JMD vs. TKD1) (Breitenbuecher et al., 2009b; Mack, Dissertation, 2014). FLT3-TKD1 mutants showed a

reduction in apoptotic cell death upon treatment with TKIs when compared to JMD-ITD mutants, despite a complete abrogation of FLT3 auto-phosphorylation. Here, the sensitivity of both novel FLT3-ITD mutants was investigated - ITDL601H(10) and ITDFV605YF(14) - and compared to previously characterized FLT3-ITD mutants.

5.1.5.1. Apoptotic cell death in ITDL601H(10) and ITDFV605YF(14) mutants

Since a constitutive activation of the FLT3 receptor enhances anti-apoptotic and proliferative signals, the treatment of transformed cells with TKIs mainly leads to cellular death. In this work, the sensitivity of ITDL601H(10) and ITDFV605YF(14) mutants to TKIs was evaluated using two different drugs: PKC412 (Midostaurin) and AC220 (Quizartinib). PKC412 is a N-benzyl-staurosporine originally developed as a protein kinase C inhibitor but with additional effects on other kinases including FLT3 (Figure 16, left). Several studies have demonstrated the inhibitory efficacy of PKC412 on FLT3-ITD positive cell lines and primary AML blasts (Weisberg et al., 2002; Armstrong et al., 2003; Knapper et al., 2006; Park et al., 2015). The second inhibitor, AC220, belongs to the second-generation FLT3 inhibitors with a higher selectivity and sensitivity against FLT3 mutations and promising activity in AML clinical trials (Chao et al., 2009; Zarrinkar et al., 2009; Gunawardane et al., 2013; Kampa-Schittenhelm et al., 2013; Park et al., 2015) (Figure 16, right).
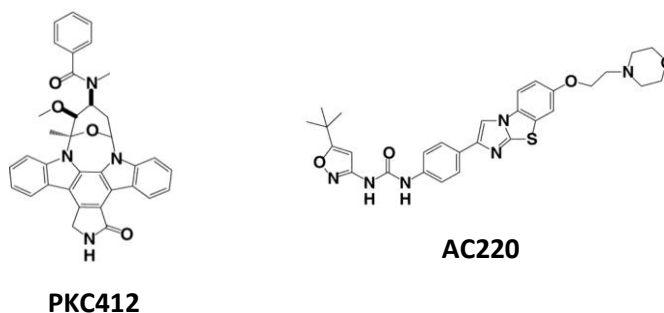
Figure 16. Chemical structure of both FLT3 inhibitors investigated. Left panel: PKC412 (Midostaurin); Right panel: AC220 (Quizartinib) (Image from Zarrinkar et al., 2009).

To assess the biological response to PKC412 and AC220 *in vitro*, equal numbers of Ba/F3 transformed cells were cultured with different concentrations of each TKI (10 nM, 50 nM and 100 nM) for 24 hours. The dissolvent of each drug was used as negative control (DMSO for PKC412 and H_2O for AC220), and a *standard* ITD mutant was included as positive control. Apoptosis was measured by flow cytometry analysis after staining the cells with propidium iodide (Nicoletti et al., 1991). This method effectively separates apoptotic cells from viable

cells according to the DNA content; cells with a DNA content less than 2n (*subG1 cells*) were defined as apoptotic. After 24 hours, PKC412 treatment resulted in a dose-dependent increase in apoptosis in ITDL601H(10) mutants (from 16.7% at 10 nM to 27.2% at 50 nM and 30.7% at 100 nM) and ITDFV605YF(14) mutants (from 9.5% at 10 nM to 13.1% at 50 nM and 16.4% at 100 nM) (Figure 17A). Moreover, these results were compared to data that was previously generated in our group using different mutants (Mack, Dissertation, 2014). Here, ITDL601H(10) showed similar sensitivity to PKC412 over all concentrations, while ITDFV605YF(14) displayed slight decreased sensitivity at the highest concentration (100 mM) (Figure 17C). Similarly, AC220 treatment resulted in a dose-dependent increased apoptosis in ITDL601H(10) cells (from 7.9% at 10 nM to 25.6% at 50 nM and 26.7% at 100 nM) and ITDFV605YF(14) (from 6.8% at 10 nM to 14.9% at 50 nM and 16.8% at 100 nM) (Figure 17B). When grouped with other JMD-ITD mutations, the percentages of apoptosis were more comparable than in the PKC412 treated cells (Figure 17D).

Taken together, these data showed that both FLT3-ITD mutants - ITDL601H(10) and ITDFV605YF(14) - were sensitive to TKI treatment. The percentage of apoptotic cells after treatment was comparable to previously characterized FLT3-ITD mutants located within the same domain (JMD), confirming the differential sensitivity to TKIs between FLT3-ITD mutations in regard to their location site (JMD vs. TKD1).

5.1.5.2. Effect of TKIs on the signaling cascade of ITDL601H(10) and ITDFV605YF(14) mutants

Most of the tyrosine kinase inhibitors are heterocyclic molecules, including PKC412 and AC220, that block the binding of ATP to the active site in a competitive fashion (Gilliland and Griffin, 2002b; Shawver et al., 2002). To confirm the inhibitory efficacy on the novel FLT3-ITD mutants, the activation of the FLT3 receptor tyrosine kinase was examined by Western Blot analysis after inhibitor treatment. Equal cell numbers were cultured in serum-starved conditions (0.5% FBS) for 3 hours followed by an additional hour of TKI treatment. As a result, PKC412 (50 nM) treatment induced an abrogation of constitutive FLT3 phosphorylation when compared to DMSO control, while FLT3 protein was equally expressed in all samples (Figure 18; lane 1 and lane 2). Furthermore, downstream signaling nodes are known to remain inactive as a consequence of FLT3 blockade (Pietschmann et al., 2012). In this model, activation of both STAT5 and ERK1/2 was equally inhibited upon TKI treatment in all FLT3-ITD mutants (Figure 18; lane 3 and lane 5), while total STAT5 and ERK1/2 were equally expressed in all samples (Figure 18; lane 4 and lane 6). The enzyme GAPDH was used as loading control (Figure 18; lane 5).
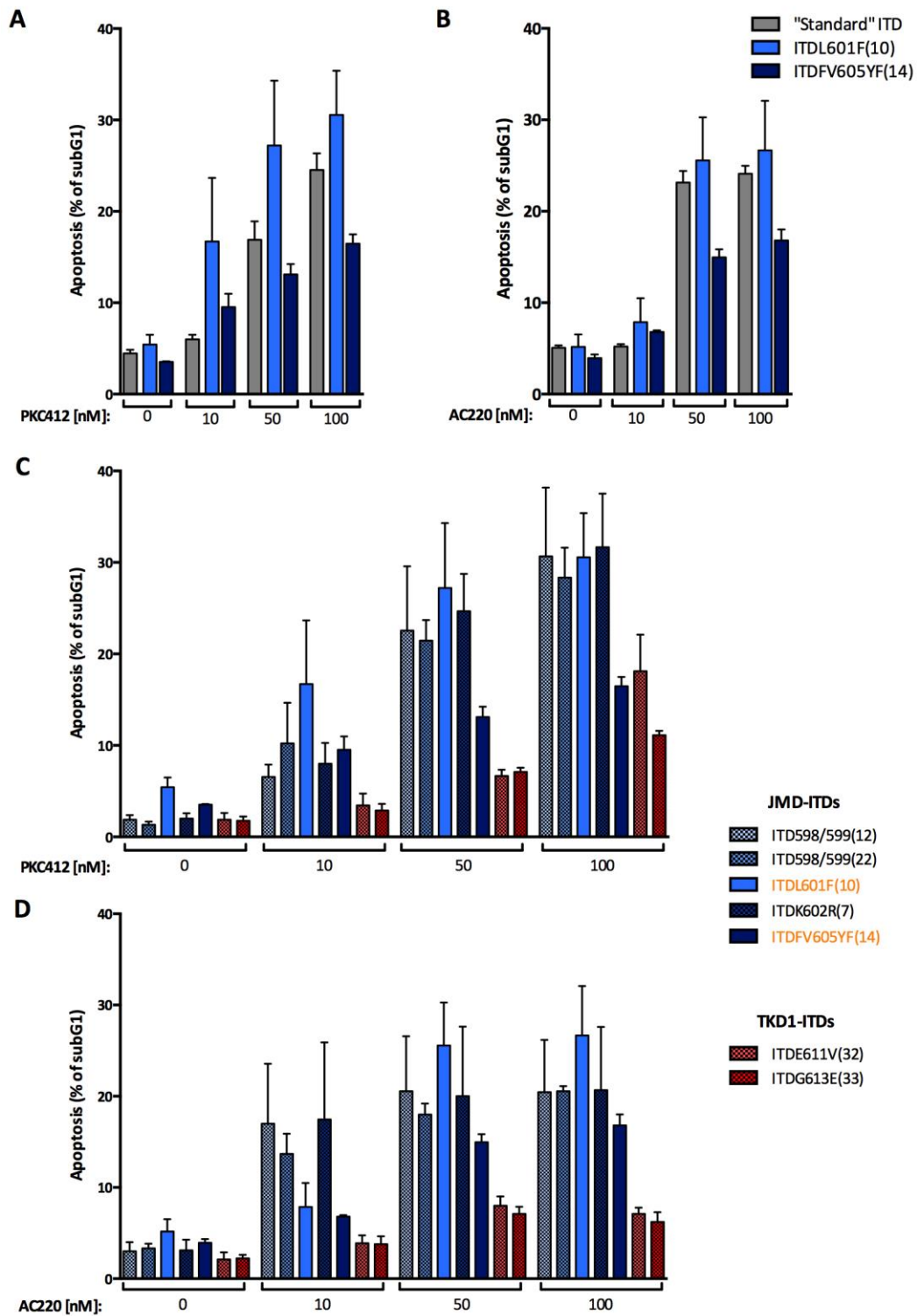
Figure 17. Inhibitory efficacy of PKC412 and AC220 in FLT3-ITD transduced Ba/F3 cells. A, B) Thirty thousand cells seeded in IL-3 free medium were treated with different concentrations (10 nM, 50 nM, 100 nM) of either PKC412 (A) or AC220 (B). A "standard" ITD (ITD598/599(12)) was included in the analysis as a positive control. DMSO (A) and water (B) were included as negative controls. After 24 hours, the percentage of apoptotic cells was determined by propidium iodide (PI) staining. Ba/F3 cells transduced with the novel FLT3-ITD mutations – ITDL601F(10) and ITDFV605YF(14) – showed a dose-dependent sensitivity to PKC412 and AC220 (n=3; mean ±SD). **C, D)** Analysis of previously described JMD-ITDs (blue) and TKD1-ITDs (red) along with the newly identified FLT3-ITDs. Efficacy of TKIs on ITDL601F(10) and ITDFV605YF(14) mutants was comparable to other JMD-ITDs in contrast to the decreased sensitivity observed in TKD1-ITDs.

| **Results**

Altogether, these results confirmed the inhibitory efficacy of PKC412 treatment on both FLT3-ITD mutants with a complete abrogation of FLT3 signaling. Moreover, the inhibitory effect was comparable to other FLT3-ITD mutations located within the JMD or TKD1 regions.
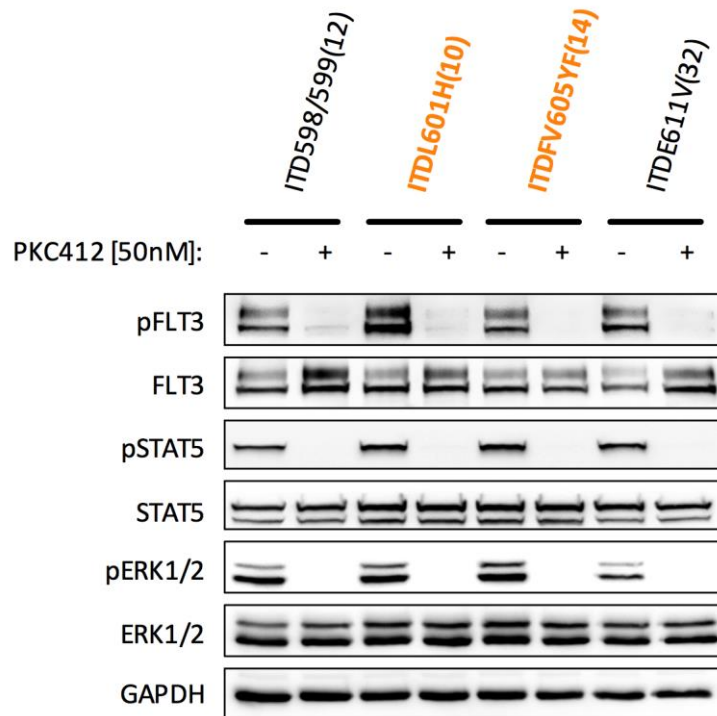
Figure 18. Inhibition of FLT3 signaling and its downstream targets STAT5 and ERK1/2 in FLT3-ITD mutants. Western blot analysis of Ba/F3 transduced cells. Cells were starved for 3 hours and then treated with 50 nM PKC412 or DMSO control, respectively, for 1 hour before preparation of total cell lysates. Inhibitory efficacy in both novel FLT3-ITD mutants (orange) was comparable to JMD-ITD (ITD598/599(12)) and TKD1-ITD (ITDE611V(32)) mutants. Novel FLT3-ITD and previously characterized FLT3-ITD mutants showed equal sensitivity to PKC412 indicated by the loss of constitutive FLT3 phosphorylation (lane 1) and the downstream signaling molecules STAT5 (lane 3) and ERK1/2 (lane 5). Total FLT3, STAT5 and ERK1/2 protein expression remained unchanged in all FLT3-ITD mutants (lane 2, lane 4 and lane 6, respectively). GAPDH was used as a loading control (lane 7). Representative blot of three independent experiments is shown.

60

5.2. Functional characterization of FLT3-ITD mutations *in vivo*

Up to date, all FLT3-ITD mutations that have been investigated were located within the JMD region (Kelly et al., 2002; Lee et al., 2005; Lee et al., 2007; Li et al., 2008; Fortier and Graubert, 2010). Therefore, a main goal of this work was to investigate the functional significance and transforming potential of several FLT3-ITD mutations grouped by their location (JMD vs. TKD1) using an *in vivo* model.

5.2.1. Retroviral bone marrow transplant model

To assess the functional role of the different FLT3-ITD mutations *in vivo*, a retroviral bone marrow transplant (BMT) model was used. As illustrated in Figure 19, donor BALB/c mice were treated intravenously by lateral tail vein injection with 5-fluorouracil (150 mg/kg) in order to deplete lineage-committed progenitors and stimulate cell cycle entry of more immature and quiescent stem cells (Radley and Scurfield, 1979). Bone marrow cells were harvested 5 days post-treatment and transduced with virus-containing supernatant for each FLT3_PIG construct. Viral particles were produced using the same retroviral pMSCV-PIG constructs as described earlier for *in vitro* studies. Transduced cells were selected with puromycin (1 ng/µl) starting 48 hours after infection, and, after 36 additional hours, transduction efficiency was analyzed by flow cytometry for expression of the GFP reporter gene (GFP$^+$). To ensure a comparative investigation of each FLT3-ITD mutation, equal fractions of GFP$^+$ cells (70000 cells) were injected along with 5×10^5 supporter cells into lethally irradiated (13 Gy) female recipient BALB/c mice. Percentage of GFP$^+$ cells in the peripheral blood was measured by flow cytometry four weeks post-transplant in order to confirm engraftment. A preliminary experiment with a well-characterized FLT3-ITD construct (ITDK602R(7)) was performed to establish the BMT model. As a result, all recipient mice succumbed to the disease. However, the amount of transformed cells (GFP$^+$) was already too high at week 4 post-transplant and disease penetrance was too fast with a survival up to 49 days (Figure 20A-B). In order to extend the time frame of disease development, the number of supporter cells was finally increased from 2.5×10^5 up to 5×10^5 cells.

Retroviral transduction

Bone marrow transplant
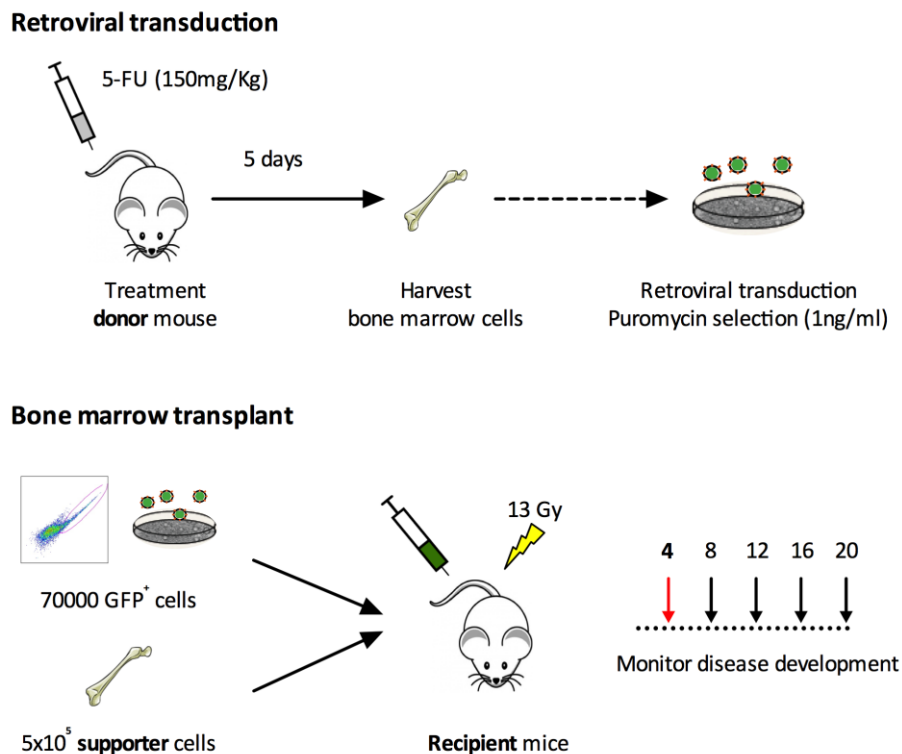
Figure 19. Experimental scheme of the retroviral bone marrow transplant model. Donor mice (BALB/c) were injected with 5-FU (150 mg/kg) to deplete mature cells and induce cell cycle entry of progenitor cells. After 5 days, primary bone marrow cells were harvested and transduced with retroviral particles of the respective ITD construct followed by selection with puromycin for 36 hours. Equal numbers of GFP$^+$ cells were injected along with supporter cells into lethally irradiated (13 Gy) female recipient mice. Cell engraftment was measured 4 weeks post-transplant (red arrow), while disease development was monitored every 4 weeks or under signs of sickness.

Transplantation of FLT3-ITD mutated cells is known to induce a lethal hematopoietic disorder characterized by an increased white blood cell count (leukocytosis) and spleen enlargement produced by extramedullary organ infiltration (splenomegaly) (Kelly et al., 2002; Grundler et al., 2005; Fortier and Graubert, 2010). Recipient mice were regularly monitored for signs of disease, including peripheral blood analysis and physical examination (fur, motility, posture, loss of weight and other signs of distress), in order to determine the time of sacrifice. Peripheral blood was analyzed by flow cytometry to determine the amount of GFP$^+$ cells, and the blood count was analyzed using an ADVIA 2120 analyzer. Since disease progression did not always follow the same pattern, each sign of disease was thoroughly scored to ensure the welfare of the animal (Appendix 1).
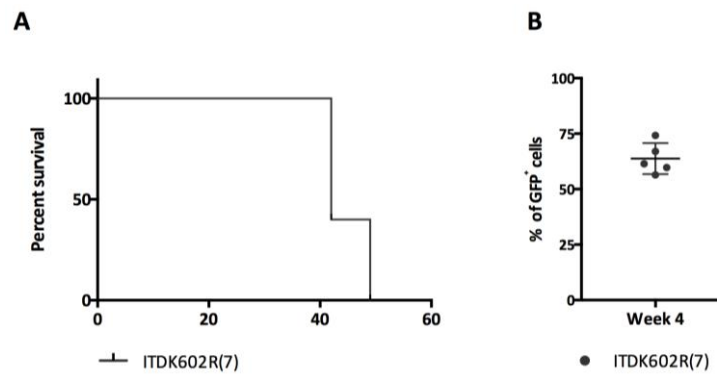
Figure 20. Preliminary BMT experiments using a well-characterized FLT3-ITD construct. A) Kaplan Meier survival curve of recipient mice receiving cells transformed with the ITDK602R(7) (n=5). **B)** Flow cytometry analysis of peripheral blood from recipient mice 4 weeks post-transplant. High penetrance of GFP$^+$ cells was already observed in all recipient mice (n=5; mean $\pm$SD).

5.2.2. Disease development in recipient mice transplanted with single FLT3-ITD mutations

To assess the functional biology of several FLT3-ITD mutations in regard to their location site, four JMD-ITDs - ITD598/599(12)_PIG, ITDK602R(7)_PIG, ITDL601H(10)_PIG and ITDFV605YF(14)_PIG - and two TKD1-ITDs - ITDE611V(32)_PIG and ITDG613E(33)_PIG - were investigated using the retroviral BMT model. Wild-type FLT3 and the empty pMSCV_PIG vector were included as negative controls. Transduced bone marrow cells were counted and analyzed by flow cytometry to confirm GFP expression and to further define equal numbers for transplantation. As illustrated with three representative flow analyses in Figure 21A, transduction of primary murine bone marrow cells was successful in all pMSCV-PIG_FLT3 constructs. The expression levels were equivalent between wild-type FLT3 and FLT3-ITD mutations (Figure 21B).
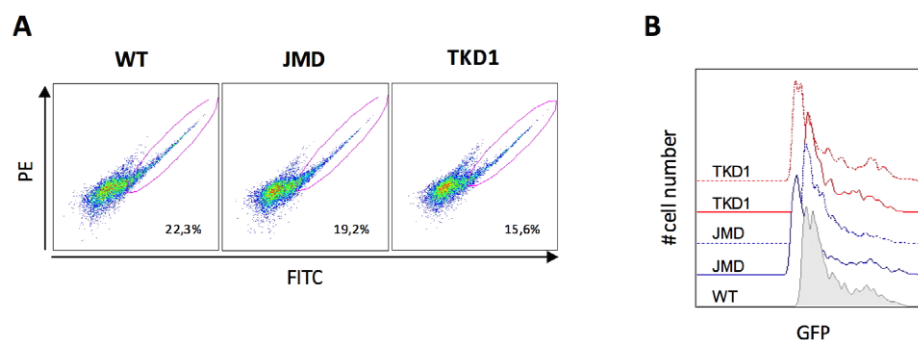
Figure 21. Expression analysis of wild-type FLT3 and FLT3-ITD transduced primary murine bone marrow cells. A) Bone marrow of 5-FU pre-treated mice was transduced with equivalent virus volume for different FLT3 constructs. After infection and selection with puromycin, transduction efficiency was analyzed by flow cytometry. The GFP$^+$ population was gated in a FITC against PE channel dot plot to exclude auto-fluorescence. Representative data of each group – wild-type FLT3 (WT), JMD and TKD1 – is shown. Viable GFP$^+$ cells are encircled and the percentage is indicated. **B)** GFP expression following retroviral transduction with different ITD constructs was analyzed in a histogram plot. Comparable GFP expression levels were observed in primary murine bone marrow cells transduced with the different FLT3 construct.

Mice receiving bone marrow cells transduced with either wild-type FLT3 or the empty pMSCV_PIG vector successfully engrafted with a mean of 7.38% and 7.53% GFP$^+$ cells, respectively, as analyzed in peripheral blood 4 weeks post-transplant. Although the percentage of GFP$^+$ cells slightly dropped over time, a continuous presence of transformed cells was observed in peripheral blood until the experimental endpoint. Control mice had normal survival with a follow-up of more than 140 days (Figure 22A; Table 18). In contrast, mice receiving cells transduced with either JMD-ITD or TKD1-ITD mutations showed differences in disease development depending on the ITD location site. All JMD-ITD mutations induced a lethal hematopoietic disorder, while TKD1-ITDs showed higher disease latency compared to JMD-ITDs. Approximately 95% of recipient mice transplanted with JMD-ITD mutations (17 of 18 mice) succumbed to the disease after a median survival of 101 days (Figure 22B; Table 18). When analyzed separately, each JMD-ITD mutation showed similar median survivals (ITDVF605YF(14) 70 days, ITDL601F(10) 98 days, ITDK602R(7) 105 days and ITD598/599(12) 112 days) (Figure 22B; Table 19). Interestingly, FLT3-ITDs located within the TKD1 region led to a lower degree of penetrance and delayed onset of disease with only 15% of lethality (2 of 13 mice) (Figure 22A; Table 18). While ITDE611V(32) showed less than 25% disease penetrance, no mouse receiving cells transduced with ITDG613E(33) succumbed to disease (Figure 22B; Table 19). Unexpectedly, JMD-ITD mutations revealed a significant increased lethality and penetrance when compared to TKD1-ITD mutations (Figure 22A; $p < 0.0001$). These data suggest a distinct transforming potential between FLT3-ITD mutations in regard to their ITD location.

Table 18. Summary of control, JMD-ITD and TKD1-ITD recipient mice. Transplanted mice were grouped by control, JMD-ITD and TKD1-ITD mutations. Analyzed data include number of mice, survival time in days, number of WBC counts, spleen enlargement and percentage of GFP$^+$ transformed cells in bone marrow. Median values are shown in brackets.

Group	No. of mice	Survival time, d (median)	WBC counts, 10^9 per L (median)	Spleen weight, mg (median)	GFP$^+$ cells in BM, % (median)
Control	12	140 (140)	4.1-16.8 (9.35)	80-140 (100)	0.6-9.7 (2.925)
JMD-ITD	18	49-140 (101)	3-198.7 (22.8)	110-670 (290)	8.63-98.5 (37.2)
TKD1-ITD	13	119-140 (140)	3.4-87.9 (9.2)	60-950 (100)	0.084-98.7 (1.63)

A

B
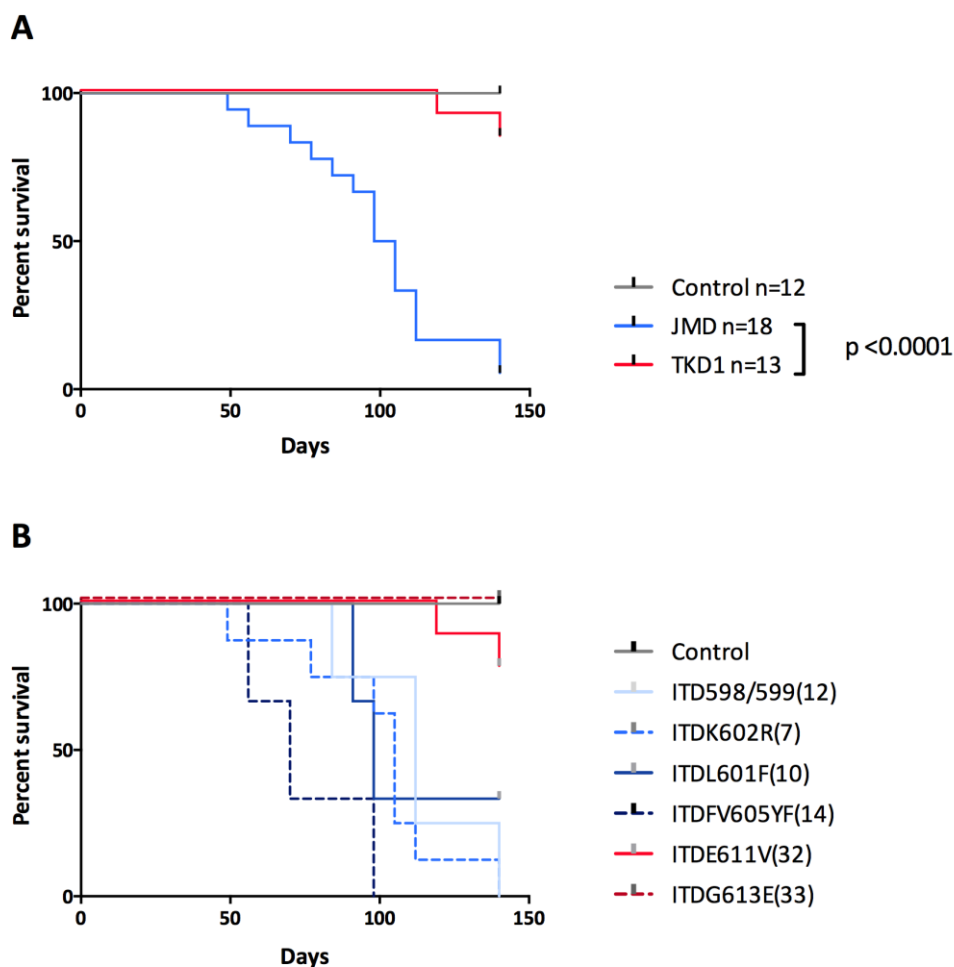
Figure 22. Kaplan-Meier survival curves of control and FLT3-ITD transplanted mice. A) All mice transplanted with transduced primary bone marrow cells were grouped by ITD location site. TKD1-ITD transduced cells (red) showed a significant delayed onset of disease and reduced penetrance with a survival percentage >80% compared to <10% in JMD-ITDs (blue). Survival analysis was calculated using a Log-rank (Mantel Cox) test. (n=13 TKD1-ITD vs. n=18 JMD-ITD; p<0.0001). **B)** Survival curve of mice transplanted with ITD598/599(12) (n=4), ITDK602R(7) (n=8), ITDL601F(10) (n=3), ITDFV605YF(14) (n=3), ITDE611V(32) (n=9) and ITDG613E(33) (n=4). Control represents mice transplanted with either empty pMSCV-PIG (n=8) or wild-type FLT3 (n=4) transduced cells.

Table 19. Summary of mice transplanted with different FLT3-ITD mutation. Transplanted mice were separated by FLT3-ITD mutation (construct). Analyzed data includes number of mice with diseased mice in brackets, survival time in days, number of WBC counts, spleen enlargement and percentage of GFP$^+$ transformed cells in bone marrow. Median values are shown in brackets.

Construct	No. of mice (diseased)	Survival time, d (median)	WBC counts, 10^9 per L (median)	Spleen weight, mg (median)	GFP$^+$ cells in BM, % (median)
598/599(12)	4 (4)	84-140 (112)	12.1-121 (18.05)	110-670 (225)	30.3-77.2 (53.85)
L601F(10)	3 (2)	91-140 (98)	5.6-19.3 (16.5)	90-190 (160)	8.63-17.4 (13.2)
K602R(7)	8 (8)	49-140 (105)	3-198.7 (25.81)	160-560 (305)	12.9-98.5 (66.8)
FV605YF(14)	3 (3)	56-98 (70)	8.5-37.4 (25.3)	200-440 (290)	10.3-37.7 (11.2)
E611V(32)	9 (2)	119-140 (-)	3.4-87.9 (11.2)	70-950 (100)	0.29-98.7 (2.77)
G613E(33)	4 (0)	140 (-)	5.9-18.7 (7.8)	60-120 (75)	0.1-1.41 (0.23)

5.2.3. Characterization of the disease phenotype induced by FLT3-ITD mutations

Single genetic mutations are insufficient to induce AML in humans, and the same holds truth when using animal models. However, retroviral BMT models of single mutations are known to develop hematologic disorders that recapitulate the main phenotypic features of AML including high WBC count (leukocytosis), organ infiltration (splenomegaly) and lethality but with a lack of accumulation of immature cells (*blasts*). In this work, all sick mice were further analyzed to confirm that animal mortality was due to the development of a hematologic disorder.

At diagnosis, the majority of mice receiving cells transduced with JMD-ITD mutations developed marked leukocytosis with WBC counts ranging from 3×10^9 to 198.7×10^9 cells/L. In contrast, mice transplanted with cells transduced with TKD1-ITD mutations showed only a slight increase in WBC counts (3.4×10^9 to 19.4×10^9 cells/L), except for two animals that succumbed to the disease (32.2×10^9 and 87.9×10^9 cells/L). Control mice showed normal leukocyte values ranging from 4.1×10^9 to 16.8×10^9 cells/L (Figure 23A; Table 18). Physiological blood parameters are listed in Appendix 2. Several mice that succumbed to the disease lacked massive leukocytosis, and for this reason additional signs of disease were included to confirm illness. Physical examination allowed to detect signs, such as hunched back, ruffled fur and reduced motility along with cachexia. Moreover, mice that succumbed to the disease showed remarkable spleen enlargement with weights ranging from 110 mg to 607 mg in JMD-ITD cohorts and 190 mg to 950 mg in diseased TKD1-ITD mice. Control mice as well as the rest of TKD1-ITD mice showed standard spleen weights from 80 mg to 100 mg and 60 mg to 120 mg, respectively (Figure 23B; Table 18). Peripheral blood of several FLT3-ITD animals was stained with Wright-Giemsa staining in order to confirm accumulation of transformed cells (leukocytosis) in the bloodstream (Figure 23C).

In order to confirm that leukocytosis emerged from highly proliferative transduced cells, infiltration of GFP$^+$ cells in PB and BM was analyzed by flow cytometry. Mice receiving cells transduced with JMD-ITD mutations showed, in almost all cases, a marked increase of GFP$^+$ cells in PB and BM in contrast to control mice (1.74% to 67.2% JMD-ITD vs. 0.6% to 9.7% control in PB; 8.63% to 98.5% JMD-ITD vs. 0.6% to 9.7% control in BM) (Figure 23D-E; Table 18). Both diseased TKD1-ITD mice also presented elevated GFP$^+$ cell numbers in PB (18.5% and 85.3%) with a consistent BM infiltration (97.8% and 98.7%). Healthy TKD1-ITD transplanted mice maintained a low GFP expression in PB (0.1% to 7.94%) and BM (0.1% to 8.22%) (Figure 23D-E; Table 18). For each FLT3-ITD mutation, all parameters are listed in Table 19. The bone marrow of diseased mice was analyzed using lineage-specific antibodies by flow cytometry in

order to define the immunophenotype of the overgrown population (GFP$^+$ cells). Recipient mice mostly suffered from a myeloproliferative-like disorder with most of the GFP$^+$ cells co-expressing the myeloid marker Gr1; while, several animals including both TKD1-ITD diseased mice developed a lymphoid-like disorder indicated by an overgrowth of transformed cells expressing CD8 (Figure 23F).

In summary, these results confirmed that all diseased animals developed a lethal hematologic disorder characterized by leukocytosis, splenomegaly and BM infiltration.
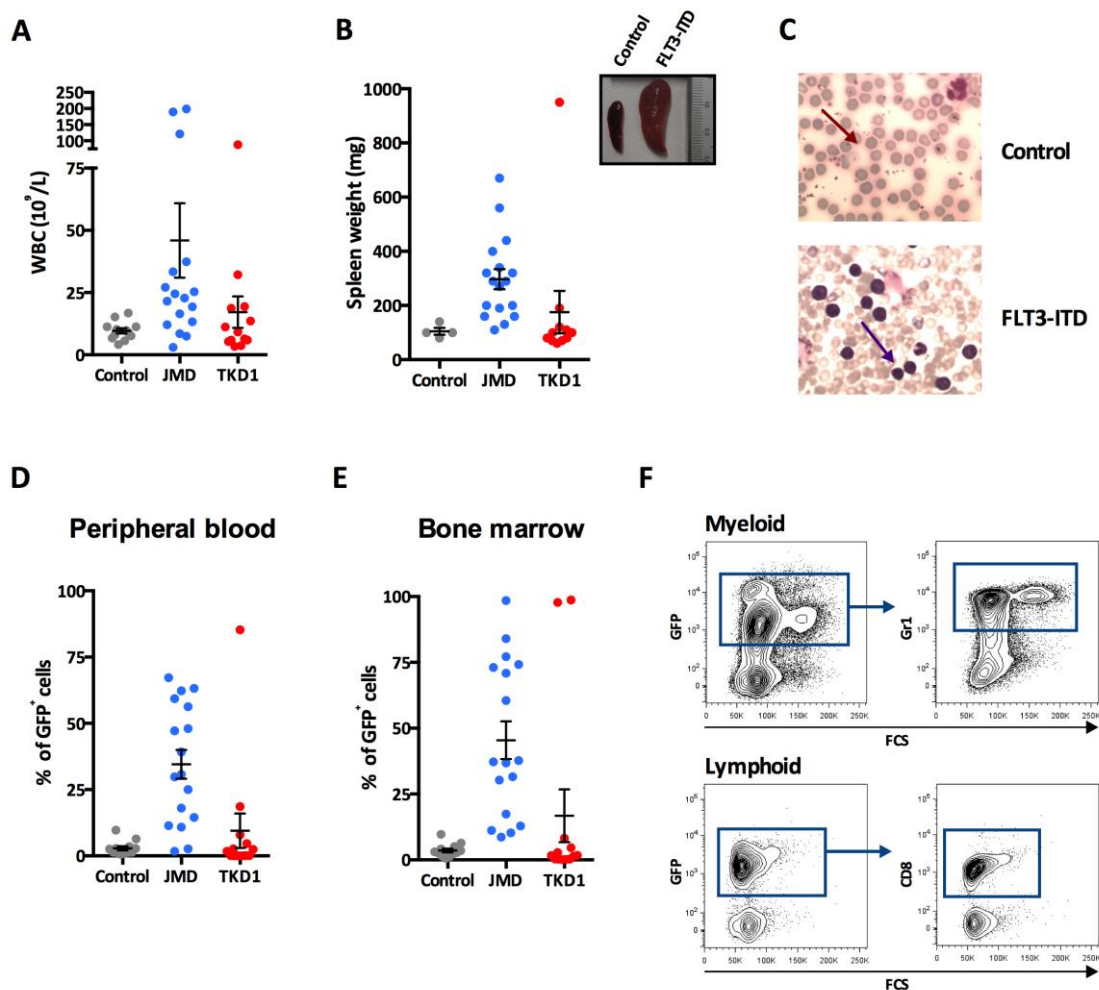
Figure 23. Disease phenotype in FLT3-ITD transplanted mice. A) Total white blood cells (WBC) counts of recipient mice - control, JMD and TKD1 - at date of sacrifice. Sick mice receiving cells transduced with JMD-ITD mutations showed an increase in WBC count compared to control. Both TKD1-ITD mice that succumbed to the disease also showed an increase in WBC counts compared to healthy TKD1-ITD mice and controls. Control represents mice transplanted with either empty pMSCV-PIG vector or wild-type FLT3 (n=12 control, n=17 JMD-ITD, n=13 TKD1-ITD; mean ±SEM). **B)** Spleen weight of recipient mice at date of sacrifice. JMD-ITD mice as well as both diseased TKD1-ITD mice showed splenomegaly compared to control mice (n=4 control, n=17 JMD-ITD, n=11 TKD1-ITD; mean ±SEM). **C)** Peripheral blood images illustrate a normal cell distribution (control) with mostly erythrocytes (red arrow) in comparison to the marked leukocytosis observed in a representative FLT3-ITD diseased recipient mouse (violet arrow) (Wright-Giemsa; magnification x63). **D, E)** Flow cytometry analysis of peripheral blood and bone marrow from recipient mice at date of sacrifice. Expansion of GFP$^+$ cells was observed in diseased mice transplanted with either JMD-ITD or TKD1-ITD mutations compared to control mice (n=12 control, n=17 JMD-ITD, n=13 TKD1-ITD; mean ±SEM) **F)** Representative flow cytometry analysis of BM cells from FLT3-ITD diseased mice. Expression levels of myeloid cells (Gr1+) and lymphoid cells (CD8+) were analyzed in viable GFP+ cells.

5.2.4. Functional biology of JMD-ITD versus TKD-ITD mutations using a competitive BMT model

Although previous *in vitro* studies revealed similar clonogenicity and proliferation between different FLT3-ITD mutations, it became evident that FLT3-ITDs located within the JMD region conferred stronger transforming potential than TKD1-ITD mutations to primary murine bone marrow cells *in vivo*. These findings suggested a divergence in proliferative and engraftment capacity between the different mutations. To assess whether JMD-ITD mutations lead to a proliferative advantage over TKD1-ITDs *in vivo*, a competitive BMT model was designed (Figure 24). Four main changes were included when compared to the standard BMT model: 1) a second vector system expressing a different reporter gene was included, 2) transduced cells were selected using fluorescence-activated cell sorting (FACS), 3) reduced cell numbers were transplanted into recipient mice and 4) two different FLT3-ITD mutations were transplanted into the same recipient mouse. The purpose of the competitive model was to transplant two populations of cells, each transduced with a different FLT3-ITD mutation, into the same recipient mouse in order to reduce experimental inter-variability (JMD vs. TKD1). A new vector system expressing a yellow fluorescent protein (YFP) was included in the experimental model in order to distinguish between both populations using flow cytometry (GFP vs. YFP). The YFP reporter gene derives from the green fluorescence protein and generates a longer wavelength emission (528nm) when compared to wild-type GFP (504-508nm) (Wachter et al., 1998). In this work, ITDK602R(7)_PIG and ITD598/599(12)_PIG were cloned into a pMSCV-YFP vector following the methodology that was previously described (please see 5.1.1.). ITDE611V(32)_YFP was already available in our department. All three pMSCV-YFP constructs were transduced in Ba/F3 parental cells and characterized *in vitro* before using them in primary bone marrow cells. As previously observed in FLT3_PIG constructs, each mutation led to long-term factor-independent growth upon IL-3 withdrawal (data not shown).

Retroviral transduction

Bone marrow transplant
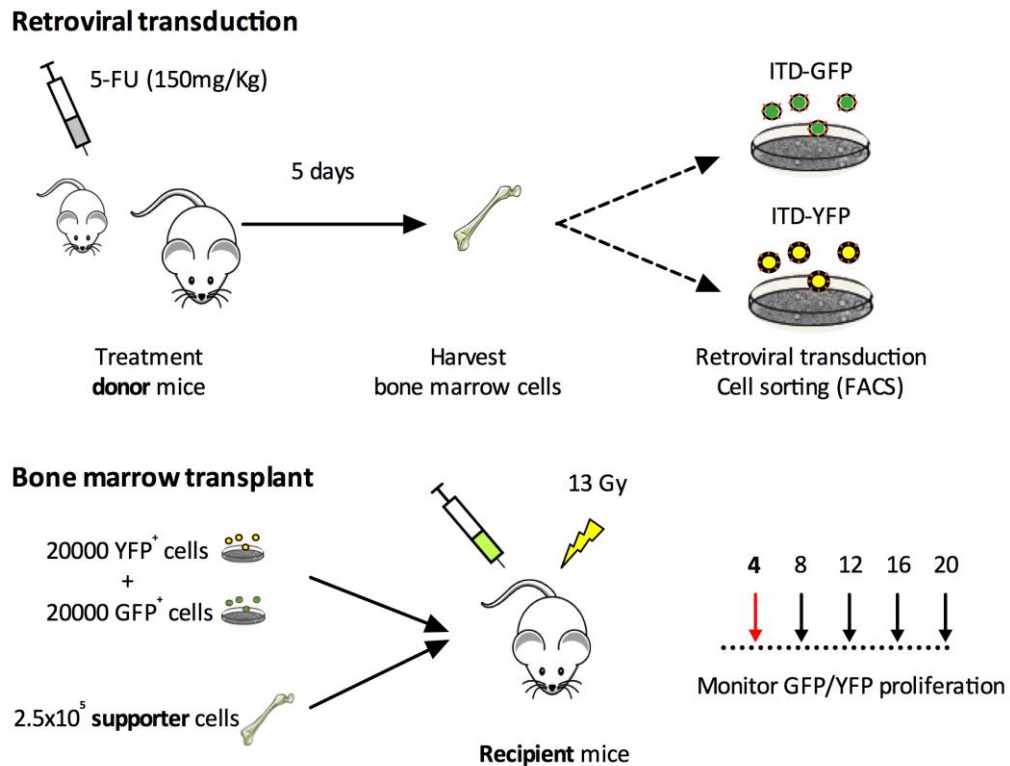
Figure 24. Experimental scheme of the retroviral competitive bone marrow transplant model. Following the BMT model previously illustrated in Figure 19, a competitive model was designed to evaluate the proliferation capacity of JMD-ITD and TKD1-ITD mutations within the same recipient mouse. Modification in the model include: 1) transduction of 5-FU pre-treated cells with two different retroviral constructs (pMSCV-PIG_ITD and pMSCV-YFP_ITD), 2) selection of transduced cells using FACS sorting, 3) transplant of equal numbers of GFP$^+$ and YFP$^+$ cells along with supporter cells into the same recipient mouse and 4) analysis of GFP and YFP expression 4 weeks post-transplant (red arrow) by flow cytometry.

Competitive bone marrow transplants were performed combining one JMD-ITD - either ITD598/599(12) or ITDK602R(7) - and one TKD1-ITD - ITDE611V(32). To avoid possible variability produced by the use of two different vector systems, both combinations (JMD_PIG vs. TKD1_YFP and JMD_YFP vs. TKD1_PIG) were investigated. Since the pMSCV-YFP vector lacks an antibiotic selection marker, transduced bone marrow cells were selected using FACS sorting. One day after sorting, equal numbers of transformed BM cells (20000 GFP$^+$/YFP$^+$ cells) for each ITD were transplanted along with 2.5 x 10^5 supporter cells into lethally irradiated (13 Gy) female recipient BALB/c mice. Disease development was monitored, and the functional biology of two different FLT3-ITD mutations was compared after transplantation. Higher levels of JMD-ITD transformed cells were detected in the peripheral blood of recipient mice when compared to TKD1-ITD cells (33.74% JMD-ITD vs. 13.78% TKD1-ITD) (Figure 25). This competitive advantage was already detected 4 weeks post-transplant and increased until the development of a lethal hematopoietic disorder.

In summary, these results confirmed the oncogenic advantage of FLT3-ITD mutations located within the JMD region compared to TKD1-ITD. By transplanting equal numbers of the

respective cells transformed with different ITD constructs into the same recipient mouse, JMD-ITDs revealed a stronger engraftment and transforming capacity than TKD1-ITD.
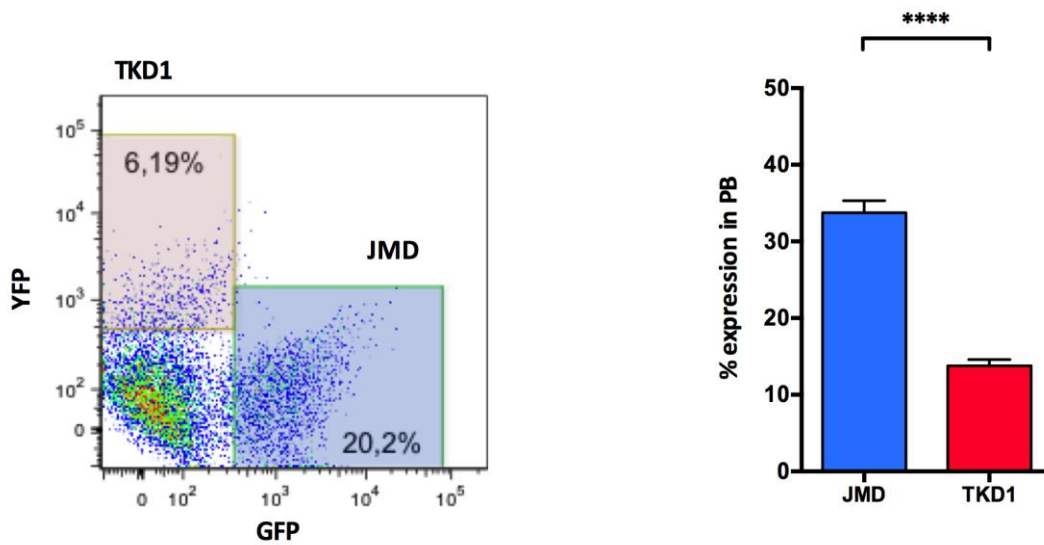
Figure 25. Analysis of recipient mice transplanted with cells harboring different FLT3-ITD mutations. Representative flow cytometry analysis of peripheral blood from mice transplanted with cells harboring different ITD mutations (JMD: blue vs. TKD1: red) (left panel); Higher expression levels of cells transduced with JMD-ITD mutations confirmed a proliferative advantage over TKD1-ITD mutations 4 weeks post-transplant. Statistical analysis was calculated using a Mann-Whitney test (n=22; mean $\pm$SEM; ****p<0.0001) (right panel).

5.2.5. Homing capacity of primary bone marrow cells transduced with FLT3-ITD mutations

The first process in bone marrow transplantation is the migration of hematopoietic cells, mostly immature stem cells, through the blood and the endothelial vasculature towards the BM niches. This process is known as homing, a fast event that involves adhesion interactions prior to engraftment and repopulation of active hematopoiesis (Lapidot et al., 2005). As described above, TKD1-ITD mutations showed reduced engraftment and disease penetrance compared to JMD-ITDs, which could be due to reduced proliferation but also to a poor homing capacity. To assess whether these findings were caused by a disability of TKD1-ITD transformed cells to reach the bone marrow niche, a homing assay was performed comparing both FLT3-ITD groups (JMD vs. TKD1). Primary bone marrow cells transduced with either ITD598/599(12)_PIG or ITDE611V(32)_PIG were transplanted into lethally irradiated mice following FACS sorting of GFP$^+$ cells. Although homing assays do not require host preconditioning by lethal irradiation, engraftment of transduced cells is dependent on this procedure in the BMT model, and identical conditions as in previous experiments were implemented. Homing of primary transduced cells was measured by flow cytometry in single femurs 16 hours after transplantation. Total cell numbers were counted in each femur prior to

flow cytometry analysis. As observed in Figure 26, both FLT3-ITD groups showed a similar number of GFP+ cells that reach the bone marrow, confirming that JMD-ITD and TKD1-ITD transduced cells possess an equivalent homing capacity.

Overall, an equal homing potential in both FLT3-ITD groups reinforced the idea that the biological differences observed between the FLT3-ITD mutations may arise from intrinsic mechanisms involved in cell proliferation and engraftment.
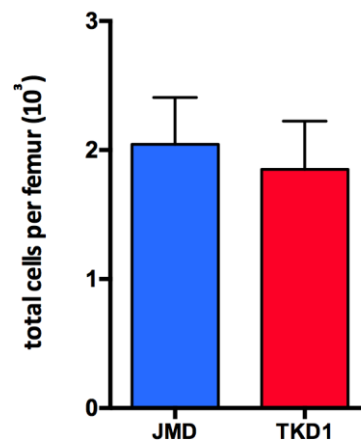
Figure 26. Homing capacity of primary bone marrow cells harboring different FLT3-ITD mutations. Sorted bone marrow cells transformed with either FLT3-ITD mutations (10.000 GFP+ cells) were transplanted into lethally irradiated recipient mice. Single femurs were harvested 16 hours post-transplant and analyzed by flow cytometry. Both FLT3-ITD mutations showed comparable numbers of cells that homed to the bone marrow. (n=3; mean ±SD).

5.2.6. Sensitivity of different FLT3-ITD mutations to tyrosine kinase inhibitors

Recently, retrospective studies have revealed a negative impact of TKD1-ITD mutations on the clinical outcome of FLT3-ITD positive AML patients (Kayser et al., 2009; Schlenk et al., 2014). Moreover, previous *in vitro* data generated in our group provided evidence that FLT3-ITD mutations located in the TKD1 region are more resistant to TKI treatment. Based on these findings, this work aimed to test the efficacy of PKC412 (Midostaurin) *in vivo*. The aim was not only to evaluate the inhibitory potential of this compound but also to compare the effect of the targeted drug on different FLT3-ITDs (JMD vs. TKD1). As experimental model, the previously described competitive BMT model was selected. After confirming engraftment, recipient mice were treated with either PKC412 (50 mg/kg/day) or vehicle control for 10 consecutive days. PKC412 was freshly prepared every day from a stock solution and administrated via oral gavage. This treatment schedule was adapted to published drug trials in mice ensuring a drug dose low enough to exclude nonspecific toxicity effects (Weisberg et al., 2002; Cools et al., 2003; Lee et al., 2005). Two weeks after the last administration of PKC412,

peripheral blood of the mice was analyzed by flow cytometry. Treatment with PKC412 led to a clear reduction of JMD-ITD transformed cells (GFP$^+$) in PB (p<0.05), while the amount of TKD1-ITD transformed cells remained unaffected (Figure 27).

Taken together, these results indicate that there is an association between ITD location and response to TKI treatment. Consistent with previous findings, FLT3-ITD mutations located within the TKD1 region showed no sensitivity to PKC412 treatment compared to JMD-ITD transformed cells *in vivo*.
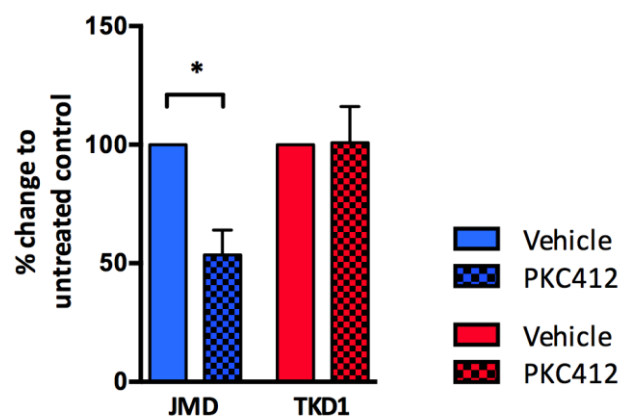
Figure 27. Inhibitory efficacy of PKC412 in mice transplanted with cells harboring different FLT3-ITD mutants. Mice transplanted with cells harboring either ITD598/599(12) or ITDE611V(32) were orally treated with PKC412 (50 mg/kg/day) for 10 days. Percentage of GFP$^+$ (JMD-ITD) and YFP$^+$ (TKD1-ITD) cells was analyzed by flow cytometry before and after treatment. JMD-ITD cells but not TKD1-ITD cells showed sensitivity to TKI treatment compare to control treatment *in vivo*. (n>5/cohort in two independent experiments; mean $\pm$SD; *p<0.05).

5.3. Assess for mechanistic consequences of distinct ITD-location

So far, the present study has shown that the ITD location alters the functional properties and response to targeted treatment of FLT3-ITD mutations. However, cellular and molecular changes involved in this differential phenotype remained unexplored. Previous studies have already reported alternative mechanisms deregulated by FLT3-ITD mutations and associated with resistance, including anti-apoptotic proteins, signaling molecules or transcription factors (Adam et al., 2006; Seedhouse et al., 2006; Sallmyr et al., 2008a; Moore et al., 2012; Puissant et al., 2014; Green et al., 2015). In order to gain insights into the mechanism underlying the biology divergence observed between FLT3-ITD mutations (JMD vs. TKD1), the transcriptional expression of target genes downstream of the FLT3 receptor was investigated in collaboration with the group of Professor Bullinger at the University Hospital Ulm. Global gene-expression profiling (GEP) on murine cells transfected with different FLT3-ITD mutations (3 JMD-ITDs and 2 TKD1-ITDs) and primary FLT3-ITD positive AML patients (33 JMD-ITD and 16 TKD1-ITD

patients) was performed. The analysis revealed 540 probe sets that were differentially expressed between JMD-ITDs and TKD1-ITDs after stringent selection (p<0.05). A closer evaluation on the basis of the expression data using a pathway enrichment analysis predicted abnormal regulation of DNA repair, chromatin organization and adhesion in TKD1-ITD mutations compared to JMD-ITDs (Arreba-Tutusaus et al., 2016). Among these regulatory mechanisms, abnormal regulation of DNA repair was selected for further validation. FLT3-ITD mutations are associated with enhanced DNA damage - especially double strand breaks (DSBs) - and aberrant DNA repair - potentially misrepair - that may lead to increased genomic instability and therapy resistance. (Seedhouse et al., 2006; Stanicka et al., 2015). In order to examine the impact of the ITD location site on DNA damage and repair, H2AX phosphorylation was investigated in different FLT3-ITD mutants using Western blot analysis. Phosphorylation of H2AX, resulting in γH2AX, is an early event and a well-established chromatin modification associated with formation of DSBs and DNA repair (Banath et al., 2004; Seedhouse et al., 2006; Muslimovic et al., 2012). In this work, DNA damage was induced in FLT3-ITD mutants using ionizing radiation (Muslimovic et al., 2012). Equal numbers of FLT3-ITD transformed Ba/F3 cells (JMD vs. TDK1) were irradiated (3 Gy), and non-irradiated cells were included as a negative control. Whole cell lysates were prepared after 60 and 120 minutes incubation in order to monitor changes in γH2AX. As a result, treated JMD-ITD and TKD-ITD mutants showed increased levels of γH2AX when compared to untreated samples, however no significant differences could be observed between the treated groups (JMD vs. TKD1) (Figure 28; lane 1). GAPDH expression was used as a loading control (Figure 28; lane 2).
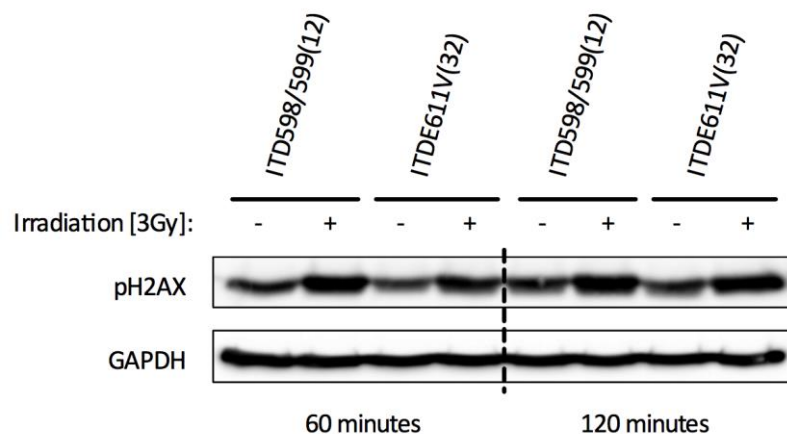
Figure 28. Expression of γH2AX in FLT3-ITD transduced Ba/F3 cells after induction of DNA damage. Transduced cells were either irradiated (3 Gy) or not treated, and then cultured for 60 and 120 minutes, respectively, before preparation of total cell lysates. Both FLT3-ITD mutants showed H2AX phosphorylation under basal conditions. Upon cellular stress (irradiation), DNA damage was induced increasing the phosphorylation of H2AX. Comparable levels of H2AX phosphorylation were observed in both FLT3-ITD groups regardless of the ITD insertion site. GAPDH was used as a loading control. Representative blot of three independent experiments is shown.

Since it was difficult to see any changes between the different ITD groups using Western blot analysis, a more sensitive and quantitative method was chosen. Immunocytochemical approaches allow the temporal and spatial quantification of individual γH2AX nuclear foci to estimate the incidence of DSB formation in single cells (Mah et al., 2010; Medunjanin et al., 2010; Podhorecka et al., 2010). Thus, FLT3-ITD transformed Ba/F3 cells were treated as described above, and γH2AX foci formation was detected by fluorescence microscopy using a phospho-antibody against γH2AX (Ser[139]). Cell nuclei were stained with DAPI (1 μg/ml). Images were analyzed using ImageJ and the average number of foci was determined. As observed in Figure 29, treated TKD1-ITD cells showed significant reduction in the average number of γH2AX foci in comparison to JMD-ITD mutants 120 minutes after induction of DNA damage (p<0.0001). In contrast, non-irradiated FLT3-ITD cells demonstrated a similar average number of γH2AX foci.

Taken together, these data suggest DNA repair as a potential mechanism in the biological divergence between FLT3-ITD mutations in regard to the ITD location (JMD vs. TKD1). After the induction of DNA damage, TKD1-ITD mutants showed less DSBs that JMD-ITDs, which may be due to higher levels of DNA repair in these cells.
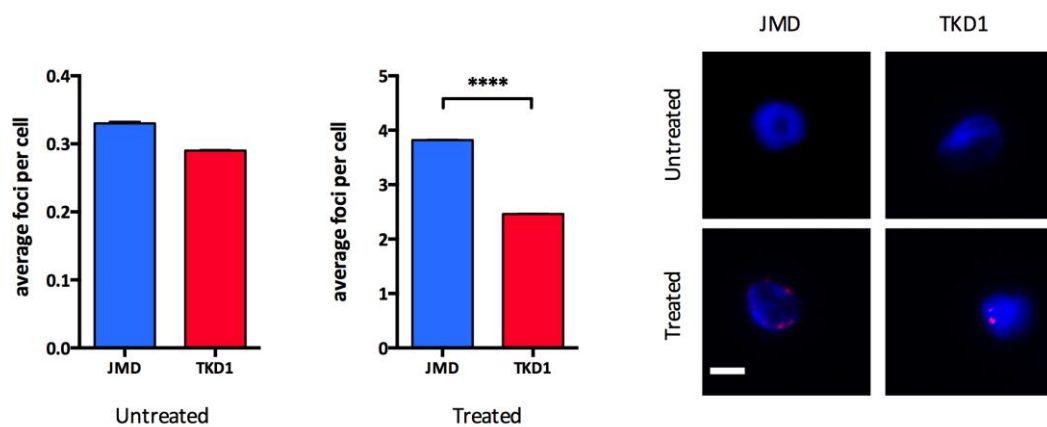
Figure 29. H2AX foci formation in FLT3-ITD transduced Ba/F3 cells. Transduced Ba/F3 cells were treated and cultured as previously described. After 120 minutes, average of γH2AX foci per cell was calculated after analyzing single cell nuclei by fluorescence microscopy. Upon cellular stress (3 Gy), TKD1-ITD cells revealed a lower average number of γH2AX foci when compared to the JMD-ITD group (right panel). A similar average of γH2AX was detectable in non-irradiated cells (left panel) (n=3; 100-300 events per experiment were counted; mean ±SEM; ****p<0.0001). Representative images illustrate the absence of foci in untreated cells and foci formation (red dots) in treated JMD-ITD and TKD1-ITD mutants (bar = 10μm).

6. Discussion

A novel subset of FLT3-ITD mutations located within the first tyrosine kinase domain (TKD1) has been identified as an independent unfavorable prognostic factor in AML (Kayser et al., 2009; Schlenk et al., 2014). Moreover, *in vitro* studies in our group suggested that murine TKD1-ITD transformed cells are significantly less sensitive to tyrosine kinase inhibitor (TKI) treatment although cellular signaling and transforming potential are comparable among FLT3-ITD mutants (JMD vs. TKD1) (Ballaschk, Dissertation, 2014; Mack, Dissertation, 2014). The present work aimed to characterize the impact of the ITD location site on the functional biology and the response to treatment of FLT3-ITD mutations *in vitro* and *in vivo*. Here, primary resistance against targeted treatment was confirmed for TKD1-ITD mutations, and surprisingly, TKD1-ITD mutations also revealed reduced transforming potential and disease penetrance *in vivo.* Additionally, early experiments combining cellular models and patient samples suggested DNA damage response as a potential mediator of the differential biology observed between FLT3-ITD mutations.

6.1. Functional characterization of two novel FLT3-ITD mutations *in vitro*

Prior *in vitro* studies have shown an equal transforming potential of FLT3-ITD mutations regardless of their location (JMD vs. TKD1). However, same activating mutations revealed differential sensitivity to first and second generation TKIs (Ballaschk, Dissertation, 2014; Mack, Dissertation, 2014). The first part of this study sought to support these findings by extending the spectrum of ITD mutations. Two novel activating FLT3 mutations were isolated, characterized and compared to previously studied FLT3-ITD mutations *in vitro*. Through the screening of genomic material from FLT3-ITD positive AML patients and human cell lines, such as MV4;11 and Molm13, two novel FLT3-ITD mutations were successfully identified and cloned. Both genetic aberrations belonged to the group of JMD-ITDs. The mutation isolated from patient material, ITDL601H(10), is inserted in the JM-zipper region. In contrast to the well-characterized ITDK602R(7) (Kelly et al., 2002; Lee et al., 2007) also located within the same region, ITDL601H(10) contains a longer duplication of 10 amino acids (AA) and includes both tyrosine residues present in the amino acid motif: **Y**VDFREYE**Y** (Tyr591-Tyr599). In addition, ITDL601H(10) exchanges a hydrophobic and uncharged leucine by a positive charged histidine, whereas the AA substitution in ITDK602R(7) involves the exchange of positive charged amino acids by replacing lysine to arginine. The mutation isolated from the human cell

line MV4;11, ITDFV605YF(14), is the first mutation located in the hinge region with a length of 14 amino acids. Another distinctive feature of this mutation is the replacement of two amino acids with hydrophobic side chain, phenylalanine and valine, by AA that belong to the same group, tyrosine and phenylalanine. These novel mutations as well as additional FLT3-ITDs, which were previously identified in other studies, were cloned into a pMSCV-based retroviral vector system (pMSCV-PIG).

Transduction of IL-3 dependent murine cell lines (Ba/F3 and 32D) is commonly used to investigate mutated genes involved in cell signaling (Mizuki et al., 2000; Kelly et al., 2002; Spiekermann et al., 2002; Breitenbuecher et al., 2009b; Huang et al., 2013; Janke et al., 2014; Nonami et al., 2015). The rationale behind this *in vitro* model is that the stable expression of constitutively activated genes involved in signal transduction and cellular growth, such as NRAS or FLT3, leads to an IL-3 independent survival generating single cellular models. These *in vitro* models can be used to investigate functional relevance and signaling mechanisms. In this work, new cell lines were generated for each FLT3-ITD mutation to characterize their transforming potential *in vitro*. Besides the novel ITDL601H(10)_PIG and ITDFV605YF(14)_PIG constructs, previously characterized FLT3-ITD mutations - ITD598/599(12)_PIG, ITD598/599(22)_PIG, ITDK602R(7)_PIG, ITDE611V(32)_PIG and ITDG613E(33)_PIG - were also included as controls. Each retroviral construct was successfully transduced in parental Ba/F3 and 32D cells, and the respective cellular models were established after a period of puromycin selection (Figure 13). The level of GFP expression was measured to quantify the amount of transduced cells in culture. After achieving stable gene expression, a pool of transformed cells was deprived of IL-3 and puromycin in order to select for FLT3-ITD positive cells with proliferative advantage (Figure 13). Both ITDL601H(10) and ITDFV605YF(14) mutations supported a long-term factor-independent growth, confirming their transforming capacity. As a result, two novel mutants were created providing a starting point for further functional and molecular analyses.

Internal tandem duplications are defined as gain-of-function mutations that confer uncontrolled proliferation and survival through intrinsic mechanisms. In this work, the transforming potential of each FLT3-ITD mutant was further investigated using methylcellulose-based assays. This assay assesses the ability of single transformed cells to proliferate in cytokine-free semi-solid medium. Thus, only cells with autonomous growth are able to survive and form colonies, termed colony-forming units (Mizuki et al., 2000; Miller and Lai, 2005). This experiment confirmed a factor-independent survival of both FLT3-ITD mutants - ITDL601H(10)_PIG and ITDFV605YF(14)_PIG (Figure 14A-B). These results are in line with

previous findings, in which several FLT3-ITD mutations - cloned into the pAL-based vector system - revealed similar clonal growth comparable to wild-type FLT3 cells stimulated with IL-3 (Mizuki et al., 2000; Ballaschk, Dissertation, 2014; Mack, Dissertation, 2014). However, colony-forming cell assays address the intrinsic potential of a single cell to form clones rather than provide relevant information about the proliferative activity. Therefore, a second *in vitro* assay was included in this work to evaluate the metabolic activity of transformed cells as readout of cell viability and proliferation (MTS assay). All investigated FLT3-ITD mutants showed equivalent proliferation rates comparable to wild-type FLT3 cells stimulated with IL-3 (Figure 14C-D). These data confirmed the clonogenicity and the factor-independent survival of both FLT3-ITD mutations, ITDL601H(10) and ITDFV605YF(14), which was comparable to other FLT3-ITD mutations regardless of the ITD location (JMD vs. TDK1).

Once the transforming potential of each mutation was analyzed, the next step was to confirm the deregulated function of the kinase. Internal tandem duplications are believed to destabilize the auto-inhibitory conformation of the receptor tyrosine kinase (RTK) leading to a ligand-independent *cis*-phosphorylation of important tyrosine residues, including Tyr^{589}, Tyr^{591} and Tyr^{599} (Rocnik et al., 2006; Toffalini and Demoulin, 2010; Chan, 2011). Hence, autonomous growth is sustained by a constitutive phosphorylation of FLT3 and concomitant activation of downstream signaling pathways, such as PI3K/AKT and MAPK, as well as STAT5, which is not activated in wild-type FLT3 signaling (Mizuki et al., 2000; Zhang et al., 2000; Birkenkamp et al., 2001; Brandts et al., 2005; Nabinger et al., 2013). In line with this, all FLT3-ITD mutations, including ITDL601H(10) and ITDFV605YF, led to a constitutive phosphorylation of FLT3 as well as activation of STAT5 and ERK1/2 (Figure 15A-B). In contrast, activation of STAT5 and ERK1/2 was only detected in wild-type FLT3 transformed cells upon IL-3 stimulation, while FLT3 remained de-phosphorylated due to the absence of FLT3 ligand (Figure 15B). These data defined both FLT3-ITDs - ITDL601H(10) and ITDFV605YF(14) - as gain-of-function mutations that enhance cell proliferation and survival through the constitutive activation of FLT3 and its downstream pathways.

Following the structural model proposed by Griffith et al., the constitutive activation of both FLT3-ITD mutations - ITDL601H(10) and ITDFV605YF(14) - may be explained by a disruption of the autoinhibitory conformation (Griffith et al., 2004). While ITDL601H(10) is located in the JMD-Z region, which is important to orientate and maintain the inactive conformation, ITDFV605YF(14) is inserted within the hinge region, which is involved in the transition from unattached to attached conformations. Moreover, both ITD sequences embrace the residues Tyr^{591} and Tyr^{599}, which are crucial for the activation of downstream molecules, as well as the

residue Arg[595], all included in the stretch: **Y**VDFR̲EYE**Y** (Rocnik et al., 2006; Vempati et al., 2007). *In vitro* studies have showed that this positive amino acid (Arg[595]) is critical for the transforming potential of FLT3-ITD mutations. A single duplication of this residue in wild-type FLT3 was enough to induce ligand-independent growth and constitutive activation of STAT5. The substitution of this AA in FLT3-ITD mutations disrupted its transforming potential (Vempati et al., 2007). However, further crystallographic studies of FLT3 mutations would be needed to confirm this hypothesis and to better understand conformational changes.

Overall, these data confirmed that the two novel FLT3-ITD mutations - ITDL601H(10) and ITDFV605YF(14) - conferred factor-independent transforming potential to murine hematopoietic cells through the constitutive activation of the FLT3 receptor tyrosine kinase and related downstream signaling molecules.

Activating FLT3 mutations are considered as powerful therapeutic targets in AML, leading to a constant search of efficient tyrosine kinase inhibitors (TKI). For over a decade, several TKIs have been investigated from the bench - using cellular models, patient material and mouse models - to clinical trials (Zhao et al., 2000, Naoe et al., 2001; Tse et al., 2001; Levis et al., 2002; Levis et al., 2006). However, a main obstacle faced in targeted therapy is resistance, either primary resistance or acquired resistance after long-term treatment. Previous results in our group demonstrated primary resistance of non-JMD mutants against TKI treatment *in vitro,* which questions the effectiveness of those treatments (Breitenbuecher et al., 2009a; Mack, Dissertation, 2014). The present study assessed the sensitivity of both ITDL601H(10) and ITDFV605YF(14) mutants to TKIs following identical experimental conditions as in prior studies in order to make reliable comparisons. Pharmacological inhibition of the FLT3-mutated receptor prevents its phosphorylation leading to growth disadvantage and cell death. Thereby, induction of apoptosis was measured as a read-out for the efficacy of two different kinase inhibitors. The first generation inhibitor PKC412 (Midostaurin) was tested in both FLT3-ITD mutants along with the well-established ITD598/599(12) (*standard* control). Transformed cells were incubated with four relevant concentrations of PCK412 ranging from 10 nM to 100 nM. DMSO was used as a negative control. After 24 hours, both mutants showed increased dose-dependent cell death comparable to the *standard* ITD. Of note, the ITDL601H(10) mutant showed a slightly higher sensitivity to PKC412 treatment than ITDFV605YF(14) (Figure 17A). Furthermore, these results were combined with data from previous studies that demonstrated primary resistance of TKD1-ITD mutants against TKI treatment. This data was generated in our group using different FLT3-ITD mutations and following identical experimental conditions.

Here, response to PKC412 treatment in ITDL601H(10) and ITDFV605YF(14) supported the differences between JMD- and TKD1-ITDs. Both JMD-ITD mutants showed the same trend as observed in other JMD-ITDs, revealing a higher sensitivity to PKC412 than in TKD1-ITD mutants (Figure 17C). Nevertheless, at higher concentrations the response to TKI treatment in ITDFV605YF(14) was comparable to TKD1-ITDs (Figure 17C; 100 nM). It could be possible that this specific mutant lost the sensitivity to treatment at higher concentrations. On the other hand, this mutation is the most C-terminal JMD-ITD inserted within the hinge region. This proximity to the kinase domain may influence the inhibitory efficacy as observed in TKD1-ITDs. A second inhibitor, AC220, was also tested in FLT3-ITD mutants. AC220 belongs to the second-generation of FLT3 inhibitors with a higher selectivity and sensitivity against FLT3 mutations and promising activity in early clinical trials (Chao et al., 2009; Zarrinkar et al., 2009; Gunawardane et al., 2013; Kampa-Schittenhelm et al., 2013; Wander et al., 2014; Konig and Levis, 2015; Park et al., 2015). As observed in PKC412 treatment, ITDL601H(10) and ITDFV605YF(14) mutants showed a dose-dependent apoptosis with a more pronounced response for ITDL601H(10) (Figure 17B). When compared to previous studies, both FLT3-ITD mutations showed a higher apoptotic rate than the TKD1-ITD group (Figure 17D). Furthermore, the inhibitory effect of PKC412 was confirmed on protein level in both JMD-ITD mutants. As a heterocyclic compound that blocks the binding of ATP to the active site in a competitive fashion, PKC412 treatment resulted in a complete abrogation of the constitutive phosphorylation of FLT3 and its downstream molecules STAT5 and ERK1/2 (Figure 18). Moreover, this inhibitory efficacy was comparable to other JMD and TKD1-ITDs.

Taken together, these results indicate a response of the newly identified FLT3-ITD mutants - ITDL601H(10) and ITDFV605YF(14) - to TKIs through complete abrogation of FLT3 signaling. Furthermore, the apoptotic rates after TKI treatment were comparable to other JMD-ITDs and much higher than in TKD1-ITDs, providing evidence that the ITD location site may influence response to targeted treatment.

6.2. Distinct functional properties of FLT3-ITD mutations *in vivo*

It is known that FLT3-ITD mutations lead to a lethal hematopoietic disorder in mice, however the few ITD mutations that have been investigated were exclusively located within the JMD region. Moreover, recent retrospective studies have identified ITD mutations located within the TKD1 as an unfavorable prognostic factor. Patients harboring TKD1-ITD mutations showed a worse clinical outcome with a reduction in complete remission (CR), relapse-free survival and

overall survival (OS) when compared to JMD-located ITDs (Kayser et al., 2009; Schlenk et al., 2014). These clinical findings suggest that ITDs located within the TKD1 region may play a more aggressive role in leukemogenesis, leading to resistance and relapse. A main purpose of the present project was to assess and compare for the first time the oncogenic potential of several FLT3-ITD mutations depending on their location site (JMD vs. TKD1) using an *in vivo* mouse model.

For over a decade, the transforming potential of constitutively activated receptor tyrosine kinases has been investigated using bone marrow transplant (BMT) assays. The retroviral transduction of oncogenes into primary murine bone marrow cells followed by transplantation into syngeneic recipient mice is known to recapitulate a lethal hematopoietic disorder. In 2002, Kelly et al. reported for the first time the oncogenic potential of FLT3-ITD mutations using a BMT model, providing a useful tool to evaluate activating FLT3 mutations *in vivo* (Kelly et al., 2002). The stable expression of a FLT3-ITD mutation resulted in a fatal myeloproliferative-like disorder characterized by an increased white blood cell (WBC) count (leukocytosis) and spleen enlargement produced by extramedullary infiltration (splenomegaly) (Kelly et al., 2002; Grundler et al., 2005). In contrast, FLT3 point mutations (FLT3-AL) developed a lymphoid-like disorder with a lower disease penetrance (Grundler et al., 2005). Besides the BMT model, additional *in vivo* approaches have been described in the literature to characterize gain-of-function aberrations, for instance the use of FLT3-ITD transformed Ba/F3 and 32D mutants. Both cell lines are derived from bone marrow of C3H/HeJ mice, and their transplantation into syngeneic mice led to cellular overgrowth and development of lethal disorders (Matulonis et al., 1995; Mizuki et al., 2000; Tse et al., 2000; Breitenbuecher et al., 2009a; Caldarelli et al., 2013). Furthermore, the generation of engineered mouse models has also contributed to better characterize FLT3 mutations *in vivo* (Lee et al., 2005; Lee et al., 2007; Li et al., 2008; Chu et al., 2012). Transgenic mice expressing human FLT3-ITD, which is under the control of the hematopoietic cell-specific *vav* promoter, mainly induced a myeloproliferative syndrome with long latency (6 to 10 months) and reduced aggressiveness. However, this transgenic model also reported animals that succumbed to immature B- and T-lymphoid diseases (Lee et al., 2005). Knock-in of FLT3-ITD in mice resulted entirely in a myeloproliferative disorder with long latency (6 to 20 months) and conferred myeloid expansion on HSPCs along with a lack of B-cell development (Lee et al., 2007; Li et al., 2008; Chu et al., 2012). Importantly, all these models demonstrate that FLT3-ITD expression alone is sufficient to enhance expansion and accumulation of transformed cells but not to develop AML. In this work, the BMT model was chosen to characterize the oncogenic potential of each

FLT3-ITD mutation. Transplantation of FLT3-ITD transformed Ba/F3 or 32D mutants was excluded as it was considered inappropriate on grounds of lack of information. Despite the fact that an overgrowth of transplanted cell lines would have confirmed the transforming potential of the oncogene, this is an artificial model that does not represent physiological conditions. For instance, both Ba/F3 and 32D cells belong to specific hematopoietic lineages - pro-B and myeloid cells, respectively -, and therefore, it is not possible to evaluate the transforming potential on immature HSPCs or to characterize the biological phenotypes of the hematopoietic disorder. Moreover, since no genetically engineered knock-in models for each ITD construct were available, the BMT model was the most suitable system providing a stable expression of our gene of interest in primary murine bone marrow cells and an adequate latency to monitor disease development. Several issues were taken under consideration for the design of the experimental model. First, the stable integration of each mutation into primary hematopoietic cells was successfully accomplished by using a pMSCV-based retroviral vector system. Second, previous findings suggested that disease latency depends on the level of FLT3-ITD protein expression and the number of transplanted cells (Grundler et al., 2005). In order to achieve a comparative investigation between the different FLT3-ITD mutations, it was important to exclude differences in the expression levels of the FLT3 protein and to transplant comparable amounts of transformed cells into recipient mice. Virus production and subsequent retroviral infection of primary bone marrow cells was performed under identical conditions in each experiment. All pMSCV-PIG_FLT3 constructs successfully expressed equivalent levels of GFP supporting comparable transgene expression (Figure 21A-B). Moreover, transduction efficiency was always analyzed shortly before transplantation by flow cytometry in order to inject equal numbers of transformed cells. Third, an optimal time frame was needed to monitor disease development and to ensure a gradual manifestation of disease signs. Previous studies reported median survival times ranging from 15 days up to 60 days using BMT models (Kelly et al., 2002; Grundler et al., 2005). Such variability was more likely due to the transplantation of different cell numbers and populations. Kelly et al. observed a median latency of 40 to 50 days using 0.5×10^6 total cells. Grundler and colleagues used low- and high-copy expression vectors and transplanted 1×10^5-1.5×10^5 transformed FLT3-ITD cells, reporting a median latency of approximately 15 to 60 days. In this work, the number of transformed cells (GFP$^+$) and supporter cells was established in order to extend disease latency and to better evaluate the functional properties in both groups (JMD vs. TKD1) (Figure 20). Last, inbred BALB/c mice were chosen as it has been shown that activating FLT3-ITD mutations exclusively develop lethal hematopoietic disorders in this specific background (Kim et al., 2008). This strain harbors hypomorphic alleles of the tumor suppressor gene Cdkn2a, resulting

in a reduced activity of the cyclin-dependent kinase inhibitor protein p16INK4a and a defective ability to inhibit Rb phosphorylation (Zhang et al., 1998; Mori, 2010). Consequently, BALB/c mice are sensitive to radiation-induced lymphoma development, and this genetic background may enhance transforming properties of FLT3-ITD mutations. In order to regulate the influence of the myeloblative conditioning, it was always confirmed that the hematopoietic disorders arose from transformed cells (GFP$^+$). Moreover, two different cohorts receiving either wild-type FLT3 or empty pMSCV_PIG transduced cells were included as negative controls.

The BMT model used in this work was designed to investigate the biological impact of several FLT3-ITD mutations and to determine whether TKD1-ITDs lead to a more aggressive phenotype. As expected, only animals receiving FLT3-ITD transformed cells succumbed to the disease (Figure 22). However, TKD1-ITD recipient mice showed a significant reduction in disease penetrance, rejecting that TKD1-ITD might confer a stronger oncogenic potential than JMD-ITDs (Figure 22B; Table 18). While all JMD-ITD mutations caused a fatal hematopoietic disorder characterized by leukocytosis, extramedullary hematopoiesis (splenomegaly) and a median latency of 101 days, TKD1-ITD mutations led to a remarkably delayed onset of disease and decreased penetrance accounting for 15% of lethality (Figure 23-A-E). Although FLT3-ITD mutations have long been characterized using murine models, this was the first study to assess the biological impact of TKD1-ITD mutations *in vivo.* Additional BMT experiments in our group confirmed a direct correlation between disease latency and number of transplanted cells. Using twice the number of transformed cells, TKD1-ITD mutations showed a 100% penetrance with a slight delay in disease progression when compared to JMD-ITDs (Arreba-Tutusaus et al., 2016). Nevertheless, lower cell numbers were needed to identify differences between groups. On the other hand, it is noteworthy to mention that no significant differences in the transforming capacity of JMD-ITD and TKD1-ITD mutations could be detected *in vitro* (Figure 14C-D). Each FLT3-ITD transformed Ba/F3 mutant was generated following IL-3 withdrawal. This method selects transformed cells with proliferative advantage, which sustain factor-independent growth. Thus, this pre-selection may have masked possible functional differences between mutants, and *in vitro* experiments may have not been sensitive enough to detect differences in transforming potential and proliferation. This may be a main limitation of the *in vitro* studies highlighting the importance and functional relevance of *in vivo* animal models. Further immunophenotypical analysis of bone marrow cells revealed that mice receiving FLT3-ITD transformed cells developed either a myeloproliferative-like disease or a lymphoproliferative phenotype (Figure 23F). These results are consistent with previous reports in which oncogenes such as BCR-ABL or RAS mainly developed myeloid leukocytosis but also

frequent T-lymphomas or B-cell lymphoblastic leukemia (Dumbar et al., 1991; Hawley et al., 1995; Van Etten, 2002; Wertheim et al., 2002; Chan et al., 2014). Unfortunately, it is not possible to draw a clear conclusion on the biological phenotype induced by each group of mutations, in particular by TKD1-ITD mutations due to the low number of diseased animals. This aspect should be investigated in more detail in future studies. The human FLT3-ITD transgenic model driven by a *vav* promoter already reported different leukemic phenotypes, including myeloproliferative as well as T-cell and B-cell lymphoid disorders (Lee et al., 2005). Moreover, FLT3 point mutations exclusively developed lymphoproliferative disorders using a BMT model, suggesting that activating FLT3 mutations may induce distinctive phenotypes. The FLT3 receptor is highly expressed in lymphoid malignancies, and activating FLT3 mutations have also been identified in adult acute lymphoblastic leukemia (ALL), which may support the pathogenic role toward lymphoid disorders (Rosnet et al., 1996; Armstrong et al., 2003; Armstrong et al., 2004; Paietta et al., 2004; Roberts et al., 2012; Elyamany et al., 2014). Further experimental investigations should assess the biological phenotype induced by TKD1-ITD mutations, for instance increasing the number of transplanted cells and recipient mice to overcome the heterogeneity of previous results. It would also be useful to generate a specific TKD1-ITD knock-in mouse model to better characterize the disease phenotype. This knock-in model would also allow investigating more deeply the role of TKD1-ITD on HSPC homeostasis and leukemogenesis. For instance, knock-in of JMD-ITD in mice enhanced proliferation and survival of the HSC compartment leading to its exhaustion, while in FLT3-AL knock-in mice the same pool of immature cells remained unaffected (Chu et al., 2012; Bailey et al., 2013). In recent years, there has been a controversial discussion whether the ITD length has a negative impact on clinical outcome (Stirewalt et al., 2006; Schnittger et al., 2012; Kim et al., 2015). In the present work, several JMD-ITDs with different lengths were characterized but no significant differences could be detected due to disease outcome (Figure 22B; Table 19). Indeed, the longest ITD mutations - ITDE611V(32) and ITDG613E(33) - seemed to show reduced oncogenic potential. However, these results have to be handled with care due to the small sample size. The experiment should be repeated with a higher number of recipient mice per cohort to proof statistical significance. It would also be interesting to compare ITD mutations with identical location sites but different length to avoid additional variability. Taken together, this is the first study to investigate the functional biology of activating TKD1-ITD mutations *in vivo,* showing a striking disadvantage in disease development when compared to JMD-ITDs (Figure 22). These differences in disease latency and aggressiveness between both groups (JMD vs. TKD1) suggest that ITD location may be relevant in FLT3-ITD-mediated leukemogenesis.

As aforementioned, FLT3-ITDs located within the JMD region conferred stronger transforming potential than TKD1-ITD mutations to primary murine bone marrow cells. In normal hematopoiesis, FLT3 is known to promote proliferation of early hematopoietic precursors, while activating FLT3 mutations enhance proliferation and survival potential of human and murine HSPCs (Hudak et al., 1995; Lee et al., 2007; Chu et al., 2012). In addition, cellular proliferation is a crucial event during engraftment after bone marrow transplantation (Lapidot et al., 2005). Along these lines, it could be possible that the capacity of cells to proliferate may differed between each group of mutations. As a consequence, this would influence the engraftment after transplantation and the oncogenic potential of transformed cells. To further elucidate on the biological relationship between disease onset and ITD location, this study assessed whether JMD-ITD mutations lead to a proliferative advantage over TKD1-ITDs *in vivo*. For the first time, a competitive BMT model was designed to analyze simultaneously different FLT3-ITD mutations. Following the principle of competitive repopulation assays, the strength of this experimental approach was to investigate the engraftment capacity of two pools of transduced cells harboring either JMD-ITD or TKD1-ITD mutations within the same BALB/c recipient mouse. Here, transduced cells were pre-selected by fluorescence-activating cell sorting (FACS) to increase the purity of transformed cells and, consequently, the number of transplanted cells was decreased when compared to the conventional BMT assay. The results of this study confirmed the unanticipated oncogenic advantage of FLT3-ITD mutations located within the JMD region, which showed a stronger engraftment and a faster overgrowth in comparison to TKD1-ITD mutations (Figure 25). These findings suggest that ITDs located within the TKD1 region may enhance a weaker proliferative advantage and, consequently, require a higher number of transformed cells (leukemia-initiating cells) in order to induce leukemogenesis. Cell cycle analysis would be worthwhile to estimate the proliferative status on primary murine bone marrow cells harboring different FLT3-ITDs. In this work, cell proliferation was analyzed using BrdU incorporation assays *in vivo*. However, the simultaneous detection of the fluorescent protein GFP (represents transformed cells) and the labeled BrdU cells by flow cytometry failed due to the harsh treatment of the cells during the experimental protocol. Therefore, alternative approaches would be needed to address this question, for example cell cycle analysis or proliferation assays of sorted cells *in vitro*.

Besides engraftment, bone marrow transplantation first requires the migration of hematopoietic cells toward the BM niche, a process known as homing. It could be possible that the manipulation of primary bone marrow cells *ex vivo* or even the expression of TKD1-ITD mutations itself might limit the homing capacity of transduced cells. This reduction in the

number of cells that reach the bone marrow may eventually result in less engraftment of malignant cells. However, both FLT3-ITD groups showed equivalent homing to the bone marrow, implying that the reduced oncogenic potential of TKD1-ITD mutations was due to engraftment disadvantage (Figure 26). Overall, these results prove a noteworthy impact of the ITD location site on the functional biology and oncogenic potential of FLT3-ITD mutations. Although JMD- and TKD1-ITD mutations could be defined as gain-of-function mutations with equivalent transforming potential *in vitro*, ITD location within the TKD1 region was associated with reduced engraftment and oncogenic potential when compared to JMD-ITDs *in vivo*. The present study suggests that the ITD location site may influence FLT3-ITD-driven leukemogenesis increasing the biological heterogeneity within the same genetic mutation. Interestingly, JMD-ITD mutations can be found more frequently than TKD1-ITD mutations in FLT3-ITD positive AML patients (Figure 6) (Breitenbuecher et al., 2009b; Kayser et al., 2009). Here, one could speculate that JMD-ITD mutations are more aggressive and, therefore, more frequent in AML. Nevertheless, TKD1-ITD mutations could still lead to increased resistance to treatment and relapse after remission for instance through alternative pathways or acquisition of additional mutations.

The last part of the *in vivo* studies focused on the resistant phenotype observed in TKD1-ITD mutations. This work and other studies have confirmed a reduced sensitivity of non-JMD-ITD mutants to TKIs *in vitro* (Breitenbuecher et al., 2009a; Mack, Dissertation, 2014). Based on these findings, the competitive BMT model was used to assess whether TKD1-ITD transformed bone marrow cells retain their resistant phenotype in spite of having reduced oncogenic potential *in vivo*. Treatment of recipient mice revealed sensitivity of JMD-ITD transformed cells to PKC412, whereas the amount of TKD1-ITD transformed cells remained unchanged (Figure 27). This *in vivo* data provides further evidence that the ITD location site may affect response to targeted therapy. The cause of primary resistance in TKD1-ITD mutations can only be speculated, as many cellular and molecular mechanisms may be involved and, most like, various factors interact. Previous studies have already reported the differential sensitivity of activating FLT3 mutations to TKIs, as either primary resistance or through the acquisition of additional mutations in the *FLT3* gene after long-term treatment (Bagrintseva et al., 2004; Clark et al., 2004; Heidel et al., 2006; Kindler et al., 2010; Pauwels et al., 2012; Smith and Shah, 2012). One possible explanation would be that the inhibitor efficacy might be decreased, which would lead to failure in blocking the constitutive activation of FLT3 and need of higher concentrations to reach inhibition. However, this work and other studies have shown a

comparable inhibitory efficacy of TKIs in JMD- and TKD1-mutations. Despite the resistance of TKD1-ITD mutants to treatment, TKIs completely blocked FLT3 signaling in all FLT3-ITD mutants regardless of dose and location site (Figure 18) (Mack, Dissertation, 2014). Given the proven effectiveness of TKIs, the resistance phenotype may most likely be due to alternative mechanism. In recent years, several cellular pathways and molecular changes deregulated by FLT3-ITD mutations have been suggested as compensatory mechanisms associated with resistance, including up-regulation of anti-apoptotic genes, down-regulation of pro-apoptotic signals or up-regulation of RUNX1, a transcription factor involved in normal hematopoiesis (Stölzel et al., 2010; Damdinsuren et al., 2015; Onishi et al., 2015; Hirade et al., 2016). Importantly, these studies highlight the relevance of apoptotic pathways in FLT3-ITD-mediated leukemogenesis and resistance. FLT3-ITD signaling is known to suppress apoptosis through the phosphorylation of the pro-apoptotic protein BAD and concomitant release of the anti-apoptotic proteins Bcl-2 and Bcl-X$_L$ as well as the up-regulation of the anti-apoptotic protein Mcl-1 (Yang et al., 2005; Kasper et al., 2012; Mehta et al., 2013). Along these lines, previous results in our group suggested a deregulation of Mcl-1 as a specific mechanism of primary resistance against TKIs in a prototype TKD-ITD mutation. Transformed murine cells harboring a TKD2-ITD mutation (ITDA627E) showed a significant up-regulation of Mcl-1 upon TKI treatment (Breitenbuecher et al., 2009a). In contrast, FLT3-ITD mutations located within the TKD1 region showed equivalent levels of Mcl-1 and Bcl-X$_L$ when compared to JMD-ITDs upon treatment, suggesting that deregulation of these specific anti-apoptotic signals may not be involved in TKD1-ITD-mediated resistance (Mack, Dissertation, 2014). Nevertheless, cellular apoptosis is a complex process that involved many molecules and pathways that remain unexplored. For instance, enhanced activation of STAT pathways and overexpression of BIRC5 (survivin), a member of the inhibitor of apoptosis family that negatively regulates programmed cell death, has also been suggested as a potential mechanism of resistance to FLT3 inhibitors (Zhou et al., 2009). On the other hand, additional compensatory mechanisms may be associated with FLT3-ITD-mediated resistance besides apoptosis. Indeed, a broad range of cellular functions have been suggested as relevant in FLT3-ITD-mediated transformation (Mizuki et al., 2003; Neben et al., 2005; Bullinger et al., 2008; Caldarelli et al., 2013). Therefore, further research is needed to identify potential mechanisms underlying the distinct response of FLT3-ITD mutations to targeted therapy.

In summary, the present data provides strong evidence for an impact of the ITD location site on disease biology and sensitivity to TKI treatment. These results reflect the biological heterogeneity within mutations that activate the same kinase, highlighting the molecular and

functional complexity in AML. Focusing on the implication of these findings on future research, the ITD location site should be considered when investigating the molecular biology of specific FLT3-ITD mutations and, more importantly, when designing and evaluating FLT3-targeted drugs. Furthermore, future retrospective studies and clinical trials should investigate the possible correlation between parameters describing clinical outcome and the ITD location site in order to define the impact of this feature on the outcome in AML patients. So far, the location of ITDs within the TKD1 region has been associated with unfavorable outcome either after remission or consolidation therapy regardless of the therapeutic approach (chemotherapy/autologous stem-cell transplantation versus allogeneic stem-cell transplantation). Moreover, it would be recommended to include the ITD location site in the analysis of recent clinical trials that combine conventional chemotherapy with FLT3-ITD-targeted treatment (Röllig et al., 2015; Stone et al, 2015). Patients harboring TKD1-ITDs may not benefit from treatment with FLT3-targeted drugs, and this finding may help to stratify patients toward the best possible treatment in future clinical trials.

6.3. Distinct molecular response to DNA damage repair depending on the ITD location

As discussed above, the ITD location alters disease development and response to targeted therapy *in vivo*. However, the fundamental mechanism behind this differential biology remained unclear. In order to gain insights into the cellular and molecular changes underlying the divergence between FLT3-ITD mutations (JMD vs. TKD1), transcriptional expression of target genes downstream the FLT3 receptor was investigated. Global gene-expression profiling (GEP) on murine cells transfected with different FLT3-ITD mutations (3 JMD-ITDs and 2 TKD1-ITDs) and primary material from FLT3-ITD positive AML patients (33 JMD-ITD and 16 TKD1-ITD patients) was performed in collaboration with the group of Professor Bullinger at the University Hospital Ulm. Comparative analysis on the data revealed a total of 540 probe sets differentially expressed between the groups, including molecules involved in cell signaling and regulation of apoptosis (Arreba-Tutusaus et al., 2016). A closer evaluation of cell functions and processes predicted abnormal regulation of DNA repair, chromatin organization and cell adhesion. Based on these results, the present study sought for early evidence in the potential association between the ITD location site and DNA damage and repair. In recent years, a strong relationship between DNA repair and FLT3-ITD-mediated leukemogenesis has been reported in the literature. DNA repair plays a crucial role in the preservation of genomic integrity through its association with other essential cellular events such as DNA replication,

cell cycle progression and apoptosis (Kinner et al., 2008). Deficiency in the repair process may result in cellular instability and tumorigenesis, whereas high levels of DNA repair can also lead to disease pathogenesis. Increased DNA repair can inhibit apoptotic pathways and support survival of cells with damaged DNA, which still may attempt repair, potentially misrepair, increasing the genomic instability (Seedhouse et al., 2006; Sallmyr et al., 2008b). One of the most aggressive DNA lesions are double-stand breaks (DSB), which can result from exogenous agents such as irradiation or genotoxic drugs and from endogenous production of reactive oxygen species (ROS) (Sallmyr et al., 2008b; Podhorecka et al., 2010). Several studies have associated FLT3-ITD mutations with increased DSB production and aberrant DNA repair in murine transformed cell lines, primary FLT3-ITD positive AML patients and human cell lines harboring FLT3-ITD mutations (Sallmyr et al., 2008a; Fan et al., 2010; Darling et al., 2013). In order to assess and compare the level of DNA repair between FLT3-ITD mutants, murine transformed cells (Ba/F3) were irradiated to enhance DNA damage (DSB formation), and the level of phosphorylated H2AX (γH2AX) was analyzed at different time points by Western Blot. Histone H2AX is one of the most evolutionary conserved H2A variants. Its phosphorylation in the residue Ser[139], known as γH2AX, occurs in response to DSB formation (Podhorecka et al., 2010; Muslimovic et al., 2012). Upon induced cell damage, the modification of the histone can be detected after a few minutes reaching its maximum 30 minutes later and declining with time once DSBs are repaired (Muslimovic et al., 2012). As expected, JMD- and TKD1-ITD irradiated cells showed increased levels of γH2AX when compared to control, indicating that the irradiation successfully induced DNA damage. However, JMD-ITD and TKD1-ITD treated cells, as well as control cells, showed comparable levels of γH2AX that remained unchanged over time (Figure 28). These results suggest an equivalent DSB formation and DNA repair between FLT3-ITD mutations regardless on the location site; however, no clear conclusions could be drawn due to the difficulty in reproducing this result by Western Blot analysis. The detection of the protein was hindered most likely due to its small size (15 KDa). The qualitative assessment of γH2AX may not be sensitive enough to detect changes in H2AX phosphorylation since activating FLT3 mutations *per se* present basal levels of DNA damage. A more sensitive and reliable assay was included in order to achieve more conclusive results. As mentioned above, the phosphorylation of H2AX depends on DSB formation. The presence of γH2AX in chromatin forms discrete nuclear foci that represent single DSBs and can be detected using immunocytochemical approaches. Thus, the number of γH2AX foci in individual cells estimates the incidence of DSBs and, consequently, provides valuable information about the levels of DNA damage and repair (Kinner et al., 2008). Following previous experimental conditions, nuclear foci formation was quantified in control and irradiated murine transformed

cells 2 hours after induction of DNA damage in order to evaluate DNA repair. The results revealed significantly fewer amounts of DSBs in irradiated TKD1-ITD mutants when compared to JMD-ITDs. Untreated cells (JMD vs. TKD1) showed comparable levels of γH2AX. These data indicate a deregulation in DNA repair between JMD and TKD1-ITDs and suggest that cells harboring a TKD1-ITD may repair DNA damage in a more efficient way than JMD-ITDs (Figure 29). A limitation of the current study is that only a single time point has been examined, assuming that H2AX phosphorylation decays 30 minutes after damage induction. A natural progression of this work would be to analyze γH2AX foci formation and decay over time in order to compare DSB repair kinetics between the different ITD mutations. Furthermore, a more detailed analysis of molecular events involved in DNA repair would be interesting. FLT3-ITD mutations have been associated with aberrant repair through the two major pathways of DSB repair: homologue recombination (HR) and nonhomologous end-joining (NHEJ) (Darling et al., 2013). On one hand, overexpression of RAD51, a key molecule in HR, has been related to increased rates of repair in FLT3-ITD positive cell lines and patients, which may lead to genomic instability and resistance to therapy (Raderschall et al., 2002; Seedhouse et al., 2006). Interestingly, RAD51 was found among the 540 genes significantly deregulated in the global gene-expression analysis with a higher expression in the TKD1-ITD group. It would be interesting to investigate whether homologue recombination is increased in TKD1-ITD mutations when compared to JMD-ITDs, for instance confirming the deregulated expression of *Rad51* in murine transformed cells. On the other hand, FLT3-ITD mutants are known to induce increased reactive oxygen species (ROS) production via STAT5 signaling and activation of RAC1, an essential component of ROS-producing NADPH oxidase (Sallmyr et al., 2008a; Godfrey et al., 2012; Woolley et al., 2012). Recently published data has suggested p22(phox) and p22(phox)-interacting NOX isoforms as mediators of ROS production in FLT3-ITD positive cellular systems (Stanicka et al., 2015). As a result, FLT3-ITD-driven ROS production enhances oxidative stress associated with increased DNA damage and activation of NHEJ misrepair. Indeed, an alternative and more inaccurate NHEJ pathway, mediated by PARP and DNA ligase IIIα, has been suggested as potential mechanism of error-prone repair in ROS-induced DSBs repair (Fan et al., 2010). Along these lines, ongoing investigations in our department aim to assess ROS production and oxidative stress in several FLT3-ITD mutants in regard to the ITD location site. It would be interesting to determine whether TKD1-ITD mutants induce higher levels of ROS production than JMD-ITDs and associate this phenotype to DNA misrepair.

Although not all questions could be answered in detail, these findings provide a proof of principle that DNA repair may be a potential mediator of the biological divergence observed

between JMD-ITD and TKD1-ITD mutations. In summary, it seems that TKD1-ITD mutations *per se* are less aggressive in leukemogenesis. However, their association with increased relapse and poor outcome may be due to aberrant DNA repair and resistance to therapy. Upon genotoxic treatment, enhanced DNA repair on TKD1-ITD positive leukemic cells may promote survival and increase the genomic instability through misrepair. Consequently, either the *founding clone* or a residual subclone would evolve and acquire additional driver mutations leading to disease relapse.

The present dissertation has focused on the molecular heterogeneity within one of the most relevant genetic aberration in AML. Paying particular attention to the impact of the ITD location on oncogenic potential and response to treatment of FLT3-ITD mutations, it has been shown its particular significance from a biological standpoint with potential relevance for clinical applications.

7. References

Abu-Duhier, F.M., Goodeve, A.C., Wilson, G.A., Care, R.S., Peake, I.R., and Reilly, J.T. (2001). Identification of novel FLT-3 Asp835 mutations in adult acute myeloid leukaemia. British Journal of Haematology *113*, 983-988.

Adam, M., Pogacic, V., Bendit, M., Chappuis, R., Nawijn, M.C., Duyster, J., Fox, C.J., Thompson, C.B., Cools, J., and Schwaller, J. (2006). Targeting PIM kinases impairs survival of hematopoietic cells transformed by kinase inhibitor-sensitive and kinase inhibitor-resistant forms of Fms-like tyrosine kinase 3 and BCR/ABL. Cancer Research *66*, 3828-3835.

Agnes, F., Shamoon, B., Dina, C., Rosnet, O., Birnbaum, D., and Galibert, F. (1994). Genomic structure of the downstream part of the human FLT3 gene: exon/intron structure conservation among genes encoding receptor tyrosine kinases (RTK) of subclass III. Gene *145*, 283-288.

Armstrong, S.A., Kung, A.L., Mabon, M.E., Silverman, L.B., Stam, R.W., Den Boer, Monique L, Pieters, R., Kersey, J.H., Sallan, S.E., and Fletcher, J.A., et al. (2003). Inhibition of FLT3 in MLL. Validation of a therapeutic target identified by gene expression based classification. Cancer Cell *3*, 173-183.

Armstrong, S.A., Mabon, M.E., Silverman, L.B., Li, A., Gribben, J.G., Fox, E.A., Sallan, S.E., and Korsmeyer, S.J. (2004). FLT3 mutations in childhood acute lymphoblastic leukemia. Blood *103*, 3544-3546.

Arora, D., Stopp, S., Bohmer, S.-A., Schons, J., Godfrey, R., Masson, K., Razumovskaya, E., Ronnstrand, L., Tanzer, S., and Bauer, R., et al. (2011). Protein-tyrosine phosphatase DEP-1 controls receptor tyrosine kinase FLT3 signaling. J Biol Chem *286*, 10918-10929.

Arreba-Tutusaus, P., Mack, T.S., Bullinger, L., Schnöder, T.M., Polanetzki, A., Weinert, S., Ballaschk, A., Wang, Z., Deshpande, A.J., and Armstrong, S.A., et al. (2016). Impact of FLT3-ITD location on sensitivity to TKI-therapy in vitro and in vivo. Leukemia *30*, 1220-5.

Badar, T., Patel, K.P., Thompson, P.A., DiNardo, C., Takahashi, K., Cabrero, M., Borthakur, G., Cortes, J., Konopleva, M., and Kadia, T., et al. (2015). Detectable FLT3-ITD or RAS mutation at the time of transformation from MDS to AML predicts for very poor outcomes. Leukemia Research *39*, 1367-1374.

Bagrintseva, K., Schwab, R., Kohl, T.M., Schnittger, S., Eichenlaub, S., Ellwart, J.W., Hiddemann, W., and Spiekermann, K. (2004). Mutations in the tyrosine kinase domain of FLT3 define a new molecular mechanism of acquired drug resistance to PTK inhibitors in FLT3-ITD-transformed hematopoietic cells. Blood *103*, 2266-2275.

Bailey, E., Li, L., Duffield, A.S., Ma, H.S., Huso, D.L., and Small, D. (2013). FLT3/D835Y mutation knock-in mice display less aggressive disease compared with FLT3/internal tandem duplication (ITD) mice. Proceedings of the National Academy of Sciences of the United States of America *110*, 21113-21118.

Ballaschk, A. (2014). Identifikation und funktionelle Charakterisierung von Internen Tandemduplikationen des FLT3-Rezeptors bei akuter myeloischer Leukämie. Magdeburg Univ., Med. Fak,. Dissertation.

Banath, J.P., Macphail, S.H., and Olive, P.L. (2004). Radiation sensitivity, H2AX phosphorylation, and kinetics of repair of DNA strand breaks in irradiated cervical cancer cell lines. Cancer Research *64*, 7144-7149.

Birkenkamp, K.U., Geugien, M., Lemmink, H.H., Kruijer, W., and Vellenga, E. (2001). Regulation of constitutive STAT5 phosphorylation in acute myeloid leukemia blasts. Leukemia *15*, 1923-1931.

Böhmer, S.-A., Weibrecht, I., Söderberg, O., and Böhmer, F.-D. (2013). Association of the protein-tyrosine phosphatase DEP-1 with its substrate FLT3 visualized by in situ proximity ligation assay. PloS One *8*, e62871.

Boyer, S.W., Schroeder, A.V., Smith-Berdan, S., and Forsberg, E.C. (2011). All hematopoietic cells develop from hematopoietic stem cells through Flk2/Flt3-positive progenitor cells. Cell Stem Cell *9*, 64-73.

Brandts, C.H., Sargin, B., Rode, M., Biermann, C., Lindtner, B., Schwäble, J., Buerger, H., Müller-Tidow, C., Choudhary, C., and McMahon, M., et al. (2005). Constitutive activation of Akt by Flt3 internal tandem duplications is necessary for increased survival, proliferation, and myeloid transformation. Cancer Research *65*, 9643-9650.

Brasel, K., Escobar, S., Anderberg, R., Vries, P. de, Gruss, H.J., and Lyman, S.D. (1995). Expression of the flt3 receptor and its ligand on hematopoietic cells. Leukemia *9*, 1212-1218.

Breitenbuecher, F., Markova, B., Kasper, S., Carius, B., Stauder, T., Böhmer, F.D., Masson, K., Rönnstrand, L., Huber, C., and Kindler, T., et al. (2009a). A novel molecular mechanism of primary resistance to FLT3-kinase inhibitors in AML. Blood *113*, 4063-4073.

Breitenbuecher, F., Schnittger, S., Grundler, R., Markova, B., Carius, B., Brecht, A., Duyster, J., Haferlach, T., Huber, C., and Fischer, T. (2009b). Identification of a novel type of ITD mutations located in nonjuxtamembrane domains of the FLT3 tyrosine kinase receptor. Blood *113*, 4074-4077.

Broxmeyer, H.E., Lu, L., Cooper, S., Ruggieri, L., Li, Z.H., and Lyman, S.D. (1995). Flt3 ligand stimulates/costimulates the growth of myeloid stem/progenitor cells. Experimental Hematology *23*, 1121-1129.

Brunet, S., Labopin, M., Esteve, J., Cornelissen, J., Socié, G., Iori, A.P., Verdonck, L.F., Volin, L., Gratwohl, A., and Sierra, J., et al. (2012). Impact of FLT3 internal tandem duplication on the outcome of related and unrelated hematopoietic transplantation for adult acute myeloid leukemia in first remission: a retrospective analysis. Journal of clinical oncology: official journal of the American Society of Clinical Oncology *30*, 735-741.

Bubnoff, N. von, Engh, R.A., Aberg, E., Sänger, J., Peschel, C., and Duyster, J. (2009). FMS-like tyrosine kinase 3-internal tandem duplication tyrosine kinase inhibitors display a nonoverlapping profile of resistance mutations in vitro. Cancer Research *69*, 3032-3041.

Bullinger, L., Döhner, K., Kranz, R., Stirner, C., Fröhling, S., Scholl, C., Kim, Y.H., Schlenk, R.F., Tibshirani, R., and Döhner, H., et al. (2008). An FLT3 gene-expression signature predicts clinical outcome in normal karyotype AML. Blood *111*, 4490-4495.

Caldarelli, A., Muller, J.P., Paskowski-Rogacz, M., Herrmann, K., Bauer, R., Koch, S., Heninger, A.K., Krastev, D., Ding, L., and Kasper, S., et al. (2013). A genome-wide RNAi screen identifies proteins modulating aberrant FLT3-ITD signaling. Leukemia *27*, 2301-2310.

Cancer Genome Atlas Research Network (2013). Genomic and epigenomic landscapes of adult de novo acute myeloid leukemia. The New England Journal of Medicine *368*, 2059-2074.

Casteran, N., Rottapel, R., Beslu, N., Lecocq, E., Birnbaum, D., and Dubreuil, P. (1994). Analysis of the mitogenic pathway of the FLT3 receptor and characterization in its C terminal region of a specific binding site for the PI3' kinase. Cellular and Molecular Biology *40*, 443-456.

Chan, P.M. (2011). Differential signaling of Flt3 activating mutations in acute myeloid leukemia: a working model. Protein & Cell *2*, 108-115.

Chan I.T., Kutok, J.L., Williams, I.R., Cohen, S., Kelly, L., Shigematsu, H., Johnson, L., Akashi, K., Tuveson, D.A., Jacks, T., and Gilliland D.G. (2004). Conditional expression of oncogenic *K-ras* from its endogenous promoter induces a myeloproliferative disease. Journal of Clinical Investigation *113*(4), 528–538.

Chang, F., Lee, J.T., Navolanic, P.M., Steelman, L.S., Shelton, J.G., Blalock, W.L., Franklin, R.A., and McCubrey, J.A. (2003a). Involvement of PI3K/Akt pathway in cell cycle progression, apoptosis, and neoplastic transformation: a target for cancer chemotherapy. Leukemia *17*, 590-603.

Chang, F., Steelman, L.S., Lee, J.T., Shelton, J.G., Navolanic, P.M., Blalock, W.L., Franklin, R.A., and McCubrey, J.A. (2003b). Signal transduction mediated by the Ras/Raf/MEK/ERK pathway from cytokine receptors to transcription factors: potential targeting for therapeutic intervention. Leukemia *17*, 1263-1293.

Chao, Q., Sprankle, K.G., Grotzfeld, R.M., Lai, A.G., Carter, T.A., Velasco, A.M., Gunawardane, R.N., Cramer, M.D., Gardner, M.F., and James, J., et al. (2009). Identification of N-(5-tert-butyl-isoxazol-3-yl)-N'-{4-7-(2-morpholin-4-yl-ethoxy)imidazo2,1-b1   ,3benzothiazol-2-ylphenyl}urea dihydrochloride (AC220), a uniquely potent, selective, and efficacious FMS-like tyrosine kinase-3 (FLT3) inhibitor. Journal of Medicinal Chemistry *52*, 7808-7816.

Cheung, A.M.S., Chow, H.C.H., Kwong, Y.-L., Liang, R., and Leung, A.Y.H. (2010). FLT3/internal tandem duplication subclones in acute myeloid leukemia differ in their engraftment potential in NOD/SCID mice. Leukemia Research *34*, 119-122.

Choudhary, C., Schwäble, J., Brandts, C., Tickenbrock, L., Sargin, B., Kindler, T., Fischer, T., Berdel, W.E., Müller-Tidow, C., and Serve, H. (2005). AML-associated Flt3 kinase domain mutations show signal transduction differences compared with Flt3 ITD mutations. Blood *106*, 265-273.

Chu, S.H., Heiser, D., Li, L., Kaplan, I., Collector, M., Huso, D., Sharkis, S.J., Civin, C., and Small, D. (2012). FLT3-ITD knockin impairs hematopoietic stem cell quiescence/homeostasis, leading to myeloproliferative neoplasm. Cell Stem Cell *11*, 346-358.

Clark, J.J., Cools, J., Curley, D.P., Yu, J.-C., Lokker, N.A., Giese, N.A., and Gilliland, D.G. (2004). Variable sensitivity of FLT3 activation loop mutations to the small molecule tyrosine kinase inhibitor MLN518. Blood *104*, 2867-2872.

Cools, J., Mentens, N., Furet, P., Fabbro, D., Clark, J.J., Griffin, J.D., Marynen, P., and Gilliland, D.G. (2004). Prediction of resistance to small molecule FLT3 inhibitors: implications for molecularly targeted therapy of acute leukemia. Cancer Research *64*, 6385-6389.

Cools, J., Stover, E.H., Boulton, C.L., Gotlib, J., Legare, R.D., Amaral, S.M., Curley, D.P., Duclos, N., Rowan, R., and Kutok, J.L., et al. (2003). PKC412 overcomes resistance to imatinib in a murine model of FIP1L1-PDGFRα-induced myeloproliferative disease. Cancer Cell *3*, 459-469.

Corces-Zimmerman, M.R., Hong, W.-J., Weissman, I.L., Medeiros, B.C., and Majeti, R. (2014). Preleukemic mutations in human acute myeloid leukemia affect epigenetic regulators and persist in remission. Proceedings of the National Academy of Sciences of the United States of America *111*, 2548-2553.

Damdinsuren, A., Matsushita, H., Ito, M., Tanaka, M., Jin, G., Tsukamoto, H., Asai, S., Ando, K., and Miyachi, H. (2015). FLT3-ITD drives Ara-C resistance in leukemic cells via the induction of RUNX3. Leukemia Research *39*, 1405-1413.

Darling, D.C., Mufti, G.J., and Gaymes, T.J. (2013). Internal Tandem Duplication Mutation Of FLT3 (FLT3/ITD) Induces Increased Homologous Recombination DNA Repair Activity, Drug Resistance and Sister Chromatid Exchanges In Acute Myeloid Leukaemia (AML). Blood *122*, 1244.

deLapeyriere, O., Naquet, P., Planche, J., Marchetto, S., Rottapel, R., Gambarelli, D., Rosnet, O., and Birnbaum, D. (1995). Expression of Flt3 tyrosine kinase receptor gene in mouse hematopoietic and nervous tissues. Differentiation; Research in Biological Diversity *58*, 351-359.

Ding, L., Ley, T.J., Larson, D.E., Miller, C.A., Koboldt, D.C., Welch, J.S., Ritchey, J.K., Young, M.A., Lamprecht, T., and McLellan, M.D., et al. (2012). Clonal evolution in relapsed acute myeloid leukaemia revealed by whole-genome sequencing. Nature *481*, 506-510.

Döhner, H., Estey, E.H., Amadori, S., Appelbaum, F.R., Büchner, T., Burnett, A.K., Dombret, H., Fenaux, P., Grimwade, D., and Larson, R.A., et al. (2010). Diagnosis and management of acute myeloid leukemia in adults: recommendations from an international expert panel, on behalf of the European LeukemiaNet. Blood *115*, 453-474.

Dosil, M., Wang, S., and Lemischka, I.R. (1993). Mitogenic signalling and substrate specificity of the Flk2/Flt3 receptor tyrosine kinase in fibroblasts and interleukin 3-dependent hematopoietic cells. Molecular and Cellular Biology *13*, 6572-6585.

Dunbar, C.E., Crosier, P.S., and Nienhuis, A.W. (1991) Introduction of an activated RAS oncogene into murine bone marrow lymphoid progenitors via retroviral gene transfer results in thymic lymphomas. Oncogene Research *6*, 39–51.

Elyamany, G., Awad, M., Alsuhaibani, O., Fadalla, K., Al Sharif, O., Al Shahrani, M., Alabbas, F., and Al-Abulaaly, A. (2014). FLT3 Internal Tandem Duplication and D835 Mutations in Patients with Acute Lymphoblastic Leukemia and its Clinical Significance. Mediterranean Journal of Hematology and Infectious Diseases *6*, e2014038.

Estey, E., and Döhner, H. (2006). Acute myeloid leukaemia. Lancet *368*, 1894-1907.

Fan, J., Li, L., Small, D., and Rassool, F. (2010). Cells expressing FLT3/ITD mutations exhibit elevated repair errors generated through alternative NHEJ pathways: implications for genomic instability and therapy. Blood *116*, 5298-5305.

Ferrara, F., and Schiffer, C.A. (2013). Acute myeloid leukaemia in adults. Lancet *381*, 484-495.

Fischer, T., Stone, R.M., Deangelo, D.J., Galinsky, I., Estey, E., Lanza, C., Fox, E., Ehninger, G., Feldman, E.J., and Schiller, G.J., et al. (2010). Phase IIB trial of oral Midostaurin (PKC412), the FMS-like tyrosine kinase 3 receptor (FLT3) and multi-targeted kinase inhibitor, in patients with acute myeloid leukemia and high-risk myelodysplastic syndrome with either wild-type or mutated FLT3. Journal of Clinical Oncology *28*, 4339-4345.

Fortier, J.M., and Graubert, T.A. (2010). Murine models of human acute myeloid leukemia. Cancer Treatment and Research *145*, 183-196.

Fröhling, S., Schlenk, R.F., Breitruck, J., Benner, A., Kreitmeier, S., Tobis, K., Döhner, H., and Döhner, K. (2002). Prognostic significance of activating FLT3 mutations in younger adults (16 to 60 years) with acute myeloid leukemia and normal cytogenetics: a study of the AML Study Group Ulm. Blood *100*, 4372-4380.

Fröhling, S., Scholl, C., Levine, R.L., Loriaux, M., Boggon, T.J., Bernard, O.A., Berger, R., Döhner, H., Döhner, K., and Ebert, B.L., et al. (2007). Identification of driver and passenger mutations of FLT3 by high-throughput DNA sequence analysis and functional assessment of candidate alleles. Cancer Cell *12*, 501-513.

Furuichi, Y., Goi, K., Inukai, T., Sato, H., Nemoto, A., Takahashi, K., Akahane, K., Hirose, K., Honna, H., and Kuroda, I., et al. (2007). Fms-like tyrosine kinase 3 ligand stimulation induces MLL-rearranged leukemia cells into quiescence resistant to antileukemic agents. Cancer Research *67*, 9852-9861.

Gabbianelli, M., Pelosi, E., Montesoro, E., Valtieri, M., Luchetti, L., Samoggia, P., Vitelli, L., Barberi, T., Testa, U., and Lyman, S. (1995). Multi-level effects of flt3 ligand on human hematopoiesis: expansion of putative stem cells and proliferation of granulomonocytic progenitors/monocytic precursors. Blood *86*, 1661-1670.

Garg, M., Nagata, Y., Kanojia, D., Mayakonda, A., Yoshida, K., Haridas Keloth, S., Zang, Z.J., Okuno, Y., Shiraishi, Y., and Chiba, K., et al. (2015). Profiling of somatic mutations in acute myeloid leukemia with FLT3-ITD at diagnosis and relapse. Blood *126*, 2491-2501.

Gavrilescu, L.C., and Van Etten, Richard A (2008). Murine retroviral bone marrow transplantation models for the study of human myeloproliferative disorders. Current Protocols in Pharmacology. *Chapter 14*, Unit 14.10.

Gaymes, T.J., Mufti, G.J., and Rassool, F.V. (2002). Myeloid leukemias have increased activity of the nonhomologous end-joining pathway and concomitant DNA misrepair that is dependent on the Ku70/86 heterodimer. Cancer Research *62*, 2791-2797.

Genovese, G., Kähler, A.K., Handsaker, R.E., Lindberg, J., Rose, S.A., Bakhoum, S.F., Chambert, K., Mick, E., Neale, B.M., and Fromer, M., et al. (2014). Clonal hematopoiesis and blood-cancer risk inferred from blood DNA sequence. The New England Journal of Medicine *371*, 2477-2487.

Gilliland, D.G. (2001). Hematologic malignancies. Current Opinion in Hematology *8*, 189-191.

Gilliland, D.G., and Griffin, J.D. (2002a). Role of FLT3 in leukemia. Current Opinion in Hematology *9*, 274-281.

Gilliland, D.G., and Griffin, J.D. (2002b). The roles of FLT3 in hematopoiesis and leukemia. Blood *100*, 1532-1542.

Godfrey, R., Arora, D., Bauer, R., Stopp, S., Müller, J.P., Heinrich, T., Böhmer, S.-A., Dagnell, M., Schnetzke, U., and Scholl, S., et al. (2012). Cell transformation by FLT3 ITD in acute myeloid leukemia involves oxidative inactivation of the tumor suppressor protein-tyrosine phosphatase DEP-1/ PTPRJ. Blood *119*, 4499-4511.

Green, A.S., Maciel, T.T., Hospital, M.-A., Yin, C., Mazed, F., Townsend, E.C., Pilorge, S., Lambert, M., Paubelle, E., and Jacquel, A., et al. (2015). Pim kinases modulate resistance to FLT3 tyrosine kinase inhibitors in FLT3-ITD acute myeloid leukemia. Science Advances *1*, e1500221.

Greenblatt, S., Li, L., Slape, C., Nguyen, B., Novak, R., Duffield, A., Huso, D., Desiderio, S., Borowitz, M.J., and Aplan, P., et al. (2012). Knock-in of a FLT3/ITD mutation cooperates with a NUP98-HOXD13 fusion to generate acute myeloid leukemia in a mouse model. Blood *119*, 2883-2894.

Griffith, J., Black, J., Faerman, C., Swenson, L., Wynn, M., Lu, F., Lippke, J., and Saxena, K. (2004). The structural basis for autoinhibition of FLT3 by the juxtamembrane domain. Molecular Cell *13*, 169-178.

Grossmann, V., Schnittger, S., Kohlmann, A., Eder, C., Roller, A., Dicker, F., Schmid, C., Wendtner, C.-M., Staib, P., and Serve, H., et al. (2012). A novel hierarchical prognostic model of AML solely based on molecular mutations. Blood *120*, 2963-2972.

Grove, C.S., and Vassiliou, G.S. (2014). Acute myeloid leukaemia: a paradigm for the clonal evolution of cancer?. Disease Models & mMchanisms *7*, 941-951.

Grundler, R., Miething, C., Thiede, C., Peschel, C., and Duyster, J. (2005). FLT3-ITD and tyrosine kinase domain mutants induce 2 distinct phenotypes in a murine bone marrow transplantation model. Blood *105*, 4792-4799.

Gunawardane, R.N., Nepomuceno, R.R., Rooks, A.M., Hunt, J.P., Ricono, J.M., Belli, B., and Armstrong, R.C. (2013). Transient exposure to quizartinib mediates sustained inhibition of FLT3 signaling while specifically inducing apoptosis in FLT3-activated leukemia cells. Molecular Cancer Therapeutics *12*, 438-447.

Hayakawa, F., Towatari, M., Kiyoi, H., Tanimoto, M., Kitamura, T., Saito, H., and Naoe, T. (2000). Tandem-duplicated Flt3 constitutively activates STAT5 and MAP kinase and introduces autonomous cell growth in IL-3-dependent cell lines. Oncogene *19*, 624-631.

Haylock, D.N., Horsfall, M.J., Dowse, T.L., Ramshaw, H.S., Niutta, S., Protopsaltis, S., Peng, L., Burrell, C., Rappold, I., and Buhring, H.J., et al. (1997). Increased recruitment of hematopoietic progenitor cells underlies the ex vivo expansion potential of FLT3 ligand. Blood *90*, 2260-2272.

Heidel, F., Solem, F.K., Breitenbuecher, F., Lipka, D.B., Kasper, S., Thiede, M.H., Brandts, C., Serve, H., Roesel, J., and Giles, F., et al. (2006). Clinical resistance to the kinase inhibitor PKC412 in acute myeloid leukemia by mutation of Asn-676 in the FLT3 tyrosine kinase domain. Blood *107*, 293-300.

Heiss, E., Masson, K., Sundberg, C., Pedersen, M., Sun, J., Bengtsson, S., and Ronnstrand, L. (2006). Identification of Y589 and Y599 in the juxtamembrane domain of Flt3 as ligand-induced autophosphorylation sites involved in binding of Src family kinases and the protein tyrosine phosphatase SHP2. Blood *108*, 1542-1550.

Heldin, C.-H., and Lennartsson, J. (2013). Structural and functional properties of platelet-derived growth factor and stem cell factor receptors. Cold Spring Harbor Perspectives in Biology *5*, a009100.

Herdrich, K. and Weinberger, H. (2013). Selected Schedules in the Therapy of Malignant Tumors. Part 1: Hematologic Malignancies. Frankfurt am Main, Baxter Oncology; ISBN: 3000114114 9783000114113

Hawley, R.G., Fong, A.Z., Ngan, B.Y., and Hawley, T.S. (1995) Hematopoietic transforming potential of activated ras in chimeric mice. Oncogene *11*, 1113–1123.

Hirade, T., Abe, M., Onishi, C., Taketani, T., Yamaguchi, S., and Fukuda, S. (2016). Internal tandem duplication of FLT3 deregulates proliferation and differentiation and confers resistance to the FLT3 inhibitor AC220 by Up-regulating RUNX1 expression in hematopoietic cells. International Journal of Hematology *103*, 95-106.

Hirayama, F., Lyman, S.D., Clark, S.C., and Ogawa, M. (1995). The flt3 ligand supports proliferation of lymphohematopoietic progenitors and early B-lymphoid progenitors. Blood *85*, 1762-1768.

Hole, P.S., Zabkiewicz, J., Munje, C., Newton, Z., Pearn, L., White, P., Marquez, N., Hills, R.K., Burnett, A.K., and Tonks, A., et al. (2013). Overproduction of NOX-derived ROS in AML promotes proliferation and is associated with defective oxidative stress signaling. Blood *122*, 3322-3330.

Huang, A., Ju, H., Liu, K., Zhan, G., Liu, D., Wen, S., Garcia-Manero, G., Huang, P., and Hu, Y. (2016). Metabolic alterations and drug sensitivity of tyrosine kinase inhibitor resistant leukemia cells with a FLT3/ITD mutation. Cancer Letters *377*, 149-57.

Huang, M., Thomas, D., Li, M.X., Feng, W., Chan, S.M., Majeti, R., and Mitchell, B.S. (2013). Role of cysteine 288 in nucleophosmin cytoplasmic mutations: sensitization to toxicity induced by arsenic trioxide and bortezomib. Leukemia *27*, 1970-1980.

Hudak, S., Hunte, B., Culpepper, J., Menon, S., Hannum, C., Thompson-Snipes, L., and Rennick, D. (1995). FLT3/FLK2 ligand promotes the growth of murine stem cells and the expansion of colony-forming cells and spleen colony-forming units. Blood *85*, 2747-2755.

Irish, J.M., Anensen, N., Hovland, R., Skavland, J., Borresen-Dale, A.-L., Bruserud, O., Nolan, G.P., and Gjertsen, B.T. (2007). Flt3 Y591 duplication and Bcl-2 overexpression are detected in acute myeloid leukemia cells with high levels of phosphorylated wild-type p53. Blood *109*, 2589-2596.

Jaiswal, S., Fontanillas, P., Flannick, J., Manning, A., Grauman, P.V., Mar, B.G., Lindsley, R.C., Mermel, C.H., Burtt, N., and Chavez, A., et al. (2014). Age-related clonal hematopoiesis associated with adverse outcomes. The New England Journal of Medicine *371*, 2488-2498.

Jan, M., Snyder, T.M., Corces-Zimmerman, M.R., Vyas, P., Weissman, I.L., Quake, S.R., and Majeti, R. (2012). Clonal evolution of preleukemic hematopoietic stem cells precedes human acute myeloid leukemia. Science Translational Medicine *4*, 149ra118.

Janke, H., Pastore, F., Schumacher, D., Herold, T., Hopfner, K.-P., Schneider, S., Berdel, W.E., Büchner, T., Woermann, B.J., and Subklewe, M., et al. (2014). Activating FLT3 mutants show distinct gain-of-function phenotypes in vitro and a characteristic signaling pathway profile associated with prognosis in acute myeloid leukemia. PloS One *9*, e89560.

Jayavelu, A.K., Müller, J.P., Bauer, R., Böhmer, S.-A., Lässig, J., Cerny-Reiterer, S., Sperr, W.R., Valent, P., Maurer, B., and Moriggl, R., et al. (2016). NOX4-driven ROS formation mediates PTP inactivation and cell transformation in FLT3ITD-positive AML cells. Leukemia *30*, 473-483.

Kampa-Schittenhelm, K.M., Heinrich, M.C., Akmut, F., Dohner, H., Dohner, K., and Schittenhelm, M.M. (2013). Quizartinib (AC220) is a potent second generation class III tyrosine kinase inhibitor that displays a distinct inhibition profile against mutant-FLT3, -PDGFRA and -KIT isoforms. Molecular Cancer *12*, 19.

Kasper, S., Breitenbuecher, F., Heidel, F., Hoffarth, S., Markova, B., Schuler, M., and Fischer, T. (2012). Targeting MCL-1 sensitizes FLT3-ITD-positive leukemias to cytotoxic therapies. Blood Cancer Journal *2*, e60.

Kayser, S., and Levis, M.J. (2014). FLT3 tyrosine kinase inhibitors in acute myeloid leukemia: clinical implications and limitations. Leukemia & Lymphoma *55*, 243-255.

Kayser, S., Schlenk, R.F., Londono, M.C., Breitenbuecher, F., Wittke, K., Du, J., Groner, S., Späth, D., Krauter, J., and Ganser, A., et al. (2009). Insertion of FLT3 internal tandem duplication in the tyrosine kinase domain-1 is associated with resistance to chemotherapy and inferior outcome. Blood *114*, 2386-2392.

Kelly, L.M., Liu, Q., Kutok, J.L., Williams, I.R., Boulton, C.L., and Gilliland, D.G. (2002). FLT3 internal tandem duplication mutations associated with human acute myeloid leukemias induce myeloproliferative disease in a murine bone marrow transplant model. Blood *99*, 310-318.

Kharazi, S., Mead, A.J., Mansour, A., Hultquist, A., Böiers, C., Luc, S., Buza-Vidas, N., Ma, Z., Ferry, H., and Atkinson, D., et al. (2011). Impact of gene dosage, loss of wild-type allele, and FLT3 ligand on Flt3-ITD-induced myeloproliferation. Blood *118*, 3613-3621.

Kikushige, Y., Yoshimoto, G., Miyamoto, T., Iino, T., Mori, Y., Iwasaki, H., Niiro, H., Takenaka, K., Nagafuji, K., and Harada, M., et al. (2008). Human Flt3 is expressed at the hematopoietic

stem cell and the granulocyte/macrophage progenitor stages to maintain cell survival. Journal of Immunology *180*, 7358-7367.

Kim, H.-G., Kojima, K., Swindle, C.S., Cotta, C.V., Huo, Y., Reddy, V., and Klug, C.A. (2008). FLT3-ITD cooperates with inv(16) to promote progression to acute myeloid leukemia. Blood *111*, 1567-1574.

Kim, K.-T., Levis, M., and Small, D. (2006). Constitutively activated FLT3 phosphorylates BAD partially through pim-1. British Journal of Haematology *134*, 500-509.

Kim, Y., Lee, G.D., Park, J., Yoon, J.-H., Kim, H.-J., Min, W.-S., and Kim, M. (2015). Quantitative fragment analysis of FLT3-ITD efficiently identifying poor prognostic group with high mutant allele burden or long ITD length. Blood Cancer Journal *5*, e336.

Kindler, T., Lipka, D.B., and Fischer, T. (2010). FLT3 as a therapeutic target in AML: still challenging after all these years. Blood *116*, 5089-5102.

Kinner, A., Wu, W., Staudt, C., and Iliakis, G. (2008). Gamma-H2AX in recognition and signaling of DNA double-strand breaks in the context of chromatin. Nucleic Acids Research *36*, 5678-5694.

Kiyoi, H. (2015a). FLT3 INHIBITORS: RECENT ADVANCES AND PROBLEMS FOR CLINICAL APPLICATION. Nagoya Journal of Medical Science *77*, 7-17.

Kiyoi, H. (2015b). Overview: A New Era of Cancer Genome in Myeloid Malignancies. Oncology *89 Suppl 1*, 1-3.

Kiyoi, H., Ohno, R., Ueda, R., Saito, H., and Naoe, T. (2002). Mechanism of constitutive activation of FLT3 with internal tandem duplication in the juxtamembrane domain. Oncogene *21*, 2555-2563.

Kiyoi, H., Towatari, M., Yokota, S., Hamaguchi, M., Ohno, R., Saito, H., and Naoe, T. (1998). Internal tandem duplication of the FLT3 gene is a novel modality of elongation mutation which causes constitutive activation of the product. Leukemia *12*, 1333-1337.

Knapper, S., Mills, K.I., Gilkes, A.F., Austin, S.J., Walsh, V., and Burnett, A.K. (2006). The effects of lestaurtinib (CEP701) and PKC412 on primary AML blasts: the induction of cytotoxicity varies with dependence on FLT3 signaling in both FLT3-mutated and wild-type cases. Blood *108*, 3494-3503.

Kohlmann, A., Bullinger, L., Thiede, C., Schaich, M., Schnittger, S., Dohner, K., Dugas, M., Klein, H.-U., Dohner, H., and Ehninger, G., et al. (2010). Gene expression profiling in AML with normal karyotype can predict mutations for molecular markers and allows novel insights into perturbed biological pathways. Leukemia *24*, 1216-1220.

Konig, H., and Levis, M. (2015). Targeting FLT3 to treat leukemia. Expert Opinion on Therapeutic Targets *19*, 37-54.

Kottaridis, P.D., Gale, R.E., Frew, M.E., Harrison, G., Langabeer, S.E., Belton, A.A., Walker, H., Wheatley, K., Bowen, D.T., and Burnett, A.K., et al. (2001). The presence of a FLT3 internal tandem duplication in patients with acute myeloid leukemia (AML) adds important prognostic information to cytogenetic risk group and response to the first cycle of chemotherapy: analysis of 854 patients from the United Kingdom Medical Research Council AML 10 and 12 trials. Blood *98*, 1752-1759.

Kottaridis, P.D., Gale, R.E., Langabeer, S.E., Frew, M.E., Bowen, D.T., and Linch, D.C. (2002). Studies of FLT3 mutations in paired presentation and relapse samples from patients with acute myeloid leukemia: implications for the role of FLT3 mutations in leukemogenesis,

minimal residual disease detection, and possible therapy with FLT3 inhibitors. Blood *100*, 2393-2398.

Kronke, J., Bullinger, L., Teleanu, V., Tschurtz, F., Gaidzik, V.I., Kuhn, M.W.M., Rucker, F.G., Holzmann, K., Paschka, P., and Kapp-Schworer, S., et al. (2013). Clonal evolution in relapsed NPM1-mutated acute myeloid leukemia. Blood *122*, 100-108.

Kumar, C.C. (2011). Genetic abnormalities and challenges in the treatment of acute myeloid leukemia. Genes & Cancer *2*, 95-107.

Kurosawa, S., Yamaguchi, H., Yamaguchi, T., Fukunaga, K., Yui, S., Wakita, S., Kanamori, H., Usuki, K., Uoshima, N., and Yanada, M., et al. (2016). Decision Analysis of Postremission Therapy in Cytogenetically Intermediate-Risk Acute Myeloid Leukemia: The Impact of FLT3 Internal Tandem Duplication, Nucleophosmin, and CCAAT/Enhancer Binding Protein Alpha. Biology of Blood and Marrow Transplantation *22*, 1125-32.

Laboure, G., Dulucq, S., Labopin, M., Tabrizi, R., Guerin, E., Pigneux, A., Lafarge, X., Leguay, T., Bouabdallah, K., and Dilhuydy, M.-S., et al. (2012). Potent graft-versus-leukemia effect after reduced-intensity allogeneic SCT for intermediate-risk AML with FLT3-ITD or wild-type NPM1 and CEBPA without FLT3-ITD. Biology of Blood and Marrow Transplantation *18*, 1845-1850.

Lange, B., Valtieri, M., Santoli, D., Caracciolo, D., Mavilio, F., Gemperlein, I., Griffin, C., Emanuel, B., Finan, J., and Nowell, P. (1987). Growth factor requirements of childhood acute leukemia: establishment of GM-CSF-dependent cell lines. Blood *70*, 192-199.

Lapidot, T., Dar, A., and Kollet, O. (2005). How do stem cells find their way home? Blood *106*, 1901-1910.

Lavagna-Sevenier, C., Marchetto, S., Birnbaum, D., and Rosnet, O. (1998). FLT3 signaling in hematopoietic cells involves CBL, SHC and an unknown P115 as prominent tyrosine-phosphorylated substrates. Leukemia *12*, 301-310.

Lee, B.H., Tothova, Z., Levine, R.L., Anderson, K., Buza-Vidas, N., Cullen, D.E., McDowell, E.P., Adelsperger, J., Frohling, S., and Huntly, B.J.P., et al. (2007). FLT3 mutations confer enhanced proliferation and survival properties to multipotent progenitors in a murine model of chronic myelomonocytic leukemia. Cancer Cell *12*, 367-380.

Lee, B.H., Williams, I.R., Anastasiadou, E., Boulton, C.L., Joseph, S.W., Amaral, S.M., Curley, D.P., Duclos, N., Huntly, Brian J P, and Fabbro, D., et al. (2005). FLT3 internal tandem duplication mutations induce myeloproliferative or lymphoid disease in a transgenic mouse model. Oncogene *24*, 7882-7892.

Levis, M., Allebach, J., Tse, K.-F., Zheng, R., Baldwin, B.R., Smith, B.D., Jones-Bolin, S., Ruggeri, B., Dionne, C., and Small, D. (2002). A FLT3-targeted tyrosine kinase inhibitor is cytotoxic to leukemia cells in vitro and in vivo. Blood *99*, 3885-3891.

Levis, M., Brown, P., Smith, B.D., Stine, A., Pham, R., Stone, R., DeAngelo, D., Galinsky, I., Giles, F., and Estey, E., et al. (2006). Plasma inhibitory activity (PIA): a pharmacodynamic assay reveals insights into the basis for cytotoxic response to FLT3 inhibitors. Blood *108*, 3477-3483.

Levis, M., Murphy, K.M., Pham, R., Kim, K.-T., Stine, A., Li, L., McNiece, I., Smith, B.D., and Small, D. (2005). Internal tandem duplications of the FLT3 gene are present in leukemia stem cells. Blood *106*, 673-680.

Li, L., Bailey, E., Greenblatt, S., Huso, D., and Small, D. (2011). Loss of the wild-type allele contributes to myeloid expansion and disease aggressiveness in FLT3/ITD knockin mice. Blood *118*, 4935-4945.

Li, L., Piloto, O., Kim, K.-T., Ye, Z., Nguyen, H.B., Yu, X., Levis, M., Cheng, L., and Small, D. (2007). FLT3/ITD expression increases expansion, survival and entry into cell cycle of human haematopoietic stem/progenitor cells. British Journal of Haematology *137*, 64-75.

Li, L., Piloto, O., Nguyen, H.B., Greenberg, K., Takamiya, K., Racke, F., Huso, D., and Small, D. (2008). Knock-in of an internal tandem duplication mutation into murine FLT3 confers myeloproliferative disease in a mouse model. Blood *111*, 3849-3858.

Li, Z., Herold, T., He, C., Valk, Peter J M, Chen, P., Jurinovic, V., Mansmann, U., Radmacher, M.D., Maharry, K.S., and Sun, M., et al. (2013). Identification of a 24-gene prognostic signature that improves the European LeukemiaNet risk classification of acute myeloid leukemia: an international collaborative study. Journal of Clinical Oncology *31*, 1172-1181.

Linch, D.C., Hills, R.K., Burnett, A.K., Khwaja, A., and Gale, R.E. (2014). Impact of FLT3(ITD) mutant allele level on relapse risk in intermediate-risk acute myeloid leukemia. Blood *124*, 273-276.

Lisovsky, M., Estrov, Z., Zhang, X., Consoli, U., Sanchez-Williams, G., Snell, V., Munker, R., Goodacre, A., Savchenko, V., and Andreeff, M. (1996). Flt3 ligand stimulates proliferation and inhibits apoptosis of acute myeloid leukemia cells: regulation of Bcl-2 and Bax. Blood *88*, 3987-3997.

Longley, D.B., Harkin, D.P., and Johnston, P.G. (2003). 5-fluorouracil: mechanisms of action and clinical strategies. Nature reviews. Cancer *3*, 330-338.

Lyman, S.D., James, L., Zappone, J., Sleath, P.R., Beckmann, M.P., and Bird, T. (1993). Characterization of the protein encoded by the flt3 (flk2) receptor-like tyrosine kinase gene. Oncogene *8*, 815-822.

Mack, T.M. (2014). Biologische Charakterisierung von unterschiedlichen FLT3 nicht-juxtamembranärer internen Tandemduplikationen (ITD) in der akuten myeloischen Leukämie (AML). Magdeburg Univ., Nat. Fak,. Dissertation.

Mackarehtschian, K., Hardin, J.D., Moore, K.A., Boast, S., Goff, S.P., and Lemischka, I.R. (1995). Targeted disruption of the flk2/flt3 gene leads to deficiencies in primitive hematopoietic progenitors. Immunity *3*, 147-161.

Madan, V., Shyamsunder, P., Han, L., Mayakonda, A., Nagata, Y., Sundaresan, J., Kanojia, D., Yoshida, K., Ganesan, S., and Hattori, N., et al. (2016). Comprehensive mutational analysis of primary and relapse acute promyelocytic leukemia. Leukemia.

Mah, L.-J., El-Osta, A., and Karagiannis, T.C. (2010). gammaH2AX: a sensitive molecular marker of DNA damage and repair. Leukemia *24*, 679-686.

Man, C.H., Fung, T.K., Ho, C., Han, H.H.C., Chow, H.C.H., Ma, A.C.H., Choi, W.W.L., Lok, S., Cheung, A.M.S., and Eaves, C., et al. (2012). Sorafenib treatment of FLT3-ITD(+) acute myeloid leukemia: favorable initial outcome and mechanisms of subsequent nonresponsiveness associated with the emergence of a D835 mutation. Blood *119*, 5133-5143.

Maroc, N., Rottapel, R., Rosnet, O., Marchetto, S., Lavezzi, C., Mannoni, P., Birnbaum, D., and Dubreuil, P. (1993). Biochemical characterization and analysis of the transforming potential of the FLT3/FLK2 receptor tyrosine kinase. Oncogene *8*, 909-918.

Matthews, W., Jordan, C.T., Wiegand, G.W., Pardoll, D., and Lemischka, I.R. (1991). A receptor tyrosine kinase specific to hematopoietic stem and progenitor cell-enriched populations. Cell *65*, 1143-1152.

Matulonis, U.A., Dosiou, C., Lamont, C., Freeman, G.J., Mauch, P., Nadler, L.M., and Griffin, J.D. (1995). Role of B7-1 in mediating an immune response to myeloid leukemia cells. Blood *85*, 2507-2515.

Mazzarella, L., Riva, L., Luzi, L., Ronchini, C., and Pelicci, P.G. (2014). The genomic and epigenomic landscapes of AML. Seminars in Hematology *51*, 259-272.

McCormack, E., Bruserud, O., and Gjertsen, B.T. (2005). Animal models of acute myelogenous leukaemia - development, application and future perspectives. Leukemia *19*, 687-706.

McKerrell, T., Park, N., Moreno, T., Grove, C.S., Ponstingl, H., Stephens, J., Crawley, C., Craig, J., Scott, M.A., and Hodkinson, C., et al. (2015). Leukemia-associated somatic mutations drive distinct patterns of age-related clonal hemopoiesis. Cell Reports *10*, 1239-1245.

Mead, A.J., Gale, R.E., Kottaridis, P.D., Matsuda, S., Khwaja, A., and Linch, D.C. (2008). Acute myeloid leukaemia blast cells with a tyrosine kinase domain mutation of FLT3 are less sensitive to lestaurtinib than those with a FLT3 internal tandem duplication. British Journal of Haematology *141*, 454-460.

Medunjanin, S., Weinert, S., Poitz, D., Schmeisser, A., Strasser, R.H., and Braun-Dullaeus, R.C. (2010). Transcriptional activation of DNA-dependent protein kinase catalytic subunit gene expression by oestrogen receptor-alpha. EMBO Reports *11*, 208-213.

Meggendorfer, M., Albuquerque, A. de, Nadarajah, N., Alpermann, T., Kern, W., Steuer, K., Perglerova, K., Haferlach, C., Schnittger, S., and Haferlach, T. (2015). Karyotype evolution and acquisition of FLT3 or RAS pathway alterations drive progression of myelodysplastic syndrome to acute myeloid leukemia. Haematologica *100*, e487-90.

Mehta, S.V., Shukla, S.N., and Vora, H.H. (2013). Overexpression of Bcl2 protein predicts chemoresistance in acute myeloid leukemia: its correlation with FLT3. Neoplasma *60*, 666-675.

Meshinchi, S., and Appelbaum, F.R. (2009). Structural and functional alterations of FLT3 in acute myeloid leukemia. Clinical Cancer Research *15*, 4263-4269.

Miller, C.L., and Lai, B. (2005). Human and mouse hematopoietic colony-forming cell assays. Methods in Molecular Biology *290*, 71-89.

Mizuki, M., Fenski, R., Halfter, H., Matsumura, I., Schmidt, R., Müller, C., Grüning, W., Kratz-Albers, K., Serve, S., and Steur, C., et al. (2000). Flt3 mutations from patients with acute myeloid leukemia induce transformation of 32D cells mediated by the Ras and STAT5 pathways. Blood *96*, 3907-3914.

Mizuki, M., Schwable, J., Steur, C., Choudhary, C., Agrawal, S., Sargin, B., Steffen, B., Matsumura, I., Kanakura, Y., and Bohmer, F.D., et al. (2003). Suppression of myeloid transcription factors and induction of STAT response genes by AML-specific Flt3 mutations. Blood *101*, 3164-3173.

Moore, A.S., Faisal, A., Gonzalez de Castro, D., Bavetsias, V., Sun, C., Atrash, B., Valenti, M., Haven Brandon, A. de, Avery, S., and Mair, D., et al. (2012). Selective FLT3 inhibition of FLT3-ITD+ acute myeloid leukaemia resulting in secondary D835Y mutation: a model for emerging clinical resistance patterns. Leukemia *26*, 1462-1470.

Mori, N. (2010). Two loci controlling susceptibility to radiation-induced lymphomagenesis on mouse chromosome 4: cdkn2a, a candidate for one locus, and a novel locus distinct from cdkn2a. Radiation Research *173*, 158-164.

Mrozek, K., Marcucci, G., Nicolet, D., Maharry, K.S., Becker, H., Whitman, S.P., Metzeler, K.H., Schwind, S., Wu, Y.-Z., and Kohlschmidt, J., et al. (2012). Prognostic significance of the

European LeukemiaNet standardized system for reporting cytogenetic and molecular alterations in adults with acute myeloid leukemia. Journal of Clinical Oncology *30*, 4515-4523.

Muslimovic, A., Johansson, P., and Hammarste, O. (2012). Measurement of H2AX Phosphorylation as a Marker of Ionizing Radiation Induced Cell Damage. Current Topics in Ionizing Radiation Research.

Nabinger, S.C., Li, X.J., Ramdas, B., He, Y., Zhang, X., Zeng, L., Richine, B., Bowling, J.D., Fukuda, S., and Goenka, S., et al. (2013). The protein tyrosine phosphatase, Shp2, positively contributes to FLT3-ITD-induced hematopoietic progenitor hyperproliferation and malignant disease in vivo. Leukemia *27*, 398-408.

Nakao, M., Yokota, S., Iwai, T., Kaneko, H., Horiike, S., Kashima, K., Sonoda, Y., Fujimoto, T., and Misawa, S. (1996). Internal tandem duplication of the flt3 gene found in acute myeloid leukemia. Leukemia *10*, 1911-1918.

Namikawa, R., Muench, M.O., Vries, J.E. de, and Roncarolo, M.G. (1996). The FLK2/FLT3 ligand synergizes with interleukin-7 in promoting stromal-cell-independent expansion and differentiation of human fetal pro-B cells in vitro. Blood *87*, 1881-1890.

Naoe, T., Kiyoe, H., Yamamoto, Y., Minami, Y., Yamamoto, K., Ueda, R., and Saito, H. (2001). FLT3 tyrosine kinase as a target molecule for selective antileukemia therapy. Cancer Chemotherapy and Pharmacology *48 Suppl 1*, S27-30.

Naoe, T., and Kiyoi, H. (2004). Normal and oncogenic FLT3. Cellular and Molecular Life Sciences *61*, 2932-2938.

Neben, K., Schnittger, S., Brors, B., Tews, B., Kokocinski, F., Haferlach, T., Muller, J., Hahn, M., Hiddemann, W., and Eils, R., et al. (2005). Distinct gene expression patterns associated with FLT3- and NRAS-activating mutations in acute myeloid leukemia with normal karyotype. Oncogene *24*, 1580-1588.

Nicoletti, I., Migliorati, G., Pagliacci, M.C., Grignani, F., and Riccardi, C. (1991). A rapid and simple method for measuring thymocyte apoptosis by propidium iodide staining and flow cytometry. Journal of Immunological Methods *139*, 271-279.

Nonami, A., Sattler, M., Weisberg, E., Liu, Q., Zhang, J., Patricelli, M.P., Christie, A.L., Saur, A.M., Kohl, N.E., and Kung, A.L., et al. (2015). Identification of novel therapeutic targets in acute leukemias with NRAS mutations using a pharmacologic approach. Blood *125*, 3133-3143.

Nordigarden, A., Kraft, M., Eliasson, P., Labi, V., Lam, E.W.-F., Villunger, A., and Jonsson, J.-I. (2009). BH3-only protein Bim more critical than Puma in tyrosine kinase inhibitor-induced apoptosis of human leukemic cells and transduced hematopoietic progenitors carrying oncogenic FLT3. Blood *113*, 2302-2311.

Onishi, C., Mori-Kimachi, S., Hirade, T., Abe, M., Taketani, T., Suzumiya, J., Sugimoto, T., Yamaguchi, S., Kapur, R., and Fukuda, S. (2015). Internal tandem duplication mutations in FLT3 gene augment chemotaxis to Cxcl12 protein by blocking the down-regulation of Rho-associated kinase via the Cxcl12/Cxcr4 signaling axis. The Journal of Biological Chemistry *290*, 28356.

Oshikawa, G., Nagao, T., Wu, N., Kurosu, T., and Miura, O. (2011). c-Cbl and Cbl-b ligases mediate 17-allylaminodemethoxygeldanamycin-induced degradation of autophosphorylated Flt3 kinase with internal tandem duplication through the ubiquitin proteasome pathway. Journal of Biological Chemistry *286*, 30263-30273.

Paietta, E., Ferrando, A.A., Neuberg, D., Bennett, J.M., Racevskis, J., Lazarus, H., Dewald, G., Rowe, J.M., Wiernik, P.H., and Tallman, M.S., et al. (2004). Activating FLT3 mutations in CD117/KIT(+) T-cell acute lymphoblastic leukemias. Blood *104*, 558-560.

Parcells, B.W., Ikeda, A.K., Simms-Waldrip, T., Moore, T.B., and Sakamoto, K.M. (2006). FMS-like tyrosine kinase 3 in normal hematopoiesis and acute myeloid leukemia. Stem cells *24*, 1174-1184.

Park, I.-K., Mundy-Bosse, B., Whitman, S.P., Zhang, X., Warner, S.L., Bearss, D.J., Blum, W., Marcucci, G., and Caligiuri, M.A. (2015). Receptor tyrosine kinase Axl is required for resistance of leukemic cells to FLT3-targeted therapy in acute myeloid leukemia. Leukemia *29*, 2382-9.

Parkin, B., Ouillette, P., Li, Y., Keller, J., Lam, C., Roulston, D., Li, C., Shedden, K., and Malek, S.N. (2013). Clonal evolution and devolution after chemotherapy in adult acute myelogenous leukemia. Blood *121*, 369-377.

Passegué, E., Jamieson, Catriona H M, Ailles, L.E., and Weissman, I.L. (2003). Normal and leukemic hematopoiesis: are leukemias a stem cell disorder or a reacquisition of stem cell characteristics?. Proceedings of the National Academy of Sciences of the United States of America *100*, 11842-11849.

Patel, J.P., Gönen, M., Figueroa, M.E., Fernandez, H., Sun, Z., Racevskis, J., van Vlierberghe, P., Dolgalev, I., Thomas, S., and Aminova, O., et al. (2012). Prognostic relevance of integrated genetic profiling in acute myeloid leukemia. The New England Journal of Medicine *366*, 1079-1089.

Pauwels, D., Sweron, B., and Cools, J. (2012). The N676D and G697R mutations in the kinase domain of FLT3 confer resistance to the inhibitor AC220. Haematologica *97*, 1773-1774.

Persons, D.A., Allay, J.A., Allay, E.R., Smeyne, R.J., Ashmun, R.A., Sorrentino, B.P., and Nienhuis, A.W. (1997). Retroviral-mediated transfer of the green fluorescent protein gene into murine hematopoietic cells facilitates scoring and selection of transduced progenitors in vitro and identification of genetically modified cells in vivo. Blood *90*, 1777-1786.

Pietschmann, K., Bolck, H.A., Buchwald, M., Spielberg, S., Polzer, H., Spiekermann, K., Bug, G., Heinzel, T., Bohmer, F.-D., and Kramer, O.H. (2012). Breakdown of the FLT3-ITD/STAT5 axis and synergistic apoptosis induction by the histone deacetylase inhibitor panobinostat and FLT3-specific inhibitors. Molecular Cancer Therapeutics *11*, 2373-2383.

Podhorecka, M., Skladanowski, A., and Bozko, P. (2010). H2AX Phosphorylation: Its Role in DNA Damage Response and Cancer Therapy. Journal of Nucleic Acids *2010*.

Ponziani, V., Gianfaldoni, G., Mannelli, F., Leoni, F., Ciolli, S., Guglielmelli, P., Antonioli, E., Longo, G., Bosi, A., and Vannucchi, A.M. (2006). The size of duplication does not add to the prognostic significance of FLT3 internal tandem duplication in acute myeloid leukemia patients. Leukemia *20*, 2074-2076.

Puissant, A., Fenouille, N., Alexe, G., Pikman, Y., Bassil, C.F., Mehta, S., Du, J., Kazi, J.U., Luciano, F., and Ronnstrand, L., et al. (2014). SYK is a critical regulator of FLT3 in acute myeloid leukemia. Cancer Cell *25*, 226-242.

Quentmeier, H., Reinhardt, J., Zaborski, M., and Drexler, H.G. (2003). FLT3 mutations in acute myeloid leukemia cell lines. Leukemia *17*, 120-124.

Raderschall, E., Stout, K., Freier, S., Suckow, V., Schweiger, S., and Haaf, T. (2002). Elevated levels of Rad51 recombination protein in tumor cells. Cancer Research *62*, 219-225.

Radley, J.M., and Scurfield, G. (1979). Effects of 5-fluorouracil on mouse bone marrow. British Journal of Haematology *43*, 341-351.

Radomska, H.S., Basseres, D.S., Zheng, R., Zhang, P., Dayaram, T., Yamamoto, Y., Sternberg, D.W., Lokker, N., Giese, N.A., and Bohlander, S.K., et al. (2006). Block of C/EBP alpha function by phosphorylation in acute myeloid leukemia with FLT3 activating mutations. The Journal of Experimental Medicine *203*, 371-381.

Rapin, N., Bagger, F.O., Jendholm, J., Mora-Jensen, H., Krogh, A., Kohlmann, A., Thiede, C., Borregaard, N., Bullinger, L., and Winther, O., et al. (2014). Comparing cancer vs normal gene expression profiles identifies new disease entities and common transcriptional programs in AML patients. Blood *123*, 894-904.

Ray, R.J., Paige, C.J., Furlonger, C., Lyman, S.D., and Rottapel, R. (1996). Flt3 ligand supports the differentiation of early B cell progenitors in the presence of interleukin-11 and interleukin-7. European Journal of Immunology *26*, 1504-1510.

Roberts, K.G., Morin, R.D., Zhang, J., Hirst, M., Zhao, Y., Su, X., Chen, S.-C., Payne-Turner, D., Churchman, M.L., and Harvey, R.C., et al. (2012). Genetic alterations activating kinase and cytokine receptor signaling in high-risk acute lymphoblastic leukemia. Cancer Cell *22*, 153-166.

Rocnik, J.L., Okabe, R., Yu, J.-C., Lee, B.H., Giese, N., Schenkein, D.P., and Gilliland, D.G. (2006). Roles of tyrosine 589 and 591 in STAT5 activation and transformation mediated by FLT3-ITD. Blood *108*, 1339-1345.

Röllig, C., Serve, H., Hüttmann, A., Noppeney, R., Müller-Tidow, C., Krug, U., Baldus, C.D., Brandts, C.H., Kunzmann, V., and Einsele, H., et al. (2015). Addition of sorafenib versus placebo to standard therapy in patients aged 60 years or younger with newly diagnosed acute myeloid leukaemia (SORAML). A multicentre, phase 2, randomised controlled trial. The Lancet Oncology *16*, 1691-1699.

Rosnet, O., Buhring, H.J., Marchetto, S., Rappold, I., Lavagna, C., Sainty, D., Arnoulet, C., Chabannon, C., Kanz, L., and Hannum, C., et al. (1996). Human FLT3/FLK2 receptor tyrosine kinase is expressed at the surface of normal and malignant hematopoietic cells. Leukemia *10*, 238-248.

Rosnet, O., Marchetto, S., deLapeyriere, O., and Birnbaum, D. (1991a). Murine Flt3, a gene encoding a novel tyrosine kinase receptor of the PDGFR/CSF1R family. Oncogene *6*, 1641-1650.

Rosnet, O., Mattei, M.G., Marchetto, S., and Birnbaum, D. (1991b). Isolation and chromosomal localization of a novel FMS-like tyrosine kinase gene. Genomics *9*, 380-385.

Rosnet, O., Schiff, C., Pebusque, M.J., Marchetto, S., Tonnelle, C., Toiron, Y., Birg, F., and Birnbaum, D. (1993). Human FLT3/FLK2 gene: cDNA cloning and expression in hematopoietic cells. Blood *82*, 1110-1119.

Rottapel, R., Turck, C.W., Casteran, N., Liu, X., Birnbaum, D., Pawson, T., and Dubreuil, P. (1994). Substrate specificities and identification of a putative binding site for PI3K in the carboxy tail of the murine Flt3 receptor tyrosine kinase. Oncogene *9*, 1755-1765.

Sallmyr, A., Fan, J., Datta, K., Kim, K.-T., Grosu, D., Shapiro, P., Small, D., and Rassool, F. (2008a). Internal tandem duplication of FLT3 (FLT3/ITD) induces increased ROS production, DNA damage, and misrepair: implications for poor prognosis in AML. Blood *111*, 3173-3182.

Sallmyr, A., Fan, J., and Rassool, F.V. (2008b). Genomic instability in myeloid malignancies: increased reactive oxygen species (ROS), DNA double strand breaks (DSBs) and error-prone repair. Cancer Letters *270*, 1-9.

Sanger, F., Nicklen, S., and Coulson, A.R. (1977). DNA sequencing with chain-terminating inhibitors. Proceedings of the National Academy of Sciences of the United States of America *74*, 5463-5467.

Sargin, B., Choudhary, C., Crosetto, N., Schmidt, M.H.H., Grundler, R., Rensinghoff, M., Thiessen, C., Tickenbrock, L., Schwable, J., and Brandts, C., et al. (2007). Flt3-dependent transformation by inactivating c-Cbl mutations in AML. Blood *110*, 1004-1012.

Sato, T., Yang, X., Knapper, S., White, P., Smith, B.D., Galkin, S., Small, D., Burnett, A., and Levis, M. (2011). FLT3 ligand impedes the efficacy of FLT3 inhibitors in vitro and in vivo. Blood *117*, 3286-3293.

Scheijen, B., Ngo, H.T., Kang, H., and Griffin, J.D. (2004). FLT3 receptors with internal tandem duplications promote cell viability and proliferation by signaling through Foxo proteins. Oncogene *23*, 3338-3349.

Schessl, C., Rawat, V.P.S., Cusan, M., Deshpande, A., Kohl, T.M., Rosten, P.M., Spiekermann, K., Humphries, R.K., Schnittger, S., and Kern, W., et al. (2005). The AML1-ETO fusion gene and the FLT3 length mutation collaborate in inducing acute leukemia in mice. The Journal of Clinical Investigation *115*, 2159-2168.

Schlenk, R.F., Kayser, S., Bullinger, L., Kobbe, G., Casper, J., Ringhoffer, M., Held, G., Brossart, P., Lübbert, M., and Salih, H.R., et al. (2014). Differential impact of allelic ratio and insertion site in FLT3-ITD-positive AML with respect to allogeneic transplantation. Blood *124*, 3441-3449.

Schlessinger, J. (2003). Autoinhibition control. Science *300*, 750-752.

Schnittger, S., Bacher, U., Haferlach, C., Alpermann, T., Kern, W., and Haferlach, T. (2012). Diversity of the juxtamembrane and TKD1 mutations (exons 13-15) in the FLT3 gene with regards to mutant load, sequence, length, localization, and correlation with biological data. Genes Chromosomes Cancer *51*, 910-924.

Schnittger, S., Schoch, C., Dugas, M., Kern, W., Staib, P., Wuchter, C., Löffler, H., Sauerland, C.M., Serve, H., and Büchner, T., et al. (2002). Analysis of FLT3 length mutations in 1003 patients with acute myeloid leukemia: correlation to cytogenetics, FAB subtype, and prognosis in the AMLCG study and usefulness as a marker for the detection of minimal residual disease. Blood *100*, 59-66.

Schwable, J., Choudhary, C., Thiede, C., Tickenbrock, L., Sargin, B., Steur, C., Rehage, M., Rudat, A., Brandts, C., and Berdel, W.E., et al. (2005). RGS2 is an important target gene of Flt3-ITD mutations in AML and functions in myeloid differentiation and leukemic transformation. Blood *105*, 2107-2114.

Seedhouse, C.H., Hunter, H.M., Lloyd-Lewis, B., Massip, A.-M., Pallis, M., Carter, G.I., Grundy, M., Shang, S., and Russell, N.H. (2006). DNA repair contributes to the drug-resistant phenotype of primary acute myeloid leukaemia cells with FLT3 internal tandem duplications and is reversed by the FLT3 inhibitor PKC412. Leukemia *20*, 2130-2136.

Sell, S. (2005). Leukemia: stem cells, maturation arrest, and differentiation therapy. Stem Cell Reviews *1*, 197-205.

Shah, A.J., Smogorzewska, E.M., Hannum, C., and Crooks, G.M. (1996). Flt3 ligand induces proliferation of quiescent human bone marrow CD34+CD38- cells and maintains progenitor cells in vitro. Blood *87*, 3563-3570.

Shawver, L.K., Slamon, D., and Ullrich, A. (2002). Smart drugs: tyrosine kinase inhibitors in cancer therapy. Cancer Cell *1*, 117-123.

Shibuya, M., Matsushime, H., Yamane, A., Ikeda, T., Yoshida, M.C., and Tojo, A. (1989). Isolation and characterization of new mammalian kinase genes by cross hybridization with a tyrosine kinase probe. Princess Takamatsu Symposia *20*, 103-110.

Shih, A.H., Jiang, Y., Meydan, C., Shank, K., Pandey, S., Barreyro, L., Antony-Debre, I., Viale, A., Socci, N., and Sun, Y., et al. (2015). Mutational cooperativity linked to combinatorial epigenetic gain of function in acute myeloid leukemia. Cancer Cell *27*, 502-515.

Shih, L.-Y., Lin, T.-L., Wang, P.-N., Wu, J.-H., Dunn, P., Kuo, M.-C., and Huang, C.-F. (2004). Internal tandem duplication of fms-like tyrosine kinase 3 is associated with poor outcome in patients with myelodysplastic syndrome. Cancer *101*, 989-998.

Shlush, L.I., Zandi, S., Mitchell, A., Chen, W.C., Brandwein, J.M., Gupta, V., Kennedy, J.A., Schimmer, A.D., Schuh, A.C., and Yee, K.W., et al. (2014). Identification of pre-leukaemic haematopoietic stem cells in acute leukaemia. Nature *506*, 328-333.

Shurin, M.R., Esche, C., and Lotze, M.T. (1998). FLT3: receptor and ligand. Biology and potential clinical application. Cytokine & Growth Factor Reviews *9*, 37-48.

Smith, C.C., and Shah, N.P. (2012). Mechanisms of resistance to targeted therapies in acute myeloid leukemia and chronic myeloid leukemia. American Society of Clinical Oncology, 685-689.

Smith, C.C., Wang, Q., Chin, C.-S., Salerno, S., Damon, L.E., Levis, M.J., Perl, A.E., Travers, K.J., Wang, S., and Hunt, J.P., et al. (2012a). Validation of ITD mutations in FLT3 as a therapeutic target in human acute myeloid leukaemia. Nature *485*, 260-263.

Smith, C.C., Wang, Q., Chin, C.-S., Salerno, S., Damon, L.E., Levis, M.J., Perl, A.E., Travers, K.J., Wang, S., and Hunt, J.P., et al. (2012b). Validation of ITD mutations in FLT3 as a therapeutic target in human acute myeloid leukaemia. Nature *485*, 260-263.

Smith, D.R. (1993). Restriction endonuclease digestion of DNA. Methods in Molecular Biology *18*, 427-431.

Spiekermann, K., Bagrintseva, K., Schoch, C., Haferlach, T., Hiddemann, W., and Schnittger, S. (2002). A new and recurrent activating length mutation in exon 20 of the FLT3 gene in acute myeloid leukemia. Blood *100*, 3423-3425.

Spiekermann, K., Bagrintseva, K., Schwab, R., Schmieja, K., and Hiddemann, W. (2003). Overexpression and constitutive activation of FLT3 induces STAT5 activation in primary acute myeloid leukemia blast cells. Clinical Cancer Research *9*, 2140-2150.

Stanicka, J., Russell, E.G., Woolley, J.F., and Cotter, T.G. (2015). NADPH oxidase-generated hydrogen peroxide induces DNA damage in mutant FLT3-expressing leukemia cells. Journal of Biological Chemistry *290*, 9348-9361.

Stirewalt, D.L., Kopecky, K.J., Meshinchi, S., Engel, J.H., Pogosova-Agadjanyan, E.L., Linsley, J., Slovak, M.L., Willman, C.L., and Radich, J.P. (2006). Size of FLT3 internal tandem duplication has prognostic significance in patients with acute myeloid leukemia. Blood *107*, 3724-3726.

Stirewalt, D.L., and Radich, J.P. (2003). The role of FLT3 in haematopoietic malignancies. Nature reviews. Cancer *3*, 650-665.

Stölzel, F., Steudel, C., Oelschlägel, U., Mohr, B., Koch, S., Ehninger, G., and Thiede, C. (2010). Mechanisms of resistance against PKC412 in resistant FLT3-ITD positive human acute myeloid leukemia cells. Annals of Hematology *89*, 653-662.

Stone, R.M., Angelo, J. de, Galinsky, I., Estey, E., Klimek, V., Grandin, W., Lebwohl, D., Yap, A., Cohen, P., and Fox, E., et al. (2004). PKC 412 FLT3 inhibitor therapy in AML: results of a phase II trial. Annals of Hematology *83*, S89-90.

Stone, R.M., Deangelo, D.J., Klimek, V., Galinsky, I., Estey, E., Nimer, S.D., Grandin, W., Lebwohl, D., Wang, Y., and Cohen, P., et al. (2005). Patients with acute myeloid leukemia and an activating mutation in FLT3 respond to a small-molecule FLT3 tyrosine kinase inhibitor, PKC412. Blood *105*, 54-60.

Stone, R.M, Mandrekars, S., Sanford, B.L., Geyer, S, Bloomfield, C.D., Dohner, K, Thiede, C., Marcucci, G., Lo-Coco, F., and Klisovic, R.B., et al. (2015). The Multi-Kinase Inhibitor Midostaurin (M) Prolongs Survival Compared with Placebo (P) in Combination with Daunorubicin (D)/Cytarabine (C) Induction (ind), High-Dose C Consolidation (consol), and As Maintenance (maint) Therapy in Newly Diagnosed Acute Myeloid Leukemia (AML) Patients (pts) Age 18-60 with FLT3 Mutations (muts): An International Prospective Randomized (rand) P-Controlled Double-Blind Trial (CALGB 10603/RATIFY [Alliance]). Proceedings of the American Society of Hematology Annual Meeting, Abstract #6.

Takahashi, K., Jabbour, E., Wang, X., Luthra, R., Bueso-Ramos, C., Patel, K., Pierce, S., Yang, H., Wei, Y., and Daver, N., et al. (2013). Dynamic acquisition of FLT3 or RAS alterations drive a subset of patients with lower risk MDS to secondary AML. Leukemia *27*, 2081-2083.

Takahashi, M., Ogino, T., and Baba, K. (1969). Estimation of relative molecular length of DNA by electrophoresis in agarose gel. Biochimica et Biophysica Acta *174*, 183-187.

Takahashi, S. (2011). Downstream molecular pathways of FLT3 in the pathogenesis of acute myeloid leukemia: biology and therapeutic implications. Journal of Hematology & Oncology *4*, 13.

Taskesen, E., Bullinger, L., Corbacioglu, A., Sanders, M.A., Erpelinck, C.A.J., Wouters, B.J., van der Poel-van de Luytgaarde, Sonja C, Damm, F., Krauter, J., and Ganser, A., et al. (2011). Prognostic impact, concurrent genetic mutations, and gene expression features of AML with CEBPA mutations in a cohort of 1182 cytogenetically normal AML patients: further evidence for CEBPA double mutant AML as a distinctive disease entity. Blood *117*, 2469-2475.

Testa, U., and Pelosi, E. (2013). The Impact of FLT3 Mutations on the Development of Acute Myeloid Leukemias. Leukemia Research and Treatment *2013*, 275760.

Thiede, C., Steudel, C., Mohr, B., Schaich, M., Schäkel, U., Platzbecker, U., Wermke, M., Bornhäuser, M., Ritter, M., and Neubauer, A., et al. (2002). Analysis of FLT3-activating mutations in 979 patients with acute myelogenous leukemia: association with FAB subtypes and identification of subgroups with poor prognosis. Blood *99*, 4326-4335.

Tickenbrock, L., Schwable, J., Wiedehage, M., Steffen, B., Sargin, B., Choudhary, C., Brandts, C., Berdel, W.E., Muller-Tidow, C., and Serve, H. (2005). Flt3 tandem duplication mutations cooperate with Wnt signaling in leukemic signal transduction. Blood *105*, 3699-3706.

Toffalini, F., and Demoulin, J.-B. (2010). New insights into the mechanisms of hematopoietic cell transformation by activated receptor tyrosine kinases. Blood *116*, 2429-2437.

Tse, K.F., Mukherjee, G., and Small, D. (2000). Constitutive activation of FLT3 stimulates multiple intracellular signal transducers and results in transformation. Leukemia *14*, 1766-1776.

Tse, K.F., Novelli, E., Civin, C.I., Bohmer, F.D., and Small, D. (2001). Inhibition of FLT3-mediated transformation by use of a tyrosine kinase inhibitor. Leukemia *15*, 1001-1010.

Tsuboi, I., Hirabayashi, Y., Harada, T., Hiramoto, M., Kanno, J., Inoue, T., and Aizawa, S. (2008). Predominant regeneration of B-cell lineage, instead of myeloid lineage, of the bone marrow after 1 Gy whole-body irradiation in mice: role of differential cytokine expression between B-cell stimulation by IL10, Flt3 ligand and IL7 and myeloid suppression by GM-CSF and SCF. Radiation Research *170*, 15-22.

Turner, A.M., Lin, N.L., Issarachai, S., Lyman, S.D., and Broudy, V.C. (1996). FLT3 receptor expression on the surface of normal and malignant human hematopoietic cells. Blood *88*, 3383-3390.

Vempati, S., Reindl, C., Kaza, S.K., Kern, R., Malamoussi, T., Dugas, M., Mellert, G., Schnittger, S., Hiddemann, W., and Spiekermann, K. (2007). Arginine 595 is duplicated in patients with acute leukemias carrying internal tandem duplications of FLT3 and modulates its transforming potential. Blood *110*, 686-694.

Verstraete, K., Vandriessche, G., Januar, M., Elegheert, J., Shkumatov, A.V., Desfosses, A., van Craenenbroeck, K., Svergun, D.I., Gutsche, I., and Vergauwen, B., et al. (2011). Structural insights into the extracellular assembly of the hematopoietic Flt3 signaling complex. Blood *118*, 60-68.

Van Etten, R.A. (2002). Studying the pathogenesis of *BCR–ABL*[+] leukemia in mice. Oncogene *21*, 8643–8651.

Wachter, R.M., Elsliger, M.-A., Kallio, K., Hanson, G.T., and Remington, S.J. (1998). Structural basis of spectral shifts in the yellow-emission variants of green fluorescent protein. Structure *6*, 1267-1277.

Wakita, S., Yamaguchi, H., Omori, I., Terada, K., Ueda, T., Manabe, E., Kurosawa, S., Iida, S., Ibaraki, T., and Sato, Y., et al. (2013). Mutations of the epigenetics-modifying gene (DNMT3a, TET2, IDH1/2) at diagnosis may induce FLT3-ITD at relapse in de novo acute myeloid leukemia. Leukemia *27*, 1044-1052.

Wakita, S., Yamaguchi, H., Ueki, T., Usuki, K., Kurosawa, S., Kobayashi, Y., Kawata, E., Tajika, K., Gomi, S., and Koizumi, M., et al. (2016). Complex molecular genetic abnormalities involving three or more genetic mutations are important prognostic factors for acute myeloid leukemia. Leukemia *30*, 545-554.

Wander, S.A., Levis, M.J., and Fathi, A.T. (2014). The evolving role of FLT3 inhibitors in acute myeloid leukemia: quizartinib and beyond. Therapeutic Advances in Hematology *5*, 65-77.

Weisberg, E., Boulton, C., Kelly, L.M., Manley, P., Fabbro, D., Meyer, T., Gilliland, D.G., and Griffin, J.D. (2002). Inhibition of mutant FLT3 receptors in leukemia cells by the small molecule tyrosine kinase inhibitor PKC412. Cancer Cell *1*, 433-443.

Welch, J.S., Ley, T.J., Link, D.C., Miller, C.A., Larson, D.E., Koboldt, D.C., Wartman, L.D., Lamprecht, T.L., Liu, F., and Xia, J., et al. (2012). The origin and evolution of mutations in acute myeloid leukemia. Cell *150*, 264-278.

Wertheim, J.A., Miller, J.P., Xu, L., He, Y., and Pear, W.S. (2002). The biology of chronic myelogenous leukemia:mouse models and cell adhesion. Oncogene *21*, 8612–8628.

Whitman, S.P., Archer, K.J., Feng, L., Baldus, C., Becknell, B., Carlson, B.D., Carroll, A.J., Mrozek, K., Vardiman, J.W., and George, S.L., et al. (2001). Absence of the wild-type allele predicts poor prognosis in adult de novo acute myeloid leukemia with normal cytogenetics and the internal tandem duplication of FLT3: a cancer and leukemia group B study. Cancer Research *61*, 7233-7239.

Wils, E.-J., Braakman, E., Verjans, Georges M G M, Rombouts, E.J.C., Broers, A.E.C., Niesters, H.G.M., Wagemaker, G., Staal, F.J.T., Lowenberg, B., and Spits, H., et al. (2007). Flt3 ligand

expands lymphoid progenitors prior to recovery of thymopoiesis and accelerates T cell reconstitution after bone marrow transplantation. Journal of immunology *178*, 3551-3557.

Woolley, J.F., Naughton, R., Stanicka, J., Gough, D.R., Bhatt, L., Dickinson, B.C., Chang, C.J., and Cotter, T.G. (2012). H2O2 production downstream of FLT3 is mediated by p22phox in the endoplasmic reticulum and is required for STAT5 signalling. PloS One *7*, e34050.

Yamamoto, Y., Kiyoi, H., Nakano, Y., Suzuki, R., Kodera, Y., Miyawaki, S., Asou, N., Kuriyama, K., Yagasaki, F., and Shimazaki, C., et al. (2001). Activating mutation of D835 within the activation loop of FLT3 in human hematologic malignancies. Blood *97*, 2434-2439.

Yang, X., Liu, L., Sternberg, D., Tang, L., Galinsky, I., DeAngelo, D., and Stone, R. (2005). The FLT3 internal tandem duplication mutation prevents apoptosis in interleukin-3-deprived BaF3 cells due to protein kinase A and ribosomal S6 kinase 1-mediated BAD phosphorylation at serine 112. Cancer Research *65*, 7338-7347.

Yokota, S., Kiyoi, H., Nakao, M., Iwai, T., Misawa, S., Okuda, T., Sonoda, Y., Abe, T., Kahsima, K., and Matsuo, Y., et al. (1997). Internal tandem duplication of the FLT3 gene is preferentially seen in acute myeloid leukemia and myelodysplastic syndrome among various hematological malignancies. A study on a large series of patients and cell lines. Leukemia *11*, 1605-1609.

Yoshimoto, G., Miyamoto, T., Jabbarzadeh-Tabrizi, S., Iino, T., Rocnik, J.L., Kikushige, Y., Mori, Y., Shima, T., Iwasaki, H., and Takenaka, K., et al. (2009). FLT3-ITD up-regulates MCL-1 to promote survival of stem cells in acute myeloid leukemia via FLT3-ITD-specific STAT5 activation. Blood *114*, 5034-5043.

Zarrinkar, P.P., Gunawardane, R.N., Cramer, M.D., Gardner, M.F., Brigham, D., Belli, B., Karaman, M.W., Pratz, K.W., Pallares, G., and Chao, Q., et al. (2009). AC220 is a uniquely potent and selective inhibitor of FLT3 for the treatment of acute myeloid leukemia (AML). Blood *114*, 2984-2992.

Zhang, J., Vakhrusheva, O., Bandi, S.R., Demirel, O., Kazi, J.U., Fernandes, R.G., Jakobi, K., Eichler, A., Ronnstrand, L., and Rieger, M.A., et al. (2015). The Phosphatases STS1 and STS2 Regulate Hematopoietic Stem and Progenitor Cell Fitness. Stem Cell Reports *5*, 633-646.

Zhang, S., and Broxmeyer, H.E. (2000). Flt3 ligand induces tyrosine phosphorylation of gab1 and gab2 and their association with shp-2, grb2, and PI3 kinase. Biochemical and Biophysical Research Communications *277*, 195-199.

Zhang, S., Fukuda, S., Lee, Y., Hangoc, G., Cooper, S., Spolski, R., Leonard, W.J., and Broxmeyer, H.E. (2000). Essential role of signal transducer and activator of transcription (Stat)5a but not Stat5b for Flt3-dependent signaling. Journal of Experimental Medicine *192*, 719-728.

Zhang, S., Ramsay, E.S., and Mock, B.A. (1998). Cdkn2a, the cyclin-dependent kinase inhibitor encoding p16INK4a and p19ARF, is a candidate for the plasmacytoma susceptibility locus, Pctr1. Proceedings of the National Academy of Sciences of the United States of America *95*, 2429-2434.

Zhao, M., Kiyoi, H., Yamamoto, Y., Ito, M., Towatari, M., Omura, S., Kitamura, T., Ueda, R., Saito, H., and Naoe, T. (2000). In vivo treatment of mutant FLT3-transformed murine leukemia with a tyrosine kinase inhibitor. Leukemia *14*, 374-378.

Zheng, R., and Small, D. (2005). Mutant FLT3 signaling contributes to a block in myeloid differentiation. Leukemia & Lymphoma *46*, 1679-1687.

Zhou, J., Bi, C., Chng, W.-J., Cheong, L.-L., Liu, S.-C., Mahara, S., Tay, K.-G., Zeng, Q., Li, J., and Guo, K., et al. (2011). PRL-3, a metastasis associated tyrosine phosphatase, is involved in FLT3-ITD signaling and implicated in anti-AML therapy. PloS One *6*, e19798.

Zhou, J., Bi, C., Janakakumara, J.V., Liu, S.-C., Chng, W.-J., Tay, K.-G., Poon, L.-F., Xie, Z., Palaniyandi, S., and Yu, H., et al. (2009). Enhanced activation of STAT pathways and overexpression of survivin confer resistance to FLT3 inhibitors and could be therapeutic targets in AML. Blood *113*, 4052-4062.

Zorko, N.A., Bernot, K.M., Whitman, S.P., Siebenaler, R.F., Ahmed, E.H., Marcucci, G.G., Yanes, D.A., McConnell, K.K., Mao, C., and Kalu, C., et al. (2012). Mll partial tandem duplication and Flt3 internal tandem duplication in a double knock-in mouse recapitulates features of counterpart human acute myeloid leukemias. Blood *120*, 1130-1136.

8. Appendix

8.1. Appendix 1

Animal ID

Date of experiment:

Experiment ID:

Retroviral vector:

Study ID:

Days	Date	Employee	Weight (g)	Fur	Posture	Motility	WBC	GFP+ cells	Sick?	Observations

Date of death:

Analyzed: YES   NO

8.2. Appendix 2

Physiological Data Summary - BALB/cJ (000651)

The Jackson Laboratory

Revised: December 13, 2007

Complete data with range and standard deviations available from the Mouse Phenome Database (MPD, *www.jax.org/phenome*) and enter the term "jaxpheno" into the search box, or go directly to this url: *phenome.jax.org/pub-cgi/phenome/mpdcgi?rtn-views%2Fsearch&req=jaxpheno*.
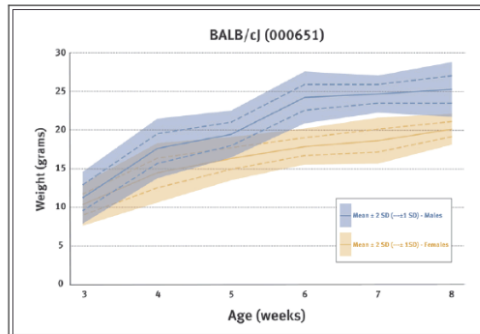
Body Weights

Age (weeks)		3	4	5	6	7	8
Female	Mean	10.45	14.50	16.36	17.91	18.69	20.18
	SD	1.38	1.91	1.41	1.17	1.49	1.00
Male	Mean	11.42	17.73	19.63	24.37	24.83	25.37
	SD	1.67	1.94	1.53	1.69	1.22	1.79

At each age, 40 mice of each sex were randomly selected from the colony, weighed, returned to the colony and excluded from further measurements. The mice were fed a diet containing 6% fat (LabDiet® 5K52/5K67) from weaning at 3 weeks of age until 8 weeks of age.

Parameter	Units	Females		Males	
Hematology					
Age	Weeks	8	16	8	16
White blood cell count (WBC)	10^3 cells/µL	3.24	-	2.86	-
Red blood cell count (RBC)	10^6 cells/µL	10.59	-	10.71	-
Hemoglobin	g/dL	17.1	-	17.3	-
Hematocrit	%	48.3	-	48.9	-
Mean cell volume (MCV)	fL	45.6	-	45.6	-
Mean cell hemoglobin (MCH)	pg	16.1	-	16.2	-
Mean cell hemoglobin concentration (MCHC)	g/dL	35.4	-	35.5	-
Platelet count	10^3 cells/µL	1001	-	994	-
Mean platelet volume (MPV)	fL	7.0	-	7.8	-
Percent reiticulocytes	%	3.2	-	2.8	-
Reticulocyte hemoglobin	pg	17.0	-	16.7	-
Reticulocyte count	10^9 cells/L	336.3	-	300.6	-
Percent neutrophils	%	14.8	-	23.1	-
Percent Lymphocytes	%	80.6	-	71.9	-
Percent Monocytes	%	0.8	-	0.9	-
Percent Eosinophils	%	3.0	-	2.9	-
Percent Basophils	%	0.2	-	0.8	-
Neutrophil count	10^3 cells/µL	0.49	-	0.60	-
Lymphocyte count	10^3 cells/µL	2.61	-	2.14	-
Monocyte count	10^3 cells/µL	0.03	-	0.02	-
Eosinophil count	10^3 cells/µL	0.10	-	0.06	-
Basophil count	10^3 cells/µL	0.01	-	0.02	-

Parameter	Units	Females		Males	
Biochemistry					
Albumin	g/dL	3.8	-	3.2	-
Total protein	g/dL	5.7	-	5.4	-
Blood urea nitrogen	mg/dL	17	-	20	-
Calcium	mg/dL	10.2	-	9.5	-
Phosphorous	mg/dL	9.5	-	9.0	-
Cholesterol	mg/dL	80	-	78	-
HDL cholesterol	mg/dL	68.8	-	76.4	-
Triglycerides	mg/dL	99	-	92	-
Free fatty acids	mEq/L	1.71	-	1.62	-
Glucose	mg/dL	112	-	114	-
Alanine tranferase	IU/L	68	-	60	-
Creatine kinase	IU/L	768	-	428	-
Thyroxine/T4	µg/dL	8.1	-	8.0	-

Parameter	Units	Females		Males	
Organ Weights					
Age	Weeks	8	16	8	16
Brain	g	0.402	-	0.406	-
	% of body weight	2.02	-	1.69	-
Heart	g	0.162	-	0.115	-
	% of body weight	0.84	-	0.48	-
Liver	g	0.993	-	1.162	-
	% of body weight	4.99	-	4.81	-
Left kidney	g	0.120	-	0.188	-
	% of body weight	0.61	-	0.78	-
Right kidney	g	0.124	-	0.189	-
	% of body weight	0.62	-	0.78	-
Spleen	g	0.082	-	0.076	-
	% of body weight	0.41	-	0.28	-

Body Composition by DEXA Analysis					
DEXA body weight	g; Total Tissue	19.14	-	23.45	-
Bone mineral density	g/cm^2	0.049	-	0.048	-
Bone mineral content	g	0.374	-	0.413	-
Bone area	cm^2	7.68	-	8.60	-
Lean tissue	g	14.9	-	18.7	-
Fat tissue	g	4.2	-	4.8	-
Percent fat tissue	%	22.2	-	20.2	-

Flow Cytometry - Spleen					
Lymphoid cells					
B cells					
B cells (B220+)	%	53.43	-	51.05	-
T cells					
CD4 T cells (CD3+, CD4+)	%	16.95	-	20.82	-
CD8 T cells (CD3+, CD8+)	%	9.45	-	10.58	-
NK cells (CD3-, NKG2D+)	%	1.75	-	2.07	-
NKT cells (CD3+, NKG2D+)	%	0.57	-	0.71	-
Myeloid cells					
Granulocytes (MAC1+, GR1+)	%	0.78	-	1.08	-
Monocytes (MAC1+, GR1-)	%	3.43	-	3.29	-

For 8 week data, mice of each sex were obtained at 8 weeks of age (BD +/- 3 days) from production rooms. All measurements are non-fasted values.

9. Acknowledgments

10. Curriculum Vitae

Personal information

Name.   Patricia Arreba-Tutusaus
Date of birth.   May 21st, 1987
Place of birth.   Barcelona (Spain)
Citizenship.   Spanish
Email.   patricia.arreba@gmail.com

Education

2011-2016   Dissertation
              Department of Hematology and Oncology
              Otto-von-Guericke University Hospital; Magdeburg (Germany)
              Supervisor: Prof. Dr. med. Florian Heidel
              Title: Impact of FLT3 internal tandem duplications (FLT3-ITD) on functional biology and sensitivity to therapy depending on their location

2010-2011   Master of Science in Biomedicine
              University of Barcelona; Barcelona (Spain)

              Master's thesis
              ENDOR Nanotechnologies, Barcelona Scientific Park; Barcelona (Spain). Supervisor: Dr. Judith Sendra
              Title: Advanced metallic nanosystems for designing new drug's delivery systems (Endor Delivery System)

2005-2010   University Degree in Biology
              University Pompeu Fabra; Barcelona (Spain)

              Degree's thesis
              Human Genetics Division, University of Southampton; Southampton (UK)
              Supervisor: Prof. Dr. Christopher G. Proud
              Title: Studying the role of 4E-HP in 5'-TOP mRNA translation

2003-2005   General Certificate of Education
              Col·legi Sagrada Familia de Gavà; Barcelona (Spain)

List of Publications

Arreba-Tutusaus P, Mack TS, Bullinger L, Polanetzki A, Schnoeder TM, Ballaschk A, Wang Z, Deshpande AJ, Armstrong SA, Döhner K, Fischer T, Heidel FH. Impact of *FLT3*-ITD location on sensitivity to TKI-therapy *in vitro* and *in vivo*. Leukemia. 2016; 30(5), 1220-5.

Schnöder TM, **Arreba-Tutusaus P**, Griehl I, Bullinger L, Buschbeck M, Lane SW, Döhner K, Plass C, Lipka DB, Heidel FH, Fischer T. Epo-induced erythroid maturation is dependent on Plcg1 signaling. Cell Death and Differentiation. 2015; 21(2): 240-8.

Heidel FH, **Arreba-Tutusaus P**, Armstrong SA, Fischer T. Evolutionary Conserved Signaling Pathways: Acting in the Shadows of AML's Genetic Diversity. Clin Cancer Res. 2015; 21(2): 240-8.

Arreba-Tutusaus P and Heidel FH. Signaling Pathways Maintaining Stemness in Adult Hematopoietic Stem Cells. In: Adult Stem Cells. 2nd Ed. New York: Springer; 2014. (Book Chapter).

Heidel FH, Bullinger L, **Arreba-Tutusaus P**, Wang Z, Gaebel J, Hirt C, Niederwieser D, Lane SW, Döhner K, Vasioukhin V, Fischer T, Armstrong SA. The cell fate determinant Llgl1 influences HSC fitness and prognosis in AML. J Exp Med. 2013; 210(1):15-22.

11. Declaration

Patricia Arreba-Tutusaus
C/ San Isidro 85, 6º 2ª
08850 Gavà, Barcelona (Spain)

Erklärung

Hiermit erkläre ich, dass ich die von mir eingereichte Dissertation zu dem Thema

Impact of FLT3 internal tandem duplications (FLT3-ITD) on functional biology

and sensitivity to therapy depending on their location

selbstständig verfasst, nicht schon als Dissertation verwendet habe und die benutzten Hilfsmittel und Quellen vollständig angegeben wurden.

Weiterhin erkläre ich, dass ich weder diese noch eine andere Arbeit zur Erlangung des akademischen Grades doctor rerum naturalium (Dr. rer. nat.) an anderen Einrichtungen eingereicht habe.